CHALMERS
UNIVERSITY OF TECHNOLOGY

STEERING EFFECTS OF ACTIVE SUSPENSIONS

Modeling and Control of AARB system to mitigate yaw disturbances and decrease driver steering effort

Master's thesis in Systems, Control and Mechatronics

AKSHAY BHARADWAJ BIRUR SATISH

Department of Mechanics and Maritime Sciences
CHALMERS UNIVERSITY OF TECHNOLOGY
Gothenburg, Sweden 2019

Master's thesis 2019:98

Steering Effects Of Active Suspensions

Modeling and Control of AARB system to mitigate yaw disturbances and decrease driver steering effort

Akshay Bharadwaj Birur Satish

Department of Mechanics and Maritime Sciences
Division of Vehicle Engineering and Autonomous Systems
Chalmers University of Technology
Gothenburg, Sweden 2019

Steering Effects Of Active Suspensions
Modeling and Control of AARB system to mitigate yaw disturbances and decrease driver steering effort
Akshay Bharadwaj Birur Satish

© Akshay Bharadwaj Birur Satish, 2019.

Supervisor: Anton Albinsson, Volvo Car Corporation
Tushar Chugh, Department of Mechanics and Maritime Sciences
Examiner: Fredrik Bruzelius, Department of Mechanics and Maritime Sciences

Master's Thesis 2019:98
Department of Mechanics and Maritime Sciences
Division of Division of Vehicle Engineering and Autonomous Systems
Chalmers University of Technology
SE-412 96 Gothenburg
Telephone +46 31 772 1000

Cover: Visualization of a car driving on a banked road.

STEERING EFFECTS OF ACTIVE SUSPENSIONS
Modeling and Control of AARB system to mitigate yaw disturbances and decrease driver steering effort
AKSHAY BHARADWAJ BIRUR SATISH
Department of Mechanics and Maritime Sciences
Chalmers University of Technology

ABSTRACT

Automotive suspension systems have traditionally been a compromise between ride comfort,road handling and load carrying. Due to these conflicting demands, semi-active suspension has been an important feature among premium car manufacturers. The type of active suspension considered in this thesis is an active anti-roll bar system (AARB). The main objective of the AARB system is to provide roll-over protection and better isolation to the passengers from the disturbances induced due to road irregularities.

While the active suspension provides better comfort by attenuating the vertical and roll disturbances to a great extent, it has certain adverse effects too. Active control of suspension triggers the lateral vehicle movement due to kinematics and compliance ($K\&C$) of the wheel suspension. The suspension parameters such as bump steer, roll steer and camber steer produces some lateral tyre force which needs to be compensated. To ensure stability of the vehicle, lateral disturbances caused by road bumps, crowned road and road banking needs to be attenuated. The master thesis involves implementation of the AARB controller to improve stability and reduce the steering effort while driving on the road with above mentioned disturbances. The controller can be integrated with active steering system to reduce the overhead on the steering actuator and increase steer-ability in auto-pilot mode. Also, the influence of $K\&C$ parameters on steering torque and yaw rate is studied using a linear kinematic model developed in CarMaker. Further, AARB controller is extended to handle cornering scenarios. The control strategy developed includes a state feedback LQR, LQI and robust $\mathcal{H}_\infty$ controller and validated with two different $K\&C$ setups and their performance is compared.

In conclusion, simulation results show that there is potential in the AARB system to reduce driver steering effort in driver-in-loop and increase steering range in autopilot while using a certain kind of $K\&C$ setup.

Keywords: Active suspension, Active anti-roll bar, $\mathcal{H}_\infty$ control, $K\&C$, linear kinematic model, Reduce steering effort.

Acknowledgements

I would like to extend my gratitude to my supervisors, Anton Albinsson and Tushar Chugh for their immense support and advice throughout the thesis. I would also like to thank the entire wheel suspension mechatronics group at Volvo cars for their support on technical and administrative part. Finally, I would like to thank Fredrik Bruzelius, my examiner at Chalmers for giving valuable inputs during the whole project. I would also like to thank Sachin Madhusudhana of Chalmers University of Technology for his valuable inputs during the thesis.

Finally, I express my gratitude to my family and friends for their continuous support without whom this accomplishment would not have been possible.

Akshay Bharadwaj Birur Satish, Gothenburg, August 2019

Contents

List of Abbreviations and Symbols

Abbreviations

DOF Degree of Freedom

EPS Electronic Power Steering

AARB Active Anti-Roll Bar

CoG Centre of Gravity

NSP Neutral Steering Point

AC Aerodynamic Center

ECU Electronic Control Unit

EPSc Column Electronic Power Steering

EPSdp Dual Pinion Electronic Power Steering

EPSapa Axis Parallel Electronic Power Steering

PID Proportional Integral Derivative controller

LQR Linear Quadratic Regulator

LQI Linear Quadratic Integral

CARE Control Algebraic Riccati Equation

SISO Single Input Single Output

LFT Linear Fractional Transformation

DoF Degree(s) of Freedom

Symbols

ψ Yaw Angle

$\dot{\psi}$ Yaw Rate or Velocity

ϕ Roll Angle

$\dot{\phi}$ Roll Rate or Velocity

θ Pitch Angle

$\dot{\theta}$ Pitch Rate or Velocity

α Tyre Slip Angle

δ Steering Angle

γ Camber Angle

δ_s Toe Angle

v_x Longitudinal velocity in wheel co-ordinates

v_y Lateral velocity in wheel co-ordinates

v_x Longitudinal velocity in wheel co-ordinates

v_y Lateral velocity in wheel co-ordinates

F_x Longitudinal Tyre Force

F_y Lateral Tyre Force

F_z Normal Load

C_α tyre cornering stiffness

CC_y Cornering Coefficient

x_s unsprung mass displacement

x_1 unsprung mass displacement FR

x_2 unsprung mass displacement FL

x_3 unsprung mass displacement RR

x_4 unsprung mass displacement RL

Z_{r1} road displacement FR

Z_{r2} road displacement FL

Z_{r3} road displacement RR

Z_{r4} road displacement RL

a_y Lateral Acceleration

F_{yf} Lateral tyre force for the front tyre

F_{yr} Lateral tyre force for the rear tyre

$\ddot{\phi}$ Yaw Acceleration

θ_{Vf} Front tire velocity angle

θ_{Vr} Rear tire velocity angle

z_s Sprung mass displacement

z_{us} Unsprung mass displacement

F_{stab} Stabilizer/Roll bar Force

T_{arb} Stabilizer/Roll bar Torque

TF Transfer Function

m Mass of the vehicle

L Wheel base

lf distance between Wheel base and front axis

lr distance between Wheel base and rear axis

w track width

c_{fl} Suspension Damping Coefficient Front Left

c_{fr} Suspension Damping Coefficient Front Right

c_{rl} Suspension Damping Coefficient Rear Left

c_{rr} Suspension Damping Coefficient Rear Right

k_{fl} Spring Stiffness Coefficient Front Left

k_{fr} Spring Stiffness Coefficient Front Right

k_{rl} Spring Stiffness Coefficient Rear Left

k_{rr} Spring Stiffness Coefficient Rear Right

k_{arf} Roll Bar Stiffness Coefficient Front

k_{arr} Roll Bar Stiffness Coefficient Rear

C_{α_f} Tyre Cornering Stiffness Front

C_{α_r} Tyre Cornering Stiffness Rear

g acceleration due to gravity

I_{xx} Roll Inertia

I_{yy} Pitch Inertia

I_{zz} Yaw Inertia

k_{tfl} Tyre Stiffness Coefficient Front Left

k_{tfr} Tyre Stiffness Coefficient Front Right

k_{trl} Tyre Stiffness Coefficient Rear Left

k_{trr} Tyre Stiffness Coefficient Rear Right

m_{fl} Wheel Mass Front Left

m_{fr} Wheel Mass Front Right

m_{rl} Wheel Mass Rear Left

m_{rr} Wheel Mass Rear Right

L_{arb} Length of AARB actuator arm length

γ_{sfl} Static Camber FL

γ_{sfr} Static Camber FR

γ_{srl} Static Camber RL

γ_{srr} Static Camber RR

$K_{fl_{stiff}}$ Camber Stiffness FL

$K_{fr_{stiff}}$ Camber Stiffness FR

$K_{rl_{stiff}}$ Camber Stiffness RL

$K_{rr_{stiff}}$ Camber Stiffness RR

C_{bsfl} Bump Steer Coefficient FL

C_{bsfr} Bump Steer Coefficient FR

C_{bsrl} Bump Steer Coefficient RL

C_{bsrr} Bump Steer Coefficient RR

C_{bcfl} Bump Camber Coefficient FL

C_{bcfr} Bump Camber Coefficient FR

C_{bcrl} Bump Camber Coefficient RL

C_{bcrr} Bump Camber Coefficient RR

List of Figures

List of Tables

1 Introduction

1.1 Motivation

The motivation of this thesis is to investigate the effects of active suspension system with active anti-roll bars on steering and yaw motion. This thesis also includes implementation of control strategies to actively control Active Anti-Roll Bar (AARB) system to compensate for the lateral road disturbances such as road bumps, banking etc. Also, the steering effort with driver-in-loop and overhead on the steering actuator are reduced thus increasing the steering capability of the pilot assist. The suspension K&C effects on steering wheel torque and yaw rate on steering is also studied.

1.2 Steering effects of Active Suspension Overview

A car is constantly subjected to a variety of forces during its normal operation which can adversely affect its trajectory. Disturbances majorly originate from external sources such as wind, road crowns and road bumps etc causing lateral-drift of the vehicle during its motion. The driver needs to compensate with steering which is not desirable from the comfort point of view. Heavy wind gusts and road crowns can be a safety issue if the driver over-compensate/under-compensate with steering.

Optimizing a passive suspension system, it is very hard to meet comfort, handling and ride stability requirements as passive suspension will always be a compromise between these properties. Active Suspension Systems has been an important field of research in vehicle dynamics. It has also become an important feature among premium car manufacturers as they provide better ride comfort, road grip and handling ability. Using active anti-roll bar it is possible to reduce the roll moment induced due to road irregularities. In addition, it is also possible to control the vertical position of the wheels axle-wise [1]. In active suspension systems, the electronically controlled actuators provides a significant increase in terms of comfort. However, depending on the system architecture and control method for the active system may be utilizing active dampers which produces optimal damping forces or active anti-roll bars. The AARB system consists of an electric motor to control the normal forces on individual tyres to counter different kind of road disturbances. Active anti-roll bar can be used to assist steering to counteract yaw motion induced due to road disturbances and wind gusts, thus reducing the steering effort of the driver.

The control strategy for an active anti-roll bar system measures body motion signal such as body roll and pitch, vertical suspension movement and control the actuators which produces desired normal force on individual wheels. However, as technology progresses, more advanced sensors are installed in new cars from which the road profile can be estimated in a good way. The downside of introducing new sensors is increase in cost. A Model based feedback control strategy is well suited for the current sensors on board to control active anti-roll bar to maintaining its stability. Optimal control strategy uses a system model to compute the optimal control signals based on the current states of the system. The drawback with linear system theory and control is that it is not possible to incorporate hard constraints such as actuator saturation in the controller design [21]. As long as actuator saturation is far from being achieved these control techniques are of great benefit as they are computationally less complex. They also provide framework to include external disturbances and uncertainties in the control design. In addition, linear system theory and controller design also is more easy to understand than its nonlinear counterpart.

Previous works have shown potential when using active anti-roll bar to drastically improve the roll stability of a vehicle to prevent rollover [4]. The $\mathcal{H}_\infty$ approach is taken to design the controller for the active anti-roll bars using a yaw-roll vehicle dynamic model. $\mathcal{H}_\infty$ control method is implemented focusing on the uncertainties due to velocity and sprung mass variation for a heavy vehicle [2]. Optimal LQR was applied to integrated model of servo-valve hydraulic model and a yaw-roll model for a single unit heavy vehicle [5]. Linear Parameter Varying (LPV) technique has been applied for active anti-roll bar combined with active brake control on a single heavy vehicle with the varying parameter being the forward velocity [6].

1.3 Active anti-roll bar Controller design goals

Upon completion of the project, the following research questions should be answered:

- How does suspension kinematics parameters effect the active anti-roll bar system and its effect on steering angle and steering wheel torque?
- How to formulate a transfer function between change in normal load to steering wheel angle?
- How to develop a controller for the anti-roll bar to attenuate yaw disturbances for high and low frequency disturbances to increase straight line stability and extend to cornering situations?
- How to utilize the AARB system to mitigate steering effort while normal driving and extend steering ability of pilot assist by decreasing overhead on steering actuator?

1.4 Scope of Thesis

The scope of the thesis is focused around the study of active roll bar system and its effects on steering. It includes design and implementation of a AARB controller to mitigate steering effort and improve steering ability of pilot assist systems which also involves analysis of suspension kinematics and propose changes required to implement the AARB controller to effect steering system. In order to implement the controller in a real car, additional work is required that will be outside of the scope. The information that is fed to the controller is assumed to be pre-processed communication with sensors and actuators in the car is assumed to be in place.

A validated IPG CarMaker car model to test and evaluate the controller is available and will be used during the project. A linear dynamic model of suspension and lateral motion is developed considering linear suspension kinematics in the model to analyze active suspension effects on steering angle. The linear system model is validated by comparing with the IPG CarMaker model. Two kinematic setups are compared and kinematic parameter effects on steering wheel torque are analyzed and the analysis is done by developing a linear kinematic model in the Carmaker. Control methods such as LQR, LQI and robust $\mathcal{H}_\infty$ techniques are used and the controllers performance are compared. The AARB controller is tested for high and low frequency road disturbances such as road bumps and banked roads. The controller is tested for straight ahead motion and then extended to cornering scenarios as well. The controller will be tuned and evaluated by assessing vehicle body motions while making sure that the actuator saturation levels are not reached.

1.5 Outline of the Thesis

- Chapter 2 contains theory about relevant vehicle dynamics and model validation results are presented. It also introduces the control problem that needs to be solved when trying to improve ride comfort with active anti-roll bar system.

- Chapter 3 contains theory about LQR, LQI and $\mathcal{H}_\infty$ methods which are used to develop the AARB controller.

- Chapter 4 describes a detailed suspension kinematics analysis. It involves comparing two existing kinematic setups and quantification of kinematic parameters on its effect on steering wheel torque.

- Chapter 5 presents simulation testing of the implemented controllers and obtained results for three different driving scenarios.

- Chapter 6 contains a discussion of the obtained results together with suggestions for future work and the conclusion of the thesis.

2
Modeling

This chapter mainly describes the mathematical modeling of 7-DOF vertical full car model and the extended bicycle model to capture the suspension and lateral dynamics of the car respectively. The dynamic model is implemented to analyze the effects of anti roll bar torque on yaw rate and overall path of the vehicle. Also, the effects of road disturbances on vehicle's roll, pitch and yaw angles are studied. Further the linear model is used in the design of AARB controller. The model is validated by comparing its states with that of CarMaker results for a maneuver. The chapter starts with the description of the vehicle motions and coordinate systems followed by the detail modeling approach. Then the two models are combined effectively to form a roll-yaw model. Finally, suspension kinematics and compliance model is added to the roll-yaw model and the active anti-roll bar control problem is formulated.

2.1 Vehicle Motions and Coordinate Systems

The coordinate system used in the entire thesis is shown in 2.1.It is in accordance to the ISO 8855 standards. According to this coordinate system, the longitudinal motion of the vehicle is described by positive X axis, the lateral motion is described by the Y axis, left of the driver being the positive orientation and the vertical motion is represented by the Z axis. The rotations about the vehicle CoG are also included in this system of coordinates. The roll, pitch and yaw rotation are the rotation around the X axis, Y axis and Z axis respectively.

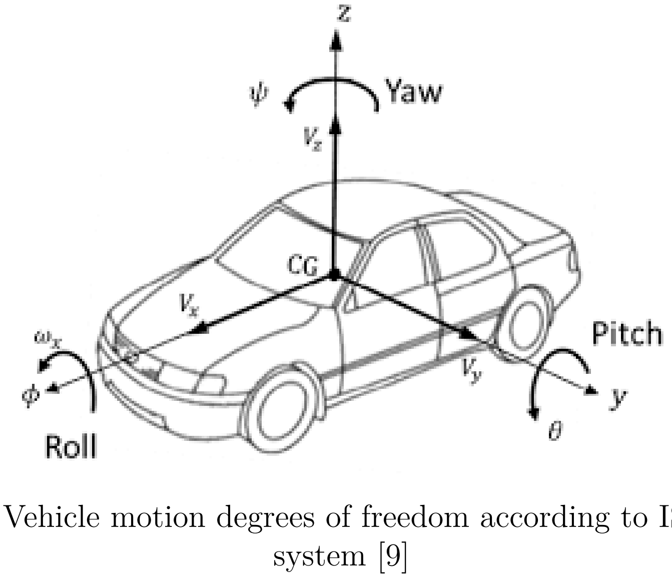

Figure 2.1: Vehicle motion degrees of freedom according to ISO coordinate system [9]

In addition to this coordinate system, a wheel is best described in its own local coordinate system for each tire, also according to ISO 8855. The forces and moments which are acting on the wheel from the ground are shown in 2.2. The other quantities, such as slip angle (α) and camber angle (γ) in figure 2.2 are the variables which have considerable effects on these forces and moments which is discussed in further chapters. The coordinate system for a single wheel can be seen in figure 2.2.

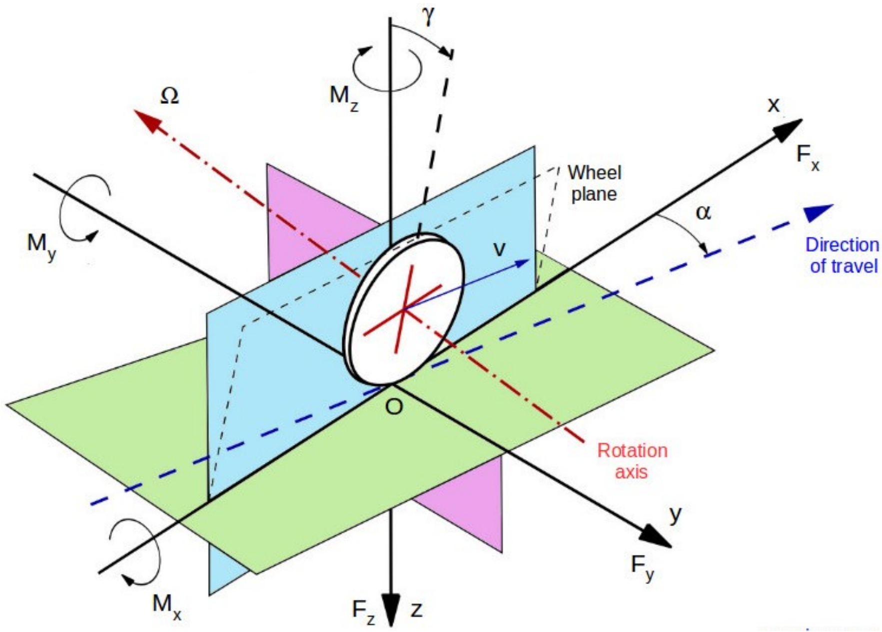

Figure 2.2: Wheel coordinate system. Forces and moments on tyre from ground from ISO 8855 [19]

The definitions of few of the wheel angles which are extensively used in this thesis is described below.

- **Steer Angle:** The Steer angle (δ) is the angle from vehicle longitudinal axis to the wheel plane about the vehicle vertical axis [9]. Assuming vehicle XY-plane is parallel to road plane, this angle is same as angle from vehicle longitudinal axis to the intersection between wheel plane and road plane.

- **Inclination angle:** The inclination angle or camber angle (γ) is the angle from vehicle longitudinal axis to the wheel plane about the vehicle longitudinal axis [9]. Camber angle is set in order to have better contact patch on the road and for the stability of the car. As seen from the front of the car, if the centre line is inclined inwards, it is called negative camber, and if it is inclined outwards, it is called positive camber.

- **Static Toe Angle:** The Static toe angle (δ_{toe}) is the angle between vehicle longitudinal axis and the wheel plane about the vehicle vertical axis, with the vehicle at rest and steering in the straight-ahead position [9]. is when forward portion of the wheel is closer to the vehicle centre line than the wheel centre.

2.2 Tire Model

Tire Model provides a mathematical model for the interaction between the vehicle tires and the road surface. The tire forces produced in longitudinal and lateral direction are generally presented as a function of tire slip angles. The example of slip curve is shown in the figure 2.3. This thesis mainly focus on the lateral tire model, thus only lateral tire forces are considered from now on.

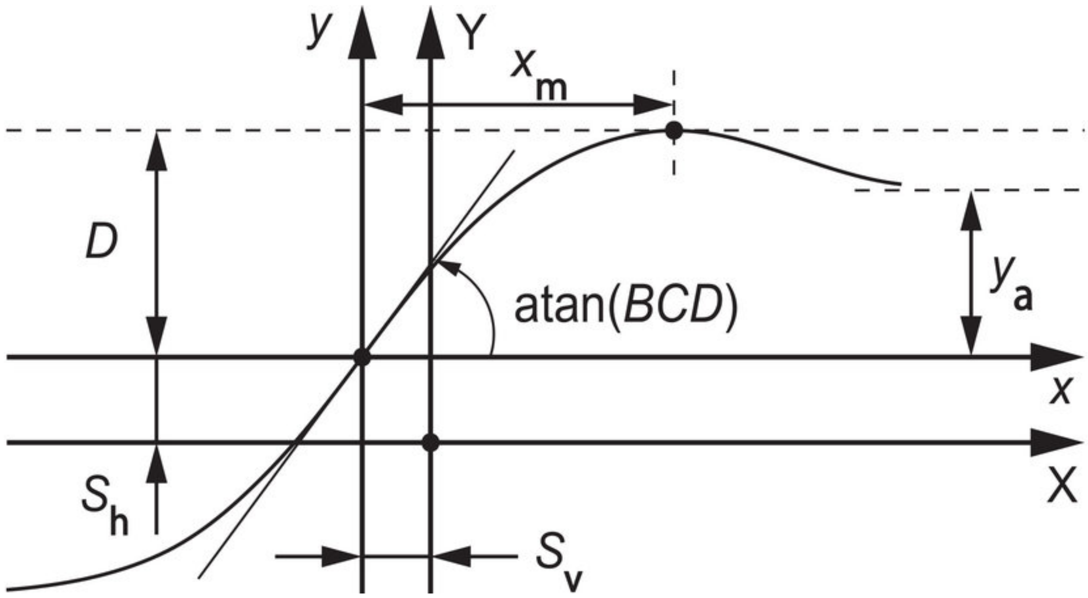

Figure 2.3: Pacejka magic formula tire parameters [7]

The slope of the curve at zero lateral slip angle is called the cornering stiffness. The lateral slip angle of the tire is given by the relation

$$\alpha = \arctan\left(v_y/v_x\right) \tag{2.1}$$

Here α is the lateral tire slip angle, v_x and v_y are the tire velocities in x and y direction in the wheel coordinate system. From figure 2.3 its evident that for small slip angle α, the lateral tire force F_y is linear and is equal to product of slip angle and the cornering stiffness. However, with the increase in slip angle the curve reaches a maximum friction coefficient µmax and F_y reaches a plateau. Other parameters such as inflation pressure of the tire, surface conditions (eg. dry/wet tarmac, snow, ice), the tire and the road temperatures also effect the lateral slip curve in a great manner. The non-linear tire models can be obtained using empirical model known as Pacejka magic formula shown in figure 2.3. The curve fit has a general form

$$\frac{F_x}{F_z} = D\sin\left(C\arctan\left(BS_x - E(BS_x - \arctan\left(BS_x\right))\right)\right) \tag{2.2}$$

Where B is a stiffness parameter, C is a shape parameter, D is a peak value parameter, and E is a curvature parameter describing the curve [7].

2.2.1 Linear Model

The tire model can be simplified by linearizing the model. The linear tire model is given by

$$F_y(\alpha) = -C_\alpha \alpha \tag{2.3}$$

F_y is the lateral tire force developed in the tire, α is lateral slip of the tire and C_α is tyre cornering stiffness [7]. This model is accurate only for small lateral tyre slip angles. This model is utilized for vehicle model linearization to generate linear plant model used for controller synthesis presented further in this chapter.

2.2.2 Influence of vertical load

The vertical load on the tire greatly influences the behaviour of the tire and is one of the important aspect of cornering performance of the vehicle.

$$C_\alpha(F_z) = CC_{\alpha_0} F_z \tag{2.4}$$

From equation 2.4, it is seen that the normal force is directly proportional to lateral force F_y. Substitute equation 2.4 in equation 2.5.

$$F_y = -C_\alpha \alpha = -CC_{\alpha_0} F_z \alpha \tag{2.5}$$

The approximation which is made here is that $C_\alpha \; \alpha \; F_z$ with proportionality coefficient $CC_{\alpha 0}$ the Cornering Coefficient (or Lateral Slip Coefficient) [7]. It is assumed that normal load depends only on the position of CoG and thus the load transfer and other effects are neglected in the vehicle model.

2.3 7-DOF Full car Vertical Model

This section describes the full-car suspension model with passive springs,dampers and anti-roll bars. The full-car model has seven degrees of freedom: heave, roll, pitch and vertical displacement of the four unsprung masses. The physical model of the full-car model is shown in figure 2.4.

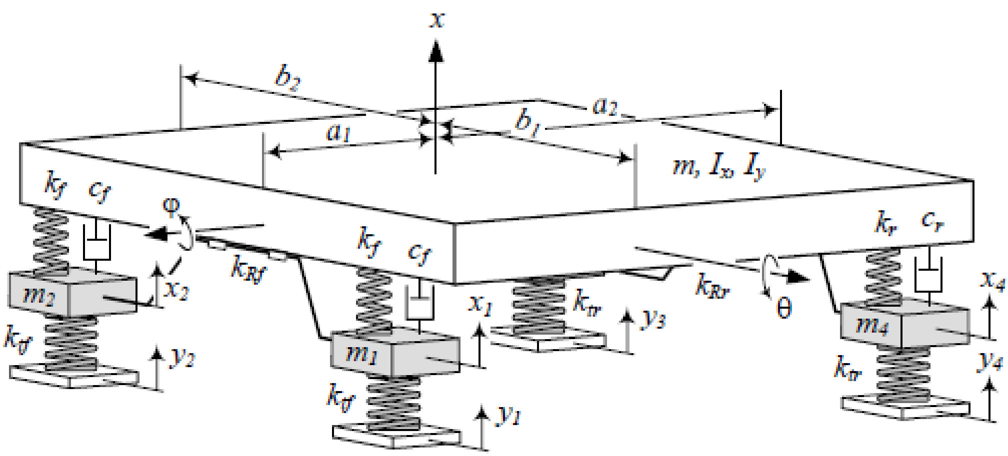

Figure 2.4: 7-DOF Full car Vertical Model [11]

In the model shown in figure 2.4,
$l_f = a_1$, $l_r = a_2$, $b_1 = b_2 = \frac{w}{2}$

equation for sprung mass acceleration:

$$\begin{aligned} m\ddot{x}_s + c_f(\dot{x_s} - \dot{x_1} + b_1\dot{\varphi} - a_1\dot{\theta}) + c_f(\dot{x_s} - \dot{x_2} - b_2\dot{\varphi} - a_1\dot{\theta}) \\ +c_r(\dot{x_s} - \dot{x_3} - b_1\dot{\varphi} + a_2\dot{\theta}) + c_r(\dot{x_s} - \dot{x_4} + b_2\dot{\varphi} + a_2\dot{\theta}) \\ +k_f(x_s - x_1 + b_1\varphi - a_1\theta) + k_f(x_s - x_2 - b_2\varphi - a_1\theta) \\ +k_r(x_s - x_3 - b_1\varphi + a_2\theta) + k_r(x_s - x_4 + b_2\varphi + a_2\theta) = 0 \end{aligned} \tag{2.6}$$

equation for body roll:

$$\begin{aligned} I_x\ddot{\varphi} + b_1c_f(\dot{x_s} - \dot{x_1} + b_1\dot{\varphi} - a_1\dot{\theta}) - b_2c_f(\dot{x_s} - \dot{x_2} - b_2\dot{\varphi} - a_1\dot{\theta}) \\ -b_1c_r(\dot{x_s} - \dot{x_3} - b_1\dot{\varphi} + a_2\dot{\theta}) + b_2c_r(\dot{x_s} - \dot{x_4} + b_2\dot{\varphi} + a_2\dot{\theta}) \\ +b_1k_f(x_s - x_1 + b_1\varphi - a_1\theta) - b_2k_f(x_s - x_2 - b_2\varphi - a_1\theta) - b_1k_r(x_s - x_3 - b_1\varphi + a_2\theta) \\ +b_2k_r(x_s - x_4 + b_2\varphi + a_2\theta) + M_R = 0 \end{aligned} \tag{2.7}$$

Equation for body pitch:

$$\begin{aligned} I_y\ddot{\theta} + a_1c_f(\dot{x_s} - \dot{x_1} + b_1\dot{\varphi} - a_1\dot{\theta}) - a_1c_f(\dot{x_s} - \dot{x_2} - b_2\dot{\varphi} - a_1\dot{\theta}) \\ +a_2c_r(\dot{x_s} - \dot{x_3} - b_1\dot{\varphi} + a_2\dot{\theta}) + a_2c_r(\dot{x_s} - \dot{x_4} + b_2\dot{\varphi} + a_2\dot{\theta}) \\ -a_1k_f(x_s - x_1 + b_1\varphi - a_1\theta) - a_1k_f(x_s - x_2 - b_2\varphi - a_1\theta) \\ +a_2k_r(x_s - x_3 - b_1\varphi + a_2\theta) + a_2k_r(x_s - x_4 + b_2\varphi + b_2\theta) = 0 \end{aligned} \tag{2.8}$$

Equation for unsprung mass FL displacement:

$$m_f\ddot{x}_1 - c_f(\dot{x_s} - \dot{x_1} + b_1\dot{\varphi} - a_1\dot{\theta}) - k_f(x_s - x_1 + b_1\varphi - a_1\theta) - k_R\frac{1}{w}(\varphi - \frac{x_1 - x_2}{w}) + k_{t_f}(x_1 - y_1) = 0 \tag{2.9}$$

Equation for unsprung mass FR displacement:

$$m_f\ddot{x}_2 - c_f(\dot{x_s} - \dot{x_2} - b_2\dot{\varphi} - a_1\dot{\theta}) - k_f(x_s - x_2 - b_2\varphi - a_1\theta) + k_R\frac{1}{w}(\varphi - \frac{x_1 - x_2}{w}) + k_{t_f}(x_2 - y_2) = 0 \tag{2.10}$$

Equation for unsprung mass RL displacement:

$$m_r\ddot{x}_3 - c_r(\dot{x_s} - \dot{x_3} - b_1\dot{\varphi} + a_2\dot{\theta}) - k_r(x_s - x_3 - b_1\varphi + a_2\theta) + k_{t_r}(x_3 - y_3) = 0 \tag{2.11}$$

Equation for unsprung mass RR displacement:

$$m_r\ddot{x}_4 - c_r(\dot{x_s} - \dot{x_4} + b_2\dot{\varphi} + a_2\dot{\theta}) - k_r(x_s - x_4 + b_2\varphi + a_2\theta) + k_{t_r}(x_4 - y_4) = 0 \tag{2.12}$$

Here we assume that,

$$m_1 = m_2 = m_f \tag{2.13}$$

$$m_3 = m_4 = m_r \tag{2.14}$$

2.3.1 Anti-Roll Bar Model

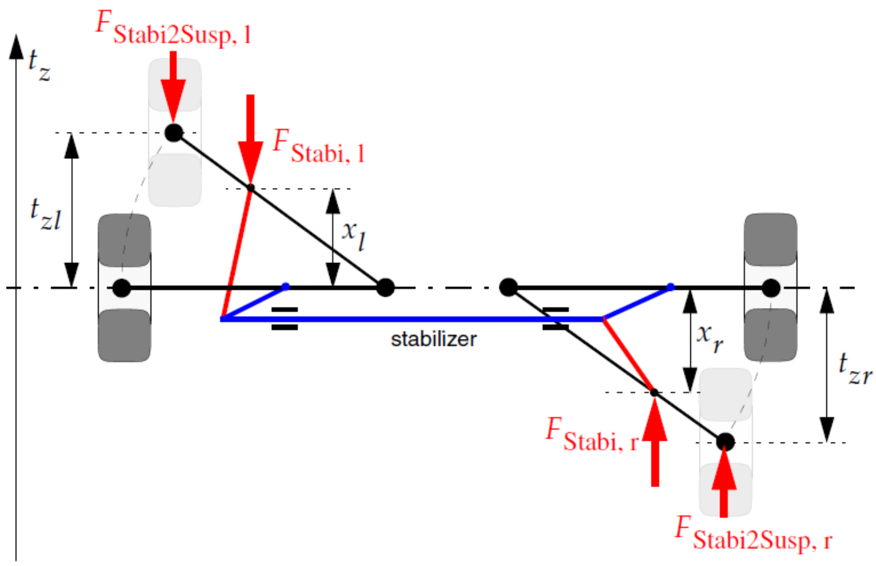

Figure 2.5: Roll bar with wheel deflection length difference [12]

Here, stabilizer deflection lengths are x_l and x_r. $F_{stabi2Susp,l}$ and $F_{stabi2Susp,r}$ are normal forces acting at the wheel centre. $F_{stabi,l}$ and $F_{stabi,r}$ are normal forces acting at the stabilizer mounting points (along the axle). t_zl and t_zr are wheel centre displacements

Electro-mechanical active AARB with controller actively generate torque T_{AARB} at the center of the bar. The reaction force of active AARB can be expressed by the model shown in 2.15.

$$F_{stab} = T_{arb}/L_{arb} \tag{2.15}$$

The passive AARB model M_R in equation 2.7 is replaced by -wF_{stab} . The F_{stabi} on two individual wheels in an axle depends on the roll distribution ratio (r) which is described as,

$$F_{stabi,front} = r * T_{arb}/L_{arb} \tag{2.16}$$

$$F_{stabi,rear} = (1 - r) * T_{arb}/L_{arb} \tag{2.17}$$

According to 2.5, the AARB force is applied at the centre of the wheel and Stabilizer force F_{stabi} is produced when right and left wheels are compressed in opposite direction. The roll bar force can be defined in two ways i.e. using a wheel deflection length difference or a deflection angle difference. Here, the model with wheel deflection difference is used.
It is also considered that for an axle, stabilizer force acting on left and right wheels are equal and opposite,

$$F_{stabi,l} = -F_{stabi,r} \tag{2.18}$$

2.4 Linear One-Track Model

One-track lateral dynamics model is considered to establish relationship between road disturbances and yaw rate. This section describes the linear single track model to describe the lateral and yaw motion of the car [4]. The physical model of the bicycle model is shown in figure 2.6.

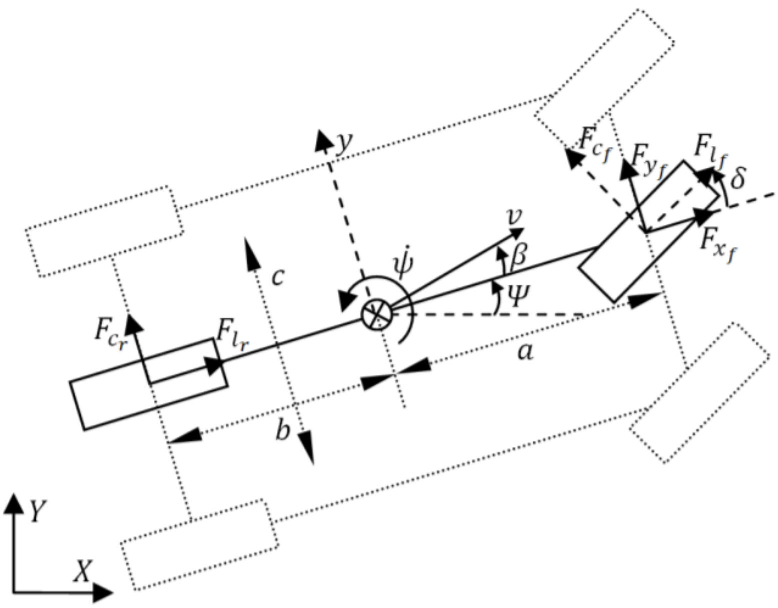

Figure 2.6: Steady State One-track model (bicycle model) [20]

From Newton's second law of motion along Y-axis,

$$ma_y = F_{y_f} + F_{y_r} \tag{2.19}$$

Here ay is the inertial acceleration of the vehicle at CoG at y axis and F_{y_f} and $F_{y_r} = F_{c_r}$ are the lateral tire forces of the front and rear wheels respectively. a_y can be written as the acceleration $\ddot{y}$ which is due to motion along the y axis and the centripetal acceleration $V_x\dot{\Psi}$.

$$a_y = \ddot{y} + V_x\dot{\Psi} \tag{2.20}$$

substitute 2.20 in 2.19 to get,

$$m(\ddot{y} + \dot{\Psi}V_x) = F_{y_f} + F_{y_r} \tag{2.21}$$

The equation for the yaw dynamics is given by taking moment about the z axis,

$$I_z \ddot{\Psi} = \ell_f F_{y_f} - \ell_r F_{y_r} \tag{2.22}$$

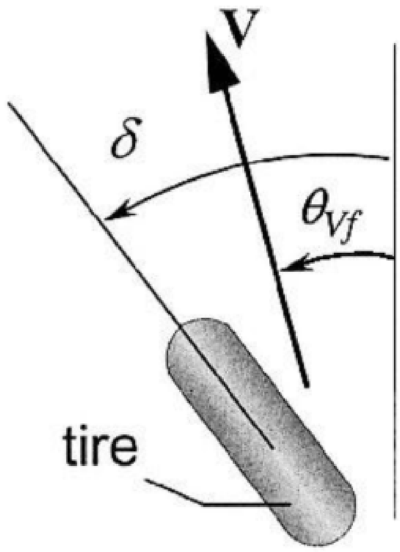

Figure 2.7: Tire Slip Angle [4]

Using a linear tyre model, the slip angle of the front and rear wheel is given by,

$$\alpha_f = \delta - \theta_{Vf} \tag{2.23}$$

$$\alpha_r = -\theta_{Vr} \tag{2.24}$$

where θ_{Vf} and θ_{Vr} are is the front and rear tire velocity angle. The lateral tyre forces for the front and rear wheel is given by,

$$F_{y_f} = 2C_{\alpha f}(\delta - \theta_{Vf}) \tag{2.25}$$

$$F_{y_r} = 2C_{\alpha r}(-\theta_{Vr}) \tag{2.26}$$

The following relations can be used to calculate θ_{Vf} and θ_{Vr} :

$$tan(\theta_{Vf}) = \frac{\dot{y} + \ell_f \dot{\Psi}}{V_x} \tag{2.27}$$

$$tan(\theta_{Vr}) = \frac{\dot{y} - \ell_r \dot{\Psi}}{V_x} \tag{2.28}$$

Using small angle approximations,

$$\theta_{Vf} = \frac{\dot{y} + \ell_f \dot{\Psi}}{V_x} \tag{2.29}$$

$$\theta_{Vr} = \frac{\dot{y} - \ell_r \dot{\Psi}}{V_x} \tag{2.30}$$

From the equations above the lateral acceleration and yaw acceleration can be written as,

$$\ddot{y} = (-\frac{2C_{\alpha f} + 2C_{\alpha r}}{mV_x})\dot{y} - (V_x + \frac{2C_{\alpha f}\ell_f - 2C_{\alpha r}\ell_r}{mV_x})\dot{\Psi} + (\frac{2C_{\alpha f}}{m})\delta \tag{2.31}$$

$$\ddot{\psi} = (-\frac{2\ell_f C_{\alpha f} - 2\ell_r C_{\alpha r}}{I_z V_x})\dot{y} - (\frac{2\ell_f^2 C_{\alpha f} - 2\ell_r^2 C_{\alpha r}}{I_z V_x})\dot{\Psi} + (\frac{2\ell_f C_{\alpha f}}{I_z})\delta \tag{2.32}$$

2.5 Suspension Kinematics and compliance

Suspension kinematics illustrates the spacial variation of a wheel caused due to change in the suspension positioning parameters (compression and steer) action. Movement of the wheel due to suspension compression and rebound is called Suspension kinematics and that due to pure steer actions is termed as steering kinematics. Some wheel movement also exist due to superposition of suspension deflection and steering in reality. Compliance describes the spacial movements of a wheel caused due to forces generated at the wheel causing elastic deformations of the wheel suspension. Suspension forces and torques produces movements of the wheel in directions other than in their effective direction due to the complexity of the vehicle suspension system [12]. Movements are explained through coordinates (primary and secondary) in an axis system as shown in figure 2.2 with wheel center as the center of the axis system.

The table 2.1 describes the context of kinematics and compliance. Primary coordinates of a wheel comprises of wheel compression and steer actions. Kinematics is defined as an effect on the secondary coordinates due to force free movements of the wheel suspension and is a function of the primary coordinates.On the contrary to the kinematics, the compliance is defined as the change of secondary coordinates due to external forces acting upon the wheel [12]. External forces and torques which affect the secondary coordinates are listed in table 2.1. In this thesis, the main focus is on the changes in toe, bump steer, camber and bump camber due to wheel compression and steering as these have the most dominating effect on yaw and steering torque. The other effects such as caster etc are not considered in the study.

Primary Coordinates	**Secondary Coordinates**	**External Forces and Torques**
Wheel compression	Toe angle	Side force
Steering	Camber angle	Longitudinal force
	Spin angle	Aligning torque
	Wheel track	Camber torque
	Wheel base	Spin torque
	Vertical wheel translation	

Table 2.1: Kinematics and Compliance [12]

2.5.1 Bump Steer Model

Bump steer or roll steer is defined as the tendency of the wheel of a car to steer itself as it goes through a suspension stroke [7]. It is generally expressed in terms of change in toe angles for a certain suspension displacement. Suspension kinematics is designed to reduce the effects of bump and roll steer. The model for this effect is obtained from Kinematics and Compliance measurement data of real production vehicle and is expressed as a linear equation as shown in equation 2.33.

$$\Delta\delta = \delta_{toe} + C_{bs}(z_s - z_{us}) \tag{2.33}$$

where, $\Delta\delta$ = Change in toe angle (degrees)
C_{bs} = Bump Steer Gradient (deg/m)
z_s = Sprung mass displacement
z_{us} = Unsprung mass displacement
The initial position of the suspension deflection is zero. Positive displacement is considered as bump and negative displacement is considered as rebound.

2.5.2 Bump Camber Model

Bump camber effect is defined as the change in camber angle as it goes through a suspension stroke [7]. It is generally expressed in terms of change in camber angles for a certain suspension displacement. This camber gain has considerable effects on the lateral forces generated by the tyres. The linear model for this effect is obtained from Kinematics and Compliance measurement data of real production vehicle as shown in equation 2.34.

$$\Delta\gamma = \gamma + C_{bc}(z_s - z_{us}) \tag{2.34}$$

where, $\Delta\gamma$ = Change in camber angle (degrees)
C_{bs} = Bump camber gradient (deg/m)
z_s = Sprung mass displacement
z_{us} = Unsprung mass displacement
The initial position of the suspension deflection is zero. Positive displacement is considered as bump and negative displacement is considered as rebound.

2.6 Roll-Yaw Model

Most studies on active anti-roll bar systems utilize the yaw-roll model with force or torque as the control signal [6]. The active anti-roll bar produces roll moment which influences both vertical and lateral motion of the car. The full car vertical model explains the relation between sprung mass displacement, body roll angle, pitch angle, unsprung mass displacement and road excitations is combined with the extended bicycle model explains the relation between lateral velocity, yaw rate and road excitation by taking steering angle as an input to the model as illustrated in sections 2.3 and 2.4. The suspension kinematics and compliance model acts as the bridge in linking the vertical and lateral model. The bump steer effects is added as additional steer angle and the camber effects is added as an lateral force component. The roll-yaw model uses the same coordinate system as the other two dynamic models. The cross terms of roll-yaw model are small and can be neglected.

$$
\begin{aligned}
\ddot{y} = (C_{\alpha_f} * (\delta_{fl} + ((C_{bsfl} * (x - x1 - (\theta * a) + (\phi * d)))) - (V_y + (a * \dot{\psi}))/(V_x)) + \\
C_{\alpha_f} * (\delta_{fr} + ((C_{bsfr} * (x - x2 - (\theta * a) - (\phi * c)))) - (V_y + (a * \dot{\psi}))/(V_x)) + \\
C_{\alpha_r} * (\delta_{rl} + ((C_{bsrl} * (x - x3 + (\theta * b) + (\phi * d)))) - (V_y - (b * \dot{\psi}))/(V_x)) + \\
C_{\alpha_r} * (\delta_{rr} + ((C_{bsrr} * (x - x4 + (\theta * b) - (\phi * c)))) - (V_y - (b * \dot{\psi}))/(V_x)) + \\
K_{fl_{stiff}} * (\gamma_{sfl} + (C_{bcfl} * (x - x1 - (\theta * a) + (\phi * d)))) + \\
K_{fr_{stiff}} * (\gamma_{sfr} + (C_{bcfr} * (x - x2 - (\theta * a) - (\phi * c)))) + \\
K_{rl_{stiff}} * (\gamma_{srl} + (C_{bcrl} * (x - x3 + (\theta * b) + (\phi * d)))) + \\
K_{rr_{stiff}} * (\gamma_{srr} + (C_{bcrr} * (x - x4 + (\theta * b) - (\phi * c)))))/m - ((V_x) * \dot{\psi})
\end{aligned}
\tag{2.35}
$$

$$
\begin{aligned}
\ddot{\psi} = (C_{\alpha_f} * a * (\delta_{fl} + ((C_{bsfl} * (x - x1 - (\theta * a) + (\phi * d)))) - (V_y + (a * \dot{\psi}))/(V_x)) + \\
C_{\alpha_f} * a * (\delta_{fr} + ((C_{bsfr} * (x - x2 - (\theta * a) - (\phi * c)))) - (V_y + (a * \dot{\psi}))/(V_x)) - \\
C_{\alpha_r} * b * (\delta_{rl} + ((C_{bsrl} * (x - x3 + (\theta * b) + (\phi * d)))) - (V_y - (b * \dot{\psi}))/(V_x)) - \\
C_{\alpha_r} * b * (\delta_{rr} + ((C_{bsrr} * (x - x4 + (\theta * b) - (\phi * c)))) - (V_y - (b * \dot{\psi}))/(V_x)) + \\
K_{fl_{stiff}} * a * (\gamma_{sfl} + (C_{bcfl} * (x - x1 - (\theta * a) + (\phi * d)))) + \\
K_{fr_{stiff}} * a * (\gamma_{sfr} + (C_{bcfr} * (x - x2 - (\theta * a) - (\phi * c)))) - \\
K_{rl_{stiff}} * b * (\gamma_{srl} + (C_{bcrl} * (x - x3))) - \\
K_{rr_{stiff}} * b * (\gamma_{srr} + (C_{bcrr} * (x - x4 + (\theta * b) - (\phi * c)))))/I_{zz}
\end{aligned}
\tag{2.36}
$$

2.7 Reduced Roll-Yaw Model

The full roll-yaw model illustrated in section 2.6 has unsprung mass displacements as degrees of freedom which is helpful in theoretical analysis of the active suspension where as it requires estimation of these states to synthesis the AARB controller. Thus to reduce the complexity of the controller, reduced roll-yaw model is utilized where unsprung mass states are replaced by road disturbances in the linearized system. This is achieved by assumption shown in equations 2.37 and 2.38.

$$x_i = Z_{ri} \tag{2.37}$$

where i= 1,2,3,4

$$
\begin{aligned}
\dot{x_1} = \dot{Z_{r1}} \\
\dot{x_2} = \dot{Z_{r2}} \\
\dot{x_3} = \dot{Z_{r3}} \\
\dot{x_4} = \dot{Z_{r4}}
\end{aligned}
\tag{2.38}
$$

The reduced roll-yaw model is obtained by substituting equations 2.37 and 2.38 in equations 2.6,2.7,2.8,2.35 and 2.36

2.8 State-Space Representation

The model analysis and control design of the active anti-roll bar system is performed by rearranging the equations of the roll-yaw model given in 2.6 and 2.7 in the state-space form. The state-space model for the roll-yaw model with active AARB is represented below.
State dynamics equation:

$$\dot{x(t)} = A_{AARB} * x(t) + B_{AARB} * u_1(t) + E_{AARB} * u_2(t) \tag{2.39}$$

Measurement equation:

$$y(t) = C_{AARB} * x(t) + D_{AARB} * u_1(t) + D_{dARB} * u_2(t) \tag{2.40}$$

The states for the roll-yaw model is represented by the vector

$$x(t) = [x \quad \dot{x} \quad \theta \quad \dot{\theta} \quad \phi \quad \dot{\phi} \quad x1 \quad \dot{x1} \quad x2 \quad \dot{x2} \quad x3 \quad \dot{x3} \quad x4 \quad \dot{x4} \quad \dot{y} \quad \dot{\psi}]^T \tag{2.41}$$

The control input for AARB system is the Combined roll torque acting on the car (front and rear).

$$u_1(t) = T_{AARB} \tag{2.42}$$

The other inputs for the model is shown in the vector

$$u_2(t) = [Z_{r1} \quad Z_{r2} \quad Z_{r3} \quad Z_{r4} \quad \delta_{fl} \quad \delta_{fr} \quad \delta_{rl} \quad \delta_{rr}]^T \tag{2.43}$$

The reduced roll-yaw model is used for controller design illustrated in further in this chapter. The states for the model is represented by the vector

$$x(t) = [x \quad \dot{x} \quad \theta \quad \dot{\theta} \quad \phi \quad \dot{\phi} \quad \dot{y} \quad \dot{\psi}]^T \tag{2.44}$$

The state-space matrices of reduced roll-yaw model are given in equations A.1, A.2, A.3 and A.4. The disturbance matrix for the AARB system is shown in A.2. The disturbance signals in the model include road excitation on front left wheel Z_{r1}, road excitation on front right wheel Z_{r2}, excitation on rear left wheel Z_{r3}, excitation on rear right wheel Z_{r4} and steering angle for all for wheels, δ_{fl}, δ_{fl}, δ_{fl}, δ_{fl}. The outputs of the system are body displacement x, body deflection rate $\dot{x}$, pitch angle θ, pitch rate $\dot{\theta}$, roll angle ϕ, roll rate $\dot{\phi}$, lateral velocity $\dot{y}$, yaw rate $\dot{\psi}$.

2.9 Dynamic Model Analysis

The eigenvalues of the system dynamical matrix A or the poles of the roll-yaw model and reduced roll-yaw model are shown below.

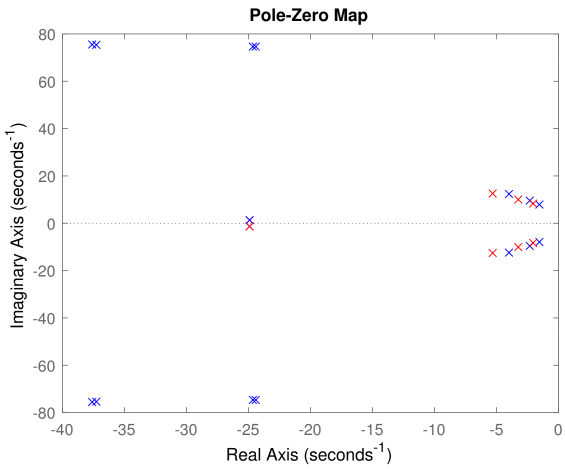

Figure 2.8: Poles of roll-yaw model and reduced order model.

All the poles of the system are in the negative half plane, thus the system is stable [14]. Both the models are not controllable but satisfies the stabilizable condition.

2.10 Model Validation Results

The aim of this section is to verify the dynamic models by comparing them to a validated vehicle model in CarMaker. The state variables of the roll-yaw model and the reduced roll-yaw model is developed in simulink uses the model parameters of an existing vehicle model and are compared with the state variables from the CarMaker model. The road profile used in the test consists of a single sided bump of amplitude 0.05m which triggers a combined motion of heave, roll and pitch. The front right wheel hits the bump first followed by the rear right wheel. The passive CarMaker model used in this test had passive suspension with passive roll bar. The road profile used in the test is shown in 2.9. From the validation results in figure 2.11 and 2.13, it can be seen that the model is not as damped as the CarMaker model as the road displacement is so fast that the linear damper assumption is not valid for relatively high frequency disturbance inputs.

Two sets of kinematic setups will be compared in this thesis. Thus two sets of roll-yaw model are implemented i.e. with kinematic setup-1 and setup-2. The validation results of kinematic setup-2 are shown in figures 2.11 and 2.13. It can be seen that for small amplitudes of road bump, state variables from the suspension match the CarMaker model quite closely. However, the dynamics are very similar when assessing the shapes of the curves. The main difference is in the amplitude of the curves. The roll-yaw model and the reduced roll-yaw model are simplified linear models which only captures state state dynamics of vertical and lateral dynamics compared to the vehicle model in CarMaker which describes the full dynamics of a real car. Thus some differences between the models are inevitable. It can also be seen that the behaviour of the reduced model is similar when compared to that roll-yaw model for smaller amplitudes of bumps. Thus reduced roll-yaw model can be utilized for controller design purposes as it has all of its states measured in the car while the un-sprung states in the full roll-yaw model needs to be estimated while designing the controller.

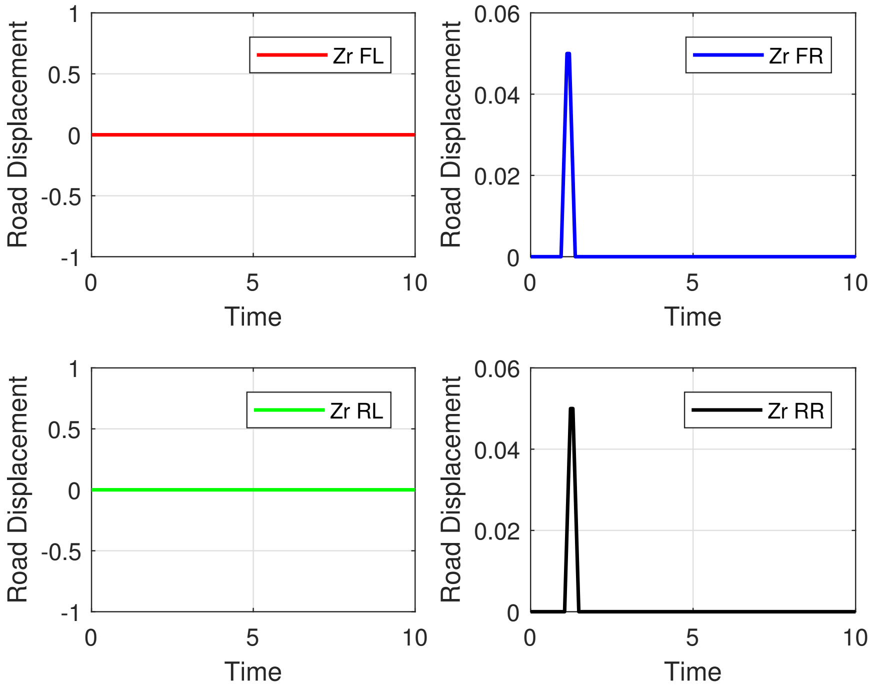

Figure 2.9: Single bump road displacement as disturbance input to the car for Roll-Yaw and reduced Roll-Yaw model validation

2.10.1 Roll-Yaw with kinematic setup-1 model validation

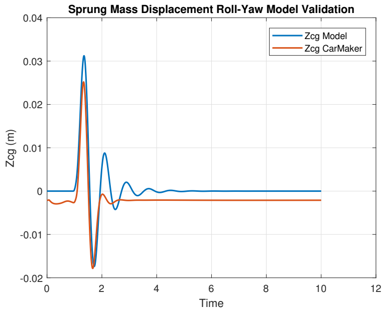

(a) Sprung mass position plot

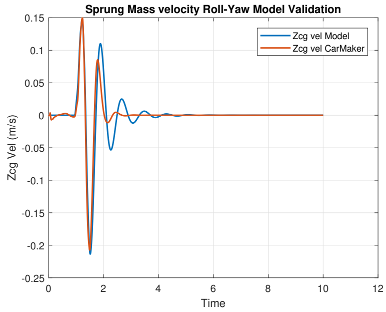

(b) Sprung mass velocity plot

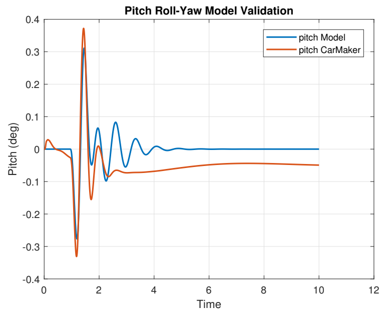

(c) Pitch plot

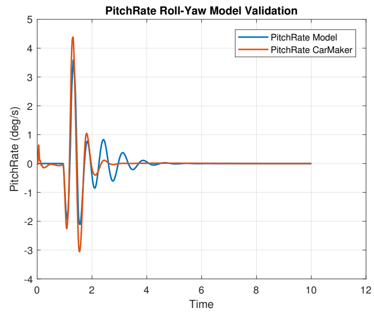

(d) Pitch rate plot

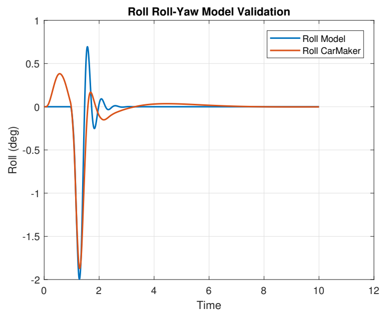

(e) Roll plot

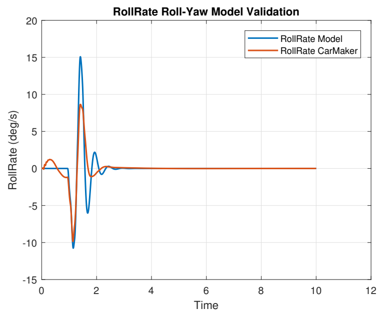

(f) Roll rate plot

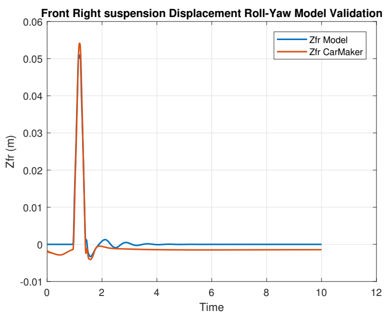

(g) Front right wheel displacement plot

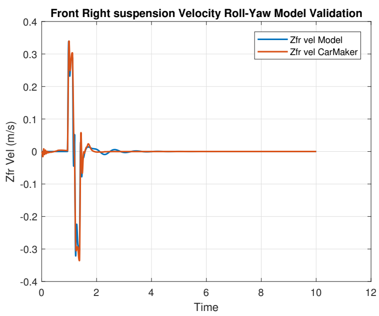

(h) Front right wheel velocity plot

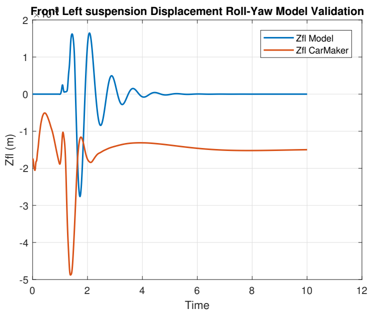

(i) Front left wheel displacement plot

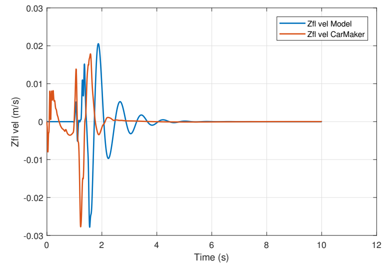

(j) Front left wheel velocity plot

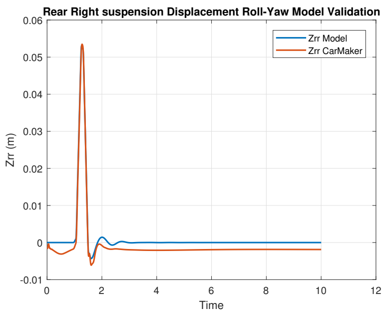

(k) Rear right wheel displacement plot

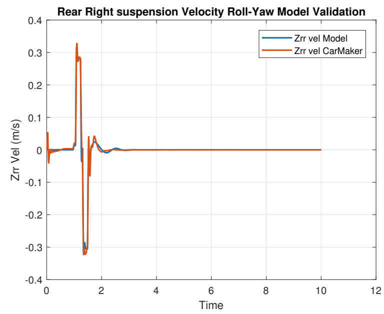

(l) Rear right wheel velocity plot

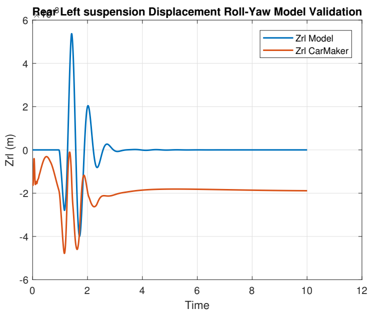

(m) Rear left wheel displacement plot

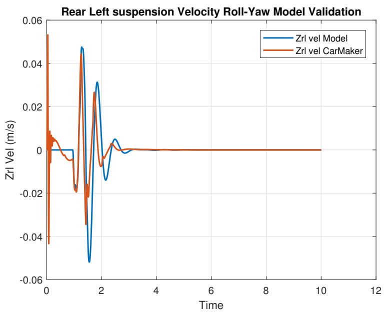

(n) Rear left wheel velocity plot

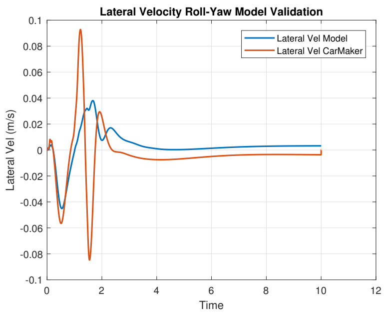

(o) Lateral Velocity plot

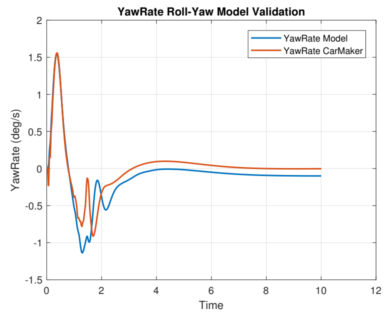

(p) Yaw rate plot

Figure 2.10: Roll-Yaw with kinematic setup-1 Model Validation results

2.10.2 Roll-Yaw with kinematic setup-2 model validation

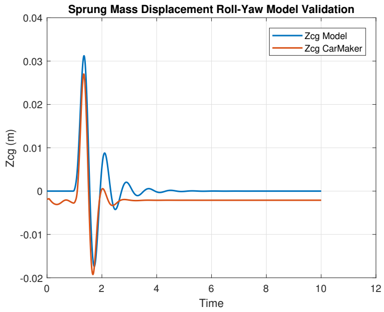

(a) Sprung mass position plot

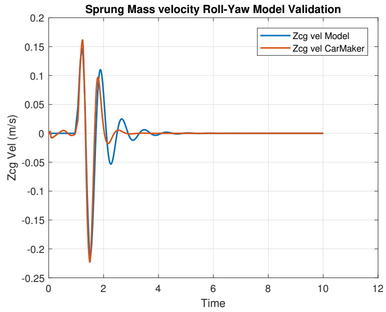

(b) Sprung mass velocity plot

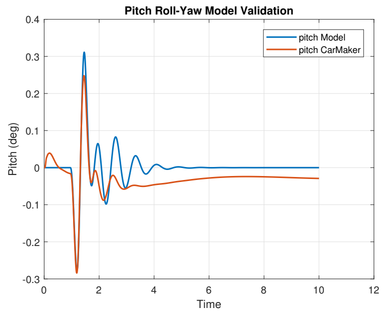

(c) Pitch plot

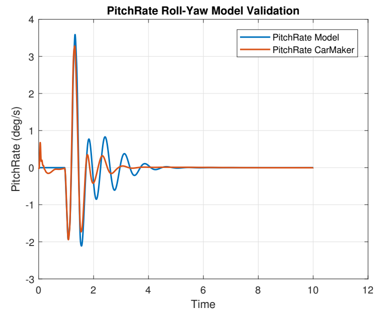

(d) Pitch rate plot

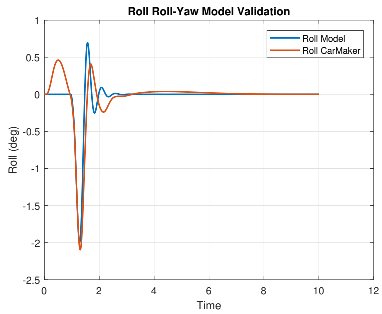

(e) Roll plot

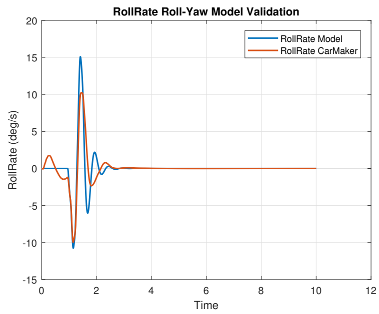

(f) Roll rate plot

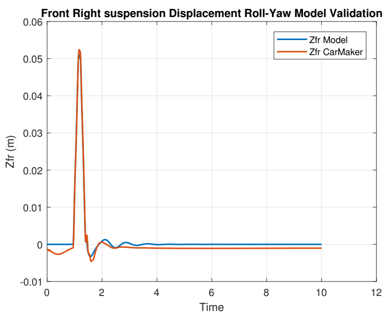

(g) Front right wheel displacement plot

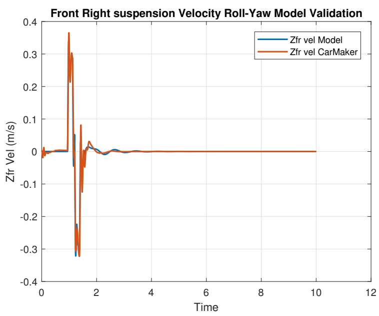

(h) Front right wheel velocity plot

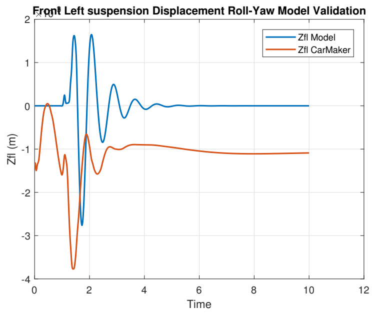

(i) Front left wheel displacement plot

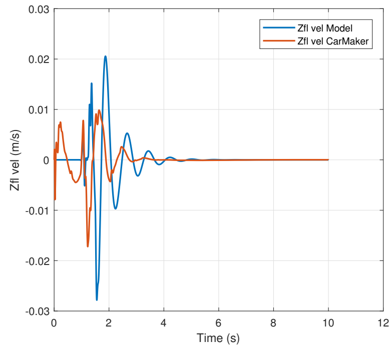

(j) Front left wheel velocity plot

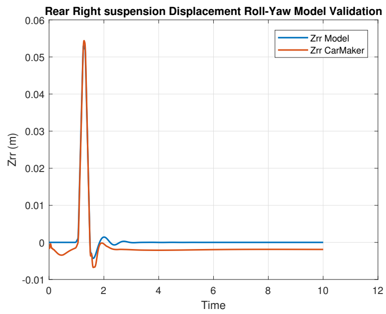

(k) Rear right wheel displacement plot

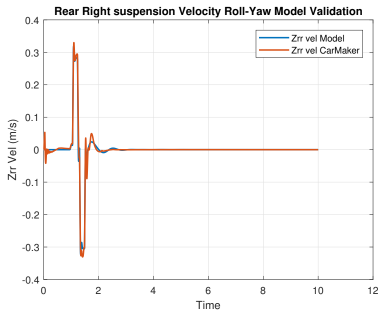

(l) Rear right wheel velocity plot

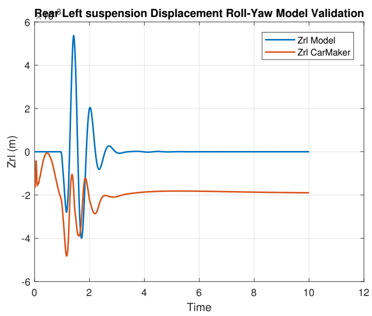

(m) Rear left wheel displacement plot

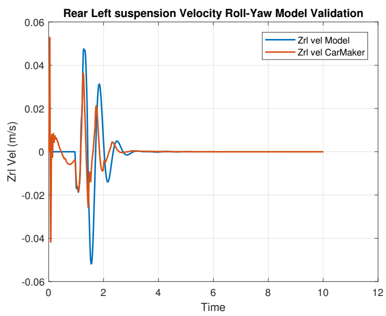

(n) Rear left wheel velocity plot

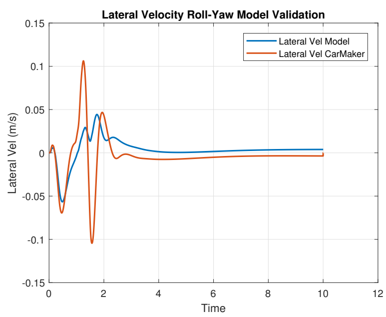

(o) Lateral Velocity plot

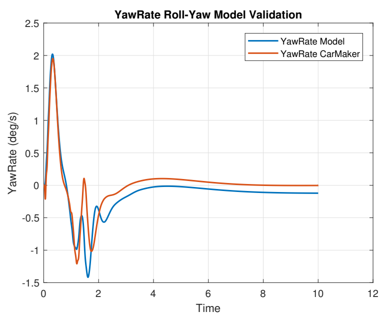

(p) Yaw rate plot

Figure 2.11: Roll-Yaw with kinematic setup-2 Model Validation results

2.10.3 Reduced Roll-Yaw with kinematic setup-1 model validation

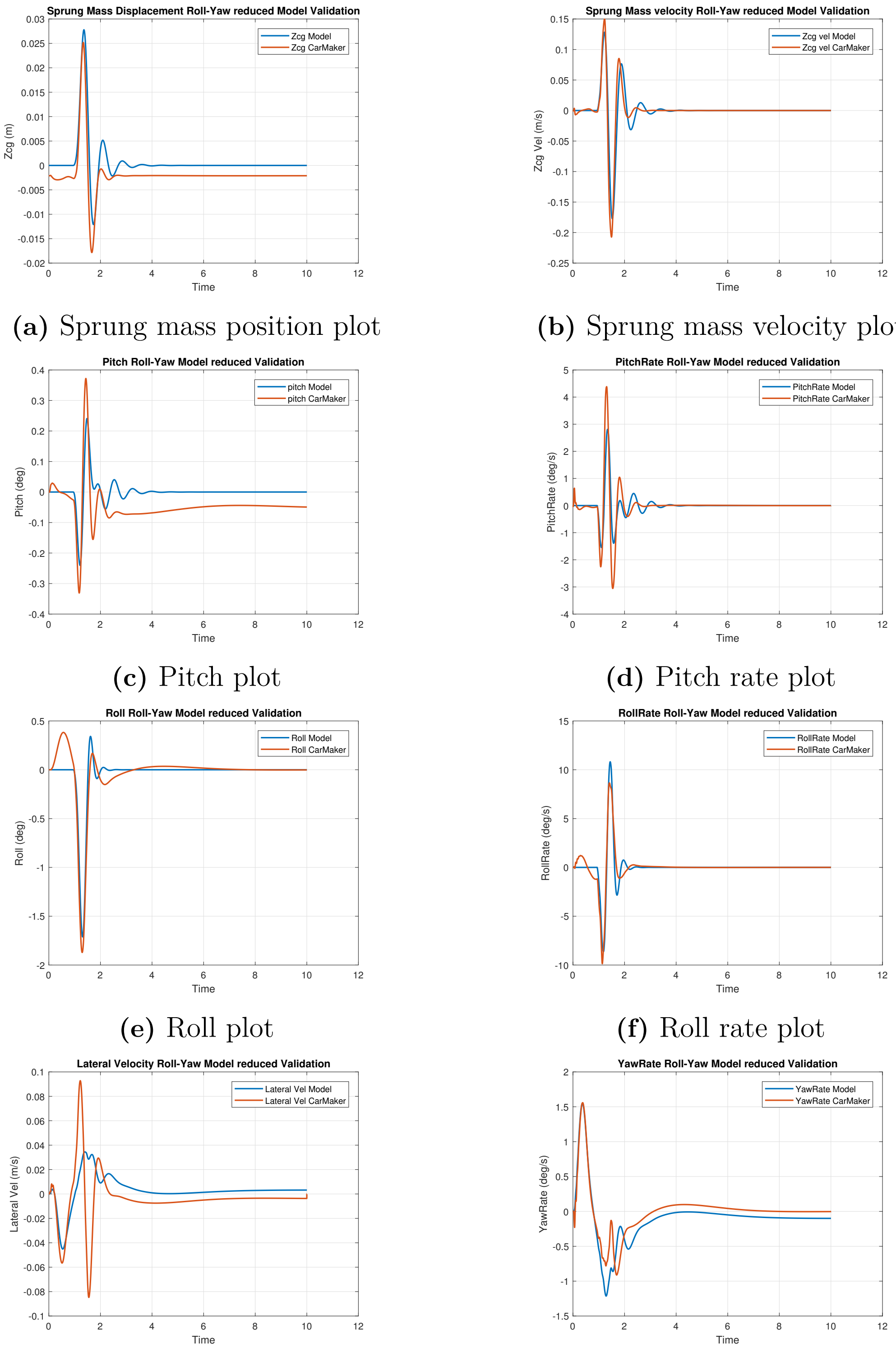

(a) Sprung mass position plot

(b) Sprung mass velocity plot

(c) Pitch plot

(d) Pitch rate plot

(e) Roll plot

(f) Roll rate plot

(g) Lateral Velocity plot

(h) Yaw rate plot

Figure 2.12: Reduced Roll-Yaw with kinematic setup-1 Model Validation results

2.10.4 Reduced Roll-Yaw with kinematic setup-2 model validation

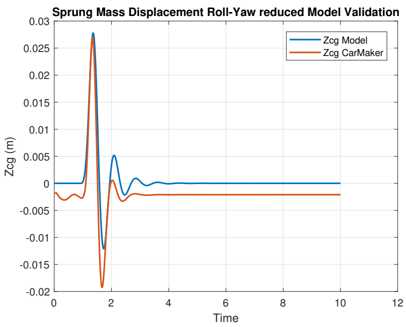

(a) Sprung mass position plot

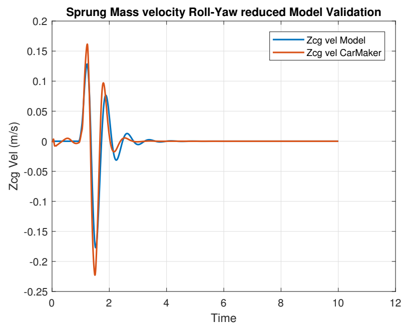

(b) Sprung mass velocity plot

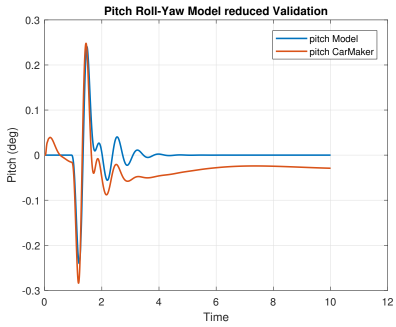

(c) Pitch plot

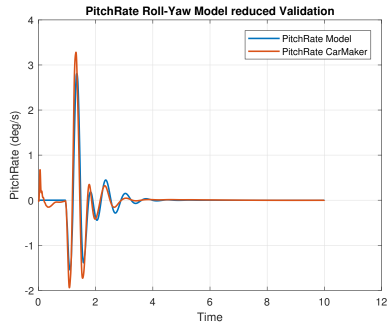

(d) Pitch rate plot

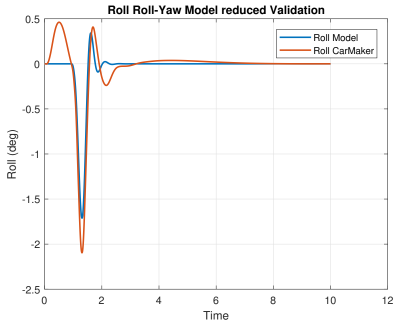

(e) Roll plot

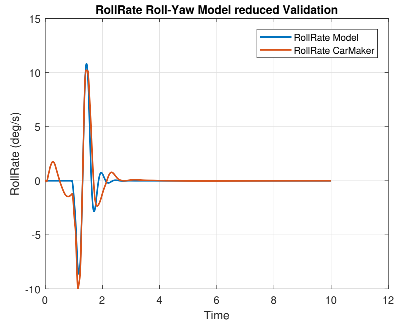

(f) Roll rate plot

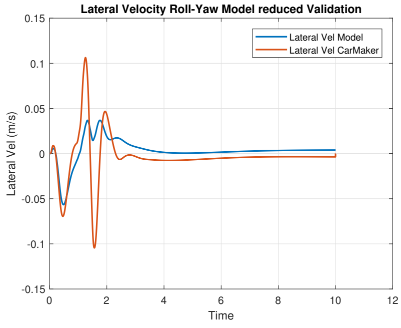

(g) Lateral Velocity plot

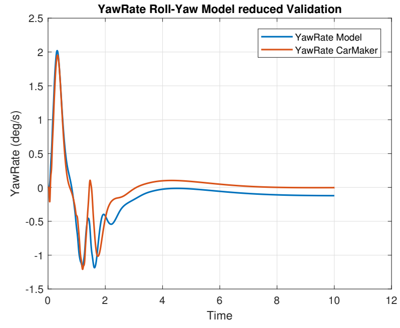

(h) Yaw rate plot

Figure 2.13: Reduced Roll-Yaw with kinematic setup-2 Model Validation results

2.11 Frequency Response of the AARB system

In this section, the frequency response of the AARB system is studied. The frequency response is characterized by the magnitude and phase response of the system, versus frequency. The AARB system has only one input which is the roll torque acting on the whole vehicle. Hence, it is sufficient to verify the effect of chassis roll torque on the yaw rate and roll angle outputs. The frequency response of the reduced roll-yaw models with setup-1 and setup-2 are obtained by plotting the magnitude and phase measurements through a Bode plot.

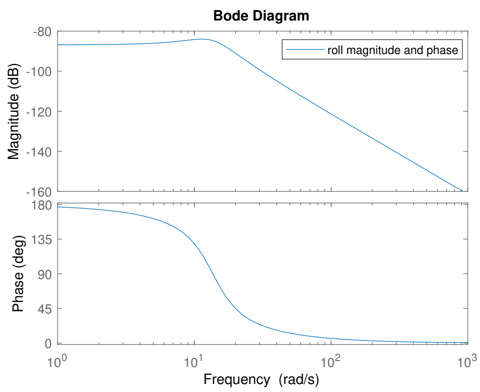

(a) Bode plot for TF($T_{arb} \rightarrow \phi$) with setup-1

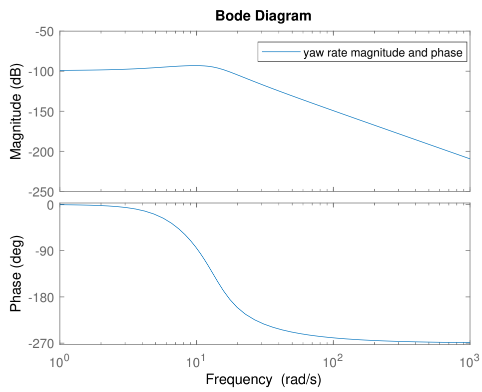

(b) Bode plot for TF($T_{arb} \rightarrow \ddot{\psi}$) with setup-1

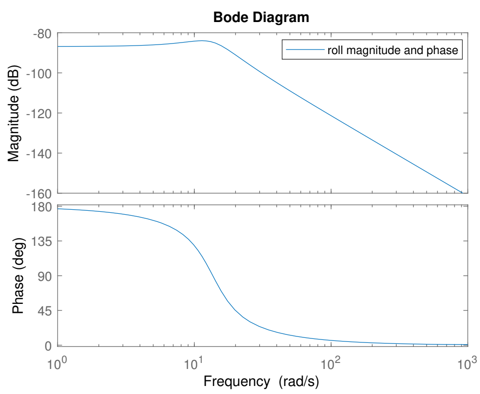

(c) Bode plot for TF($T_{arb} \rightarrow \phi$) with setup-2

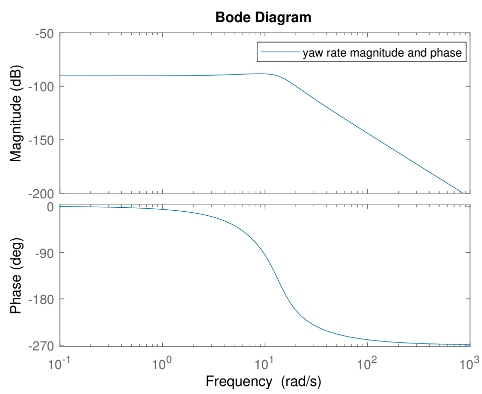

(d) Bode plot for TF($T_{arb} \rightarrow \ddot{\psi}$) with setup-2

From bode plot analysis of the TF($T_{arb} \rightarrow \phi$) and TF($T_{arb} \rightarrow \ddot{\psi}$), it can be noticed that the transfer function gain is really less and is about -85dB for both the kinematic setup. However for TF($T_{arb} \rightarrow \ddot{\psi}$), the magnitude is about -95dB and -100db for setup-1 and setup-2 respectively. From 2.14b and 2.14d, it can seen that the model with kinematic setup-1 is more understeered than that with setup-2.

Further from the bode plots it can be seen that The amount roll torque required to produce unit change in roll angle and yaw rate is very high which is not quite energy efficient. Thus AARB system can be used only to correct small yaw rate/ steering angle changes.

3

Control Theory

In this chapter the theory behind control design is presented. At first, linear state-space representation of the reduced roll-yaw dynamic model is presented and its stability is analyzed. This is followed by the control design methodology of LQR, LQI and $\mathcal{H}_\infty$ robust control techniques which are implemented to control the AARB system.

3.1 Linear Quadratic Regulator

Linear Quadratic Regulator (LQR) is an optimal control method of the class of model based controllers. An optimization problem is solved by utilizing the linearized model. A state feedback controller is designed for the AARB controller as all the states of the reduced roll-yaw model are assumed to be measurable/available.

The control input is given as,

$$u(t) = K_{LQR,AARB}x(t)_{AARB} + K_{r,AARB}r(t)_{AARB} \tag{3.1}$$

$K_{LQR,AARB}$ is the feedback gain which is computed using state-feedback LQR theory. $K_{r,AARB}$ is the reference gain, $x(t)_{AARB}$ are the states of the reduced Roll-Yaw model and $u(t)$ is the control input.

The closed loop form for the AARB controller is then described by:

$$\dot{x}_{AARB} = (A_{AARB} - B_{AARB}K_{LQR,AARB})x(t)_{AARB} + B_{AARB}K_{r,AARB}r(t)_{AARB} \tag{3.2}$$

$$y = (C_{AARB} - D_{AARB}K_{LQR,AARB})x(t)_{AARB} + D_{AARB}K_{r,AARB}r(t)_{AARB} \tag{3.3}$$

Here, $K_{r,AARB}$ is not influencing the stability of the closed loop plant so it's not used for the control design.

The LQR method is used for optimal pole placement by minimizing the cost function:

$$min(J) = \int_0^\infty \frac{1}{2}x^TQx + \frac{1}{2}u^TRu \tag{3.4}$$

The controller is synthesized for the model with fixed vehicle speed. The optimal controller gain $K_{LQR,AARB}$ is computed by using an lqr command in matlab.

The cost function J will be minimized to the obtained control input. Q matrix is used to penalize the state related energy and R penalizes the control input energy in the cost function. By increasing the values of the weights Q and R, the states and control inputs are penalized more. All eigenvalues of the plant designed with LQR control will be stable regardless of the original locations of poles guaranteed by the Riccati equation [13]. The LQR system is tuned for desired optimal performance by tuning the state cost matrix Q and an input cost matrix R. Since the system input is the torque generated by the AARB motors it is reasonable to set the weight in R as high as possible so as to use the vehicle energy cautiously. However, the R weighting needs to be set considerably small as high roll torque is required to produce a small yaw rate as seen from the bode plot shown in figure 2.14a and figure 2.14d. Further, in the Q matrix, the interesting states are the roll and yaw rate, thus it is reasonable that these states will have higher weights than other states. Each setting is tested on the IPG CarMaker model in an simulation environment.

In many scenarios it is desired that the closed loop has integral action to have no steady state error. In this thesis, yaw angle needs to be tracked on low frequency road disturbances. To impart integral action on the loop, the system is re-formulated by creating a number of additional states equal to the number of outputs for which zero steady state error must be ensured. By augmenting the state space system as shown in equations 3.7 and 3.8, integral action will be imparted onto the loop. Integral state for the yaw rate state is added so as to track yaw angle of the vehicle.

$$z(t) = \int (y_{AARB}(t) - r_{AARB}(t))dt \tag{3.5}$$

$$\dot{z(t)} = y(t) - r(t) = Cx(t) + Du(t) - r(t) \tag{3.6}$$

$$\begin{bmatrix} \dot{x(t)} \\ \dot{z(t)} \end{bmatrix} = \begin{bmatrix} A & 0_{n*q} \\ C & 0_q \end{bmatrix} \begin{bmatrix} x(t) \\ z(t) \end{bmatrix} + \begin{bmatrix} B & 0_{n*q} \\ D & -I_q \end{bmatrix} \begin{bmatrix} u(t) \\ r(t) \end{bmatrix} \tag{3.7}$$

$$y(t) = \begin{bmatrix} C & 0_q \end{bmatrix} \begin{bmatrix} x(t) \\ z(t) \end{bmatrix} + Du(t) \tag{3.8}$$

The control law for the LQI controller is given by,

$$u(t) = K_{LQR,AARB}x(t)_{AARB} + K_{r,AARB}r(t)_{AARB} + K_z z(t) \tag{3.9}$$

The optimal controller gain $K_{LQI,AARB}$ is computed by using an lqi command in matlab.

3.2 Robust $\mathcal{H}_\infty$ Control

A MIMO system is said to be robust if it possess good stability margin, low sensitivity to plant and controller variations, and good disturbance rejection to high frequency disturbance inputs [17]. The above robustness properties can be modified by altering the feedback loop and the gains associated with it. This section will illustrate the concepts of feedback manipulation to achieve a robust design using $\mathcal{H}_\infty$ control technique.

The nominal plant G consists of matrix of transfer function with roll torque as input and states as the output. The disturbance model G_d is defined by the transfer functions with road disturbance, steering angle as input and states as the output. The matrices G and G_d are given in A.1 and A.2. The interconnected system stability is check by the small gain theorem,

$$||G||_\infty * ||G_d||_\infty < 1 \tag{3.10}$$

The $\mathcal{H}_\infty$ norm of the G and G_d are given below. It can be seen that the product of them is < 1.

$$||G||_{H_\infty} = 7.9926e - 04$$
$$||G_d||_{H_\infty} = 29.1711$$

Generalized Δ-P-K structure is derived for the active roll bar system as shown in 3.1

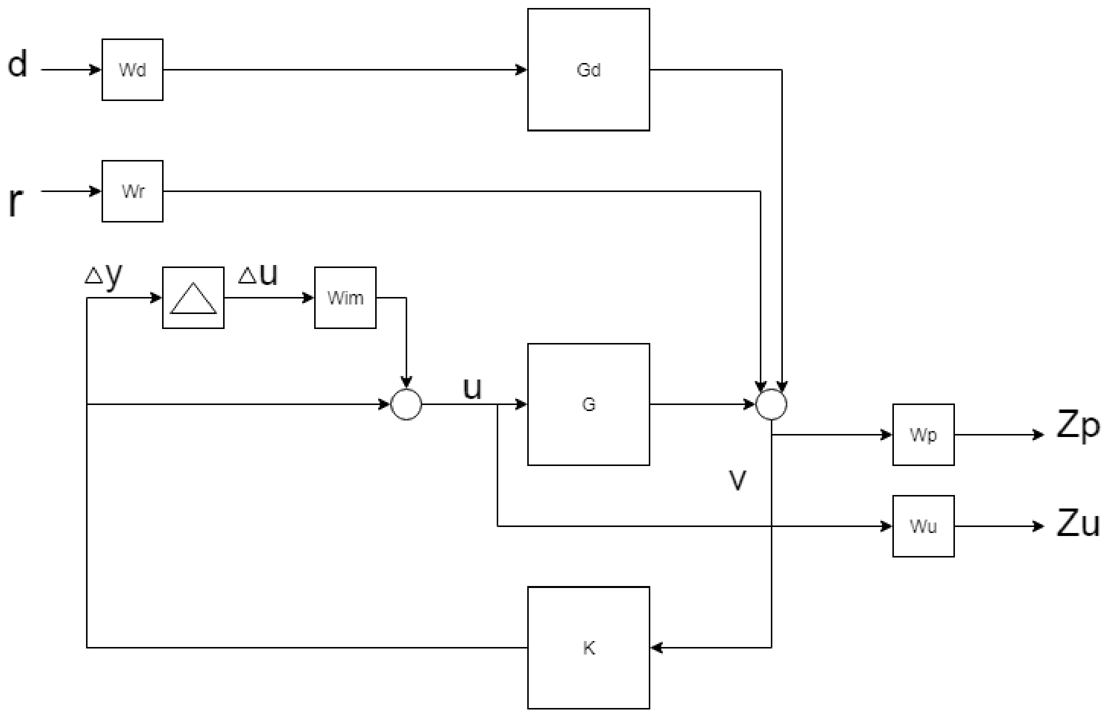

Figure 3.1:
$\mathcal{H}_\infty$ Controller structure for AARB system.

$$\begin{bmatrix} y\Delta \\ z_u \\ z_p \\ v \end{bmatrix} = \begin{bmatrix} 0 & 0_{1x8} & 0_{1x8} & 1 \\ W_u W_{im} & 0_{1x8} & 0_{1x8} & W_u \\ -W_p G_{min} W_{im} & W_p W_r & -W_p G_{dmin} W_d & -W_p G_{min} \\ -G_{min} W_{im} & W_r & -G_{dmin} W_d & -G_{min} \end{bmatrix} * \begin{bmatrix} u\Delta \\ r \\ d \\ u \end{bmatrix} \tag{3.11}$$

The augmented plant P is given by,

$$P = \begin{bmatrix} 0 & 0_{1x8} & 0_{1x8} & 1 \\ W_u W_{im} & 0_{1x8} & 0_{1x8} & W_u \\ -W_p G_{min} W_{im} & W_p W_r & -W_p G_{dmin} W_d & -W_p G_{min} \\ -G_{min} W_{im} & W_r & -G_{dmin} W_d & -G_{min} \end{bmatrix}$$

where,

$$P_{11} = \begin{bmatrix} 0 & 0_{1x8} & 0_{1x8} \\ W_u W_{im} & 0_{1x8} & 0_{1x8} \\ -W_p G_{min} W_{im} & W_p W_r & -W_p G_{dmin} W_d \end{bmatrix}$$
$$P_{12} = \begin{bmatrix} 1 \\ W_u \\ -W_p G_{min} \end{bmatrix}$$
$$P_{21} = \begin{bmatrix} -G_{min} W_{im} & W_r & -G_{dmin} W_d \end{bmatrix}$$

$$P_{22} = -G_{min}$$

The P-K structure loop is closed using a technique called (Lower) Linear Fractional Transformation, LFT, which is shown in equations below -

$$z = F_l(P, K)w = Nw$$
$$z = (P_{11} + P_{12}K(I - P_{22}K)^{-1}P_{21})w$$

where z = $\begin{bmatrix} z_p & z_u & v \end{bmatrix}^T$, w = $\begin{bmatrix} r & d & u \end{bmatrix}^T$

Formulation of the robust control problem is done in an uncertain model environment. Uncertainty/perturbations can be external disturbances at the output/input or unmodeled dynamics of the plant. It can also be parameter variations which would change the stability of the plant. Under uncertainty, the closed-loop gets the following form,

$$\begin{bmatrix} y\Delta \\ z \end{bmatrix} = \begin{bmatrix} N_{11} & N_{12} \\ N_{21} & N_{22} \end{bmatrix} * \begin{bmatrix} u\Delta \\ w \end{bmatrix} \tag{3.12}$$

where, $u\Delta = \Delta y\Delta$ and

$$F_u(N, \Delta) = N_{22} + N_{21}\Delta(I - N_{11}\Delta)^{-1}N_{12} \tag{3.13}$$

For the AARB controller,

$$N(P, K) = \begin{bmatrix} -T_i W_{iM} & KS_o W_r & -KS_o G_{dmin} W_d \\ W_u S_i W_{im} & W_u KS_o W_r & -W_u KS_o G_{dmin} W_d \\ -W_p G_{min} S_i W_{im} & W_p S_o W_r & -W_p S_o G_{dmin} W_d \end{bmatrix}$$

$$
\begin{aligned}
N_{11} &= -T_i W_{iM} \\
N_{12} &= \begin{bmatrix} KS_oW_r & -KS_oG_{dmin}W_d \\ W_uKS_oW_r & -W_uKS_oG_{dmin}W_d \end{bmatrix} \\
N_{21} &= \begin{bmatrix} W_uS_iW_{im} \\ -W_pG_{min}S_iW_{im} \end{bmatrix} \\
N_{22} &= \begin{bmatrix} W_uKS_oW_r & -W_uKS_oG_{dmin}W_d \\ W_pS_oW_r & -W_pS_oG_{dmin}W_d \end{bmatrix}
\end{aligned}
$$

The Control input is considered to be 30% uncertain as actuator dynamics is not modeled. The uncertain plant model is shown in the figure 3.2. The uncertainty layout used is input multiplicative unstructured uncertainty as shown in the plot 3.12. Thus the augmented plant model is an uncertain state-space model.

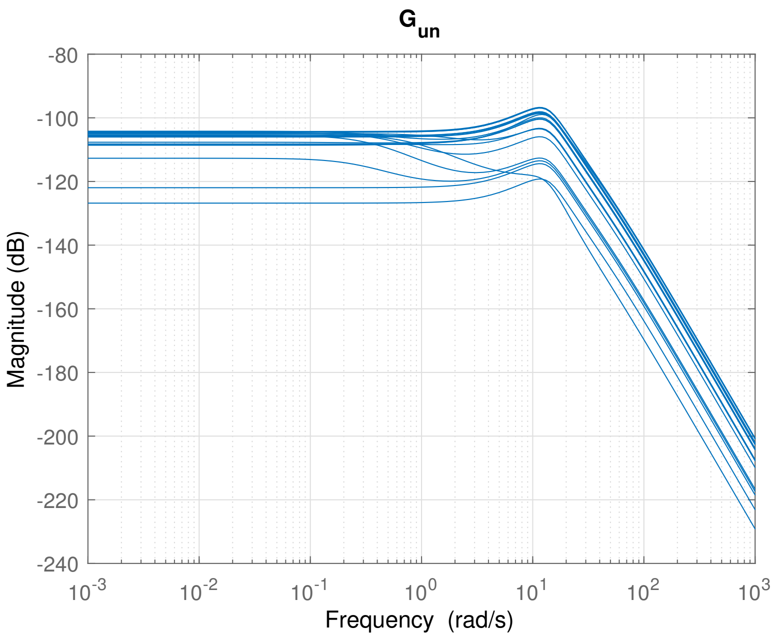

Figure 3.2: Uncertain plant model with 30% uncertainty in the control input

Weights are additional information provided for the control design. In order to formulate the standard structure for the $\mathcal{H}_\infty$ controller defined for the AARB controller, the frequency weighting functions W_p, W_u, W_d and W_r are defined to characterize the performance objectives and perform loop shaping. The performance weighting of the yaw rate is integral weighed to reduce yaw angle error and low pass filter is developed for actuator rate limitation as weighting for the control input.The bode plot for the transfer function is shown in the plot 3.3a. Also, LPF are used as weightings for disturbance and reference signals. The bode plot for the filter used for disturbance signal is given in figure 3.3b

The control law is given by,

$$u(t) = -K_{H_\infty,AARB}x(t) \tag{3.14}$$

such that $||F_l(P,K)||_\infty < \gamma$ i.e. the induced 2 norm from w to z, given x measurement is smaller than a given γ.

The cost function for the $\mathcal{H}_\infty$ control problem is min-max function and is given by,

$$min_u max_w J(u,w) = \int_0^\infty \frac{1}{2}x^T Q x + \frac{1}{2}u^T Q_u u - \gamma^2 w^T w \tag{3.15}$$

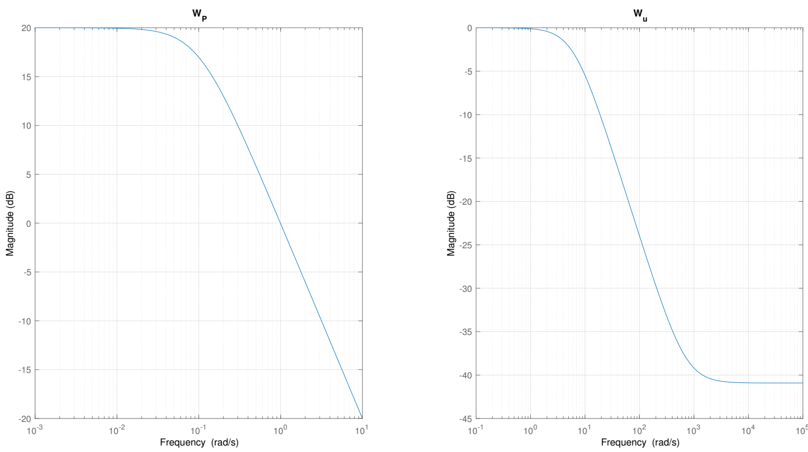

(a) bode plot for performance filters for yaw rate and control input

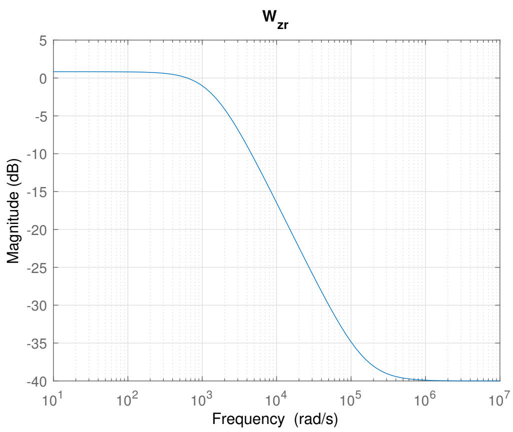

(b) bode plot for disturbance filter Z_r

γ is a parameter which acts as an upper-bound to the ∞ norm of the transfer function from w to z, which guarantees nominal performance. This kind of control problem is called a min-max problem where a saddle point exists in the solution between best case control input and worst case disturbance rejection. The state feedback $\mathcal{H}_\infty$ controller with disturbance rejection level γ can be obtained on a pre-tuned performance objective. Performance and stability of the controller is evaluated using small gain theorem to define Nominal Stability (NS), Nominal Performance (NP), Robust Stability (RS) and Robust Performance (RP). The conditions for these are given below.

- NS: Eigenvalues of N have to be negative.
- NP: NS plus $||N_{22}||_\infty < 1$ guarantees that the performance specifications are met.

- RS: NS plus $||N_{11}||_\infty < 1$, the SGT is met.
- RP: RS plus $||N||_\infty < 1$ shows stability of the closed loop.

The H_∞ controller synthesis is done using the hinfsys command in matlab.

3.3 Controller Tuning

This section illustrates the AARB controller tuning for LQR, LQI and $\mathcal{H}_\infty$ controllers for different kinematic setups. The results shown in the chapter 5 compares different control methods for two contrasting kinematic setups. Further, the controller needs to be tuned separately for driver-in-loop and driver-out-loop cases. Chapter 5 describes why different controller tuning is required for the above mentioned cases. Here, the controller performance tuning functions and matrices are presented.

3.3.1 Controller tuning for Driver-in-loop (Roll weighting) and kinematic setup-1

- LQR: Q = diag$\Big([1 \quad 1 \quad 1 \quad 1 \quad 50000000 \quad 1 \quad 1 \quad 1]\Big)$, R = 0.001
- LQI: Q = diag$\Big([1 \quad 1 \quad 1 \quad 1 \quad 50000000 \quad 1 \quad 1 \quad 1]\Big)$, R = 0.001
- $\mathcal{H}_\infty$: W_p = diag$\Big([1 \quad 1 \quad 1 \quad 1 \quad 1000000(1/(s+0.01)) \quad 1 \quad 1 \quad 1]\Big)$

3.3.2 Controller tuning for Driver-in-loop (Yaw rate weighting) and kinematic setup-1

- LQR: Q = diag$\Big([1 \quad 1 \quad 1 \quad 1 \quad 1 \quad 1 \quad 1 \quad 5000000]\Big)$, R = 0.001
- LQI: Q = diag$\Big([1 \quad 1 \quad 1 \quad 1 \quad 1 \quad 1 \quad 1 \quad 20000000 \quad 20000]\Big)$, R = 0.001
- $\mathcal{H}_\infty$: W_p = diag$\Big([1 \quad 1 \quad 1 \quad 1 \quad 1 \quad 1 \quad 1 \quad 1000000(1/(s+0.01))]\Big)$

3.3.3 Controller tuning for Driver-in-loop (Roll weighting) and kinematic setup-2

- LQR: Q = diag$\Big([1 \quad 1 \quad 1 \quad 1 \quad 50000000 \quad 1 \quad 1 \quad 1]\Big)$, R = 0.001
- LQI: Q = diag$\Big([1 \quad 1 \quad 1 \quad 1 \quad 50000000 \quad 1 \quad 1 \quad 1]\Big)$, R = 0.001
- $\mathcal{H}_\infty$: W_p = diag$\Big([1 \quad 1 \quad 1 \quad 1 \quad 1000000(1/(s+0.01)) \quad 1 \quad 1 \quad 1]\Big)$

3.3.4 Controller tuning for Driver-in-loop (Yaw rate weighting) and kinematic setup-2

- LQR: Q = diag$\left([1 \quad 1 \quad 1 \quad 1 \quad 1 \quad 1 \quad 1 \quad 5000000]\right)$, R = 0.001
- LQI: Q = diag$\left([1 \quad 1 \quad 1 \quad 1 \quad 1 \quad 1 \quad 1 \quad 20000000 \quad 20000]\right)$, R = 0.001
- $\mathcal{H}_\infty : W_p = \text{diag}\left([1 \quad 1 \quad 1 \quad 1 \quad 1 \quad 1 \quad 1 \quad 1000000(1/(s+0.01))]\right)$

3.3.5 Controller tuning for Driver-out-loop and kinematic setup-1

- LQR: Q = diag$\left([1 \quad 1 \quad 1 \quad 1 \quad 1 \quad 1 \quad 1 \quad 5000000]\right)$, R = 0.001
- LQI: Q = diag$\left([1 \quad 1 \quad 1 \quad 1 \quad 1 \quad 1 \quad 1 \quad 50000 \quad 5000000]\right)$, R = 0.001
- $\mathcal{H}_\infty : W_p = \text{diag}\left([1 \quad 1 \quad 1 \quad 1 \quad 1 \quad 1 \quad 1 \quad 100000(1/(s+0.001))]\right)$

3.3.6 Controller tuning for Driver-out-loop and kinematic setup-2

- LQR: Q = diag$\left([1 \quad 1 \quad 1 \quad 1 \quad 1 \quad 1 \quad 1 \quad 20000000]\right)$, R = 0.001
- LQI: Q = diag$\left([1 \quad 1 \quad 1 \quad 1 \quad 1 \quad 1 \quad 1 \quad 50000 \quad 50000]\right)$, R = 0.001
- $\mathcal{H}_\infty : W_p = \text{diag}\left([1 \quad 1 \quad 1 \quad 1 \quad 1 \quad 1 \quad 1 \quad 10000(1/(s+0.1))]\right)$

The makeweight function in matlab is used to design frequency based filters.

4

Suspension Kinematics

This chapter illustrates the characteristic behaviour of two suspension kinematics and compliance setups which are used to evaluate the performance of the AARB controller. This chapter also involves analysis of individual and combined effects of kinematic parameters on steering wheel torque and yaw rate under the influence of active roll torque provided by the AARB system. The Kinematic parameters are quantified using linear 3-DOF kinematics model in IPG Carmaker to lay down a marker for suspension design. The chapter starts with the description of the sign conventions and coordinate systems used in the IPG CarMaker followed by the description of the 3-DOF linear kinematic model. Further, the qualitative analysis is done for the two pre-defined non linear suspension kinematics are illustrated and individual and combined effects of suspension kinematic parameters are quantified. Finally, a marker is laid on to how the suspension kinematics needs to be setup for the AARB controller to work effectively.

4.1 IPG Carmaker: Sign conventions

The sign conventions and co-ordinate systems used in representing the suspension kinematics parameters in IPG Carmker are described below.

- **Toe Angles**: The anti-clockwise rotation of wheel when viewed from top view is considered to be positive rotation. Thus positive toe angles are represented as $+r_z$ on the right wheel and -r_z on the left wheel as shown in 4.1.

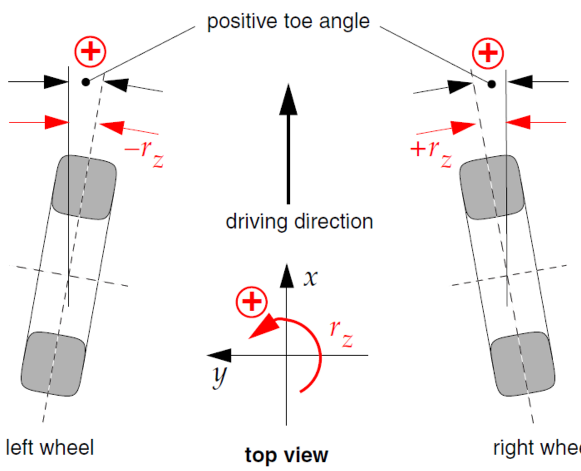

Figure 4.1: Sign convention for toe angles in CarMaker [12]

- **Camber Angles**: The clockwise rotation of wheel when viewed from rear view is considered to be positive rotation. Thus negative camber angles are represented as -r_x on the right wheel and $+r_x$ on the left wheel as shown in 4.2.

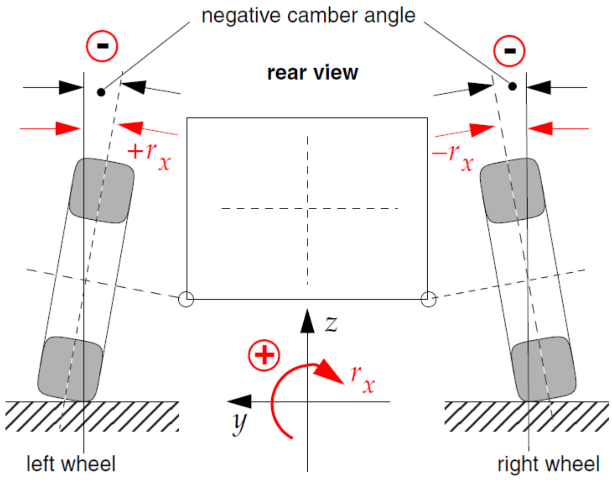

Figure 4.2: Sign convention for camber angles in CarMaker [12]

- **Wheel Compression**: The upward motion of the wheel when viewed from rear view is defined as positive compression q_0 and t_z when measured from the centre of the wheel as shown in 4.3.

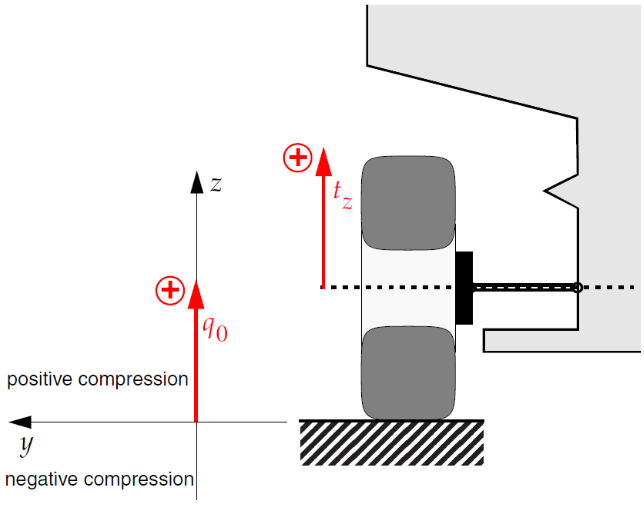

Figure 4.3: Sign convention for wheel compression in CarMaker [12]

The suspension parameters are narrowed down to static toe, static camber, bump steer and bump camber in kinematic analysis carried out in this chapter. Also, this thesis only deals with front kinematic analysis as front axle steering is considered in this thesis. Hence, rear suspension kinematics is not considered for kinematic analysis.

4.2 Kinematic and Compliance: Linear Model

In order to study and analyze the effects of the above mentioned kinematic parameters, a linear model is derived using IPG Carmaker. A linear 3-DOF model utilize linear equations to describe the kinematic movements for translations and rotations of the wheel. Linear 3-DOF model uses 3-generalized coordinates. The model linear 3 DOF can be given by an equation [12].

$$k(q0, q1, q2) = c_{off} + c0 * q0 + c1 * q1 + c2 * q2 \tag{4.1}$$

k(q0,q1,q2) = one of the three translations(t_x, t_y, t_z) or 3 cardan rotation angles(r_x, r_y, r_z) with a rotation sequence Z-X-Y.
c_{off} = offsets for q0,q1,q2.
c0 = gradient depending on compression q0.
c1 = gradient depending on compression q1 of opposite wheel.
c2 = gradient depending on steering coordinate q2.

The linear model derived above is used for quantification of kinematic parameters described in further section.

4.3 Suspension Kinematics Analysis

In this thesis, two suspension kinematic setups are used and the performance of the AARB controller with both the setups will be compared in chapter 5. The kinematic setup-1 and setup-2 are qualitatively analyzed and the results are shown in the figure 4.4. Kinematic setup-1 and setup-2 are evaluated for a sinusoidal 20 degree steering angle maneuver with period of 20 seconds. The two kinematic setups are also evaluated on handsoff mode along straight line. In both maneuvers, the vehicle is subjected to constant 2000 Nm roll torque which is further divided into front and rear roll torque. The main difference between the two setups are analyzed.

From the plot 4.4, it can be seen that for kinematic setup-1, reduction in steering wheel torque is seen when the active roll torque is produced in the direction opposite to the direction of conventional body roll during cornering. The figures 4.4a and 4.4b shows that for a +ve yaw rate, constant +2000Nm roll torque decreases the steering wheel torque. Similarly for -ve yaw rate, constant -2000Nm torque decreases the driving effort for setup-1 while its quite opposite in the case of setup-2. Similar behaviour is seen by comparing their lateral acceleration plots in figures 4.4c and 4.4d when subjected to constant roll torque.

In the handsoff mode, the results shown in 4.4e and 4.4f shows that the steering angle moves in the direction of roll torque in setup-1 while the behaviour of setup-2 is quite exactly the opposite. In the figures 4.4e and 4.4f, it can be seen that +ve roll torque produces +ve steering wheel angle while -ve roll torque produces -ve steering wheel angle for setup-1. The exact opposite trend is seen for kinematic setup-2.

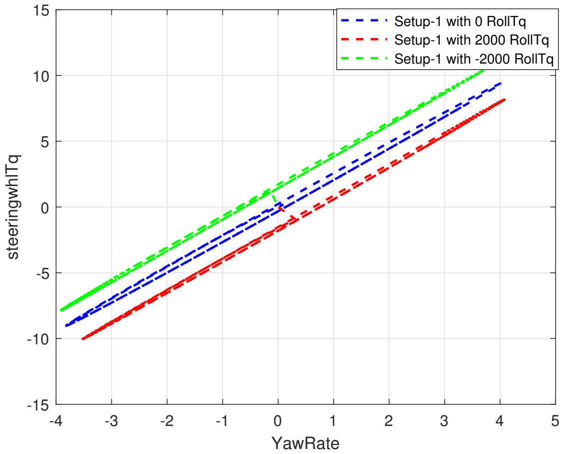

(a) Steering Wheel Torque vs Yaw rate plot for driver-in-loop with setup-1

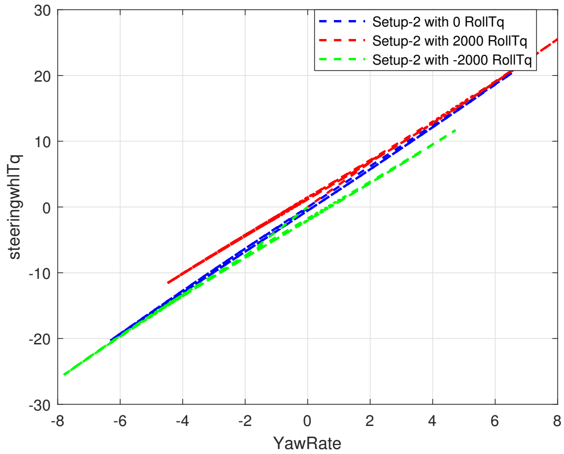

(b) Steering Wheel Torque vs Yaw rate plot for driver-in-loop with setup-2

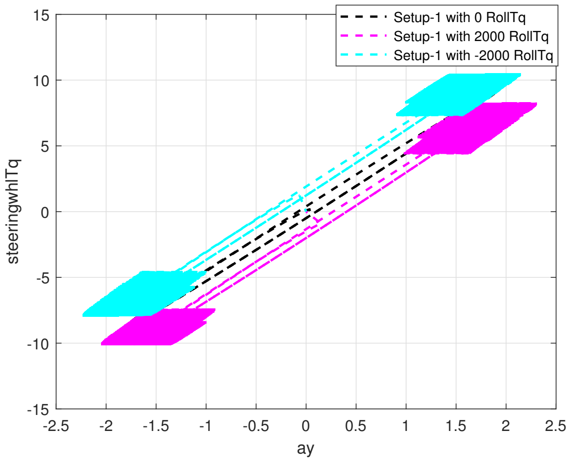

(c) Steering Wheel Torque vs Lateral acceleration plot for driver-in-loop with setup-1

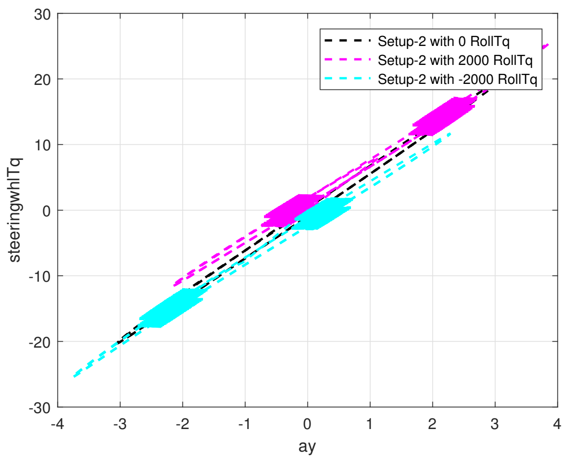

(d) Steering Wheel Torque vs Lateral acceleration plot for driver-in-loop with setup-2

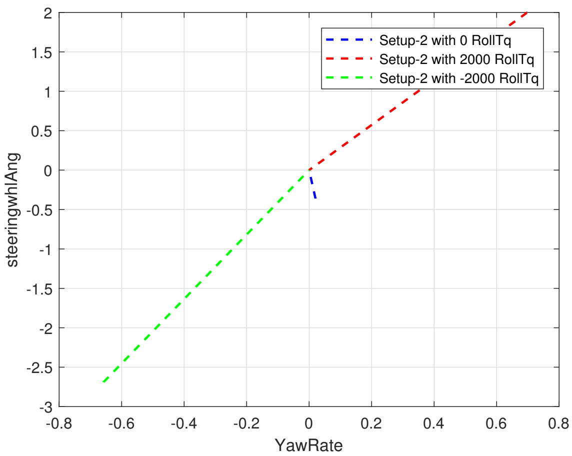

(e) Steering wheel angle vs Yaw rate plot for driver-out-loop with setup-1

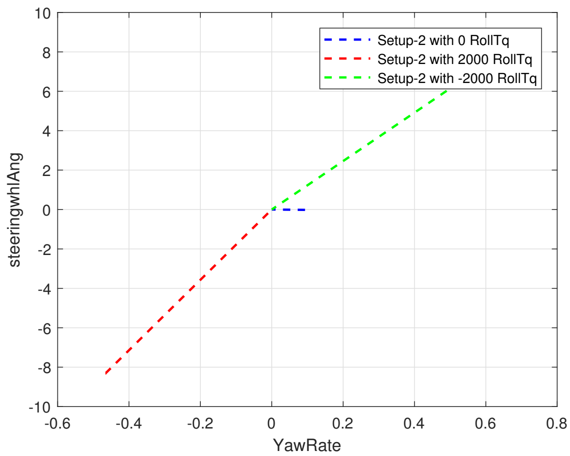

(f) Steering wheel angle vs Yaw rate plot for driver-out-loop with setup-2

Figure 4.4: Qualitative analysis of the two kinematic setups at a constant vehicle speed of 100 km/hr

4.4 Influence of KC parameters on steering torque and yaw rate

The main aim of the thesis is to reduce the steering wheel torque with the anti-roll bar controller which induces body roll, it is important to identify the effects of individual kinematic parameter on the steering wheel torque and its behaviour on application of roll torque.

The manuever used for quatification is that the steering wheel angle is set to 0 degrees and step roll torque of $\pm$ 2000 Nm is applied to the car at 100km/hr. The steering wheel torque and yaw rate are recorded for two different kinematic setup where the parameters varies by 30% in magnitude. The 3-DOF linear kinematic model in CarMaker is is used in this simulation and the results are recorded in the tables 4.1 and 4.2.

SteerTq	**BS 0.1**	**BS 0.13**	**BC 0.1**	**BC 0.13**	δ_{Toe} **0.01**	δ_{Toe} **0.013**	γ **0.01**	γ **0.013**
BS 0.1	13.2024	0	13.8706	14.0716	10.4793	9.6130	13.0081	12.9509
BS 0.13	0	17.0315	17.7127	17.9115	13.7386	12.6751	16.8077	16.7386
BC 0.1	13.8706	17.7127	0.5091	0	-0.1045	-0.2774	0.4805	0.4743
BC 0.13	14.0716	17.9115	0	0.7046	0.0555	-0.1292	0.6721	0.6646
δ_{Toe} **0.01**	10.4793	13.7386	-0.1045	0.0555	-0.6333	0	-0.5317	-0.4988
δ_{Toe} **0.013**	9.6130	12.6751	-0.2774	-0.1292	0	-0.7669	-0.6259	-0.5815
γ **0.01**	13.0081	16.8077	0.4805	0.6721	-0.5317	-0.6259	-0.1549	0
γ **0.013**	12.9509	16.7386	0.4743	0.6646	-0.4988	-0.5815	0	-0.1569

Table 4.1: Effects of BS (rad/m), BC (rad/m), toe (rad) and camber (rad) on steering wheel torque (Nm) under influence of a roll torque

YawRate	**BS 0.1**	**BS 0.13**	**BC 0.1**	**BC 0.13**	δ_{Toe} **0.01**	δ_{Toe} **0.013**	γ **0.01**	γ **0.013**
BS 0.1	2.2839	0	2.3700	2.3959	2.0475	1.9814	2.2635	2.2575
BS 0.13	0	2.8830	2.9678	2.9940	2.5899	2.5027	2.8593	2.8516
BC 0.1	2.3700	2.9678	0.2585	0	0.2318	0.2394	0.2565	0.2561
BC 0.13	2.3959	2.9940	0	0.2851	0.2538	0.2593	0.2827	0.2822
δ_{Toe} **0.01**	2.0475	2.5899	0.2318	0.2538	0.1592	0	0.1670	0.1696
δ_{Toe} **0.013**	1.9814	2.5027	0.2394	0.2593	0	0.1735	0.1839	0.1873
γ **0.01**	2.2635	2.8593	0.2565	0.2827	0.1670	0.1839	0.1696	0
γ **0.013**	2.2575	2.8516	0.2561	0.2822	0.1696	0.1873	0	0.1697

Table 4.2: Effects of BS (rad/m), BC (rad/m), toe (rad) and camber (rad) on yaw rate (deg/s) under influence of a roll torque

The diagonal elements of the tables are the effects of individual parameters. It can be noticed that the bump steer has the largest effect on both steering wheel torque and yaw rate as these parameters increases the most when bump steer is increased by 30%. In the tables 4.1 and 4.2, cross correlation terms shows the combined effects of kinematic parameters on steering wheel torque and yaw rate.

5

Simulation Results

This chapter illustrates the performance of the AARB controller in a simulation environment using simulink and IPG CarMaker. The controller design is implemented in simulink and the controller testing is done using a validated vehicle model provided by the IPG CarMaker.

This chapter mainly presents the difference in the controller performance while using two contrasting sets of kinematic setups presented in chapter 4 and the results are presented for driver-in-loop and driver-out-loop modes. In order to evaluate the performance of the AARB controller, overall three different test scenarios are created where section 5.1 and 5.2 aims to test for high and low frequency road disturbances such as road bumps and banked roads respectively. The third test in section 5.3 aims to test the controller for small steering angle changes.

In the driver-out-loop test case, to test the performance of the AARB controller, the driver hands-off scenario is created by using 0Nm steering torque as the input where as in the driver-in-loop, IPG driver produces steering angle inputs for the controller and the car.

5.1 Test Scenario-1 - Road Bumps

In this scenario, the car is subjected to high frequency disturbances on either side of the car in the form of a road bump at two different time instances on a straight track. The scenario is setup in a way that at one time instant wheels on one side of the car is subjected to a road bump while the road profile on the left hand side is a flat surface. The resulting vehicle body motion is a combined roll and pitch motion with an additional heave motion. This test scenario is interesting because it induces a yaw rate on the car. The driver needs to counter steer in order to correct the yaw rate induced to keep the car on track. The AARB controller produces a roll torque on the car using the active anti-roll bar actuator which produces counteractive yaw rate which is effectively due to the suspension kinematic setup of the car.

The road profile for the driver-in-loop test case is a straight road with two sharp bumps with one bump on either side of the car. The road displacement of the road bumps for this test is shown in the figure 5.1. The test is performed for a constant speed of 100km/h. The road profile for the driver-out-loop case is a straight road with a single bump on the right side of the car. The road displacement for this test scenario is shown in the figure 5.2.

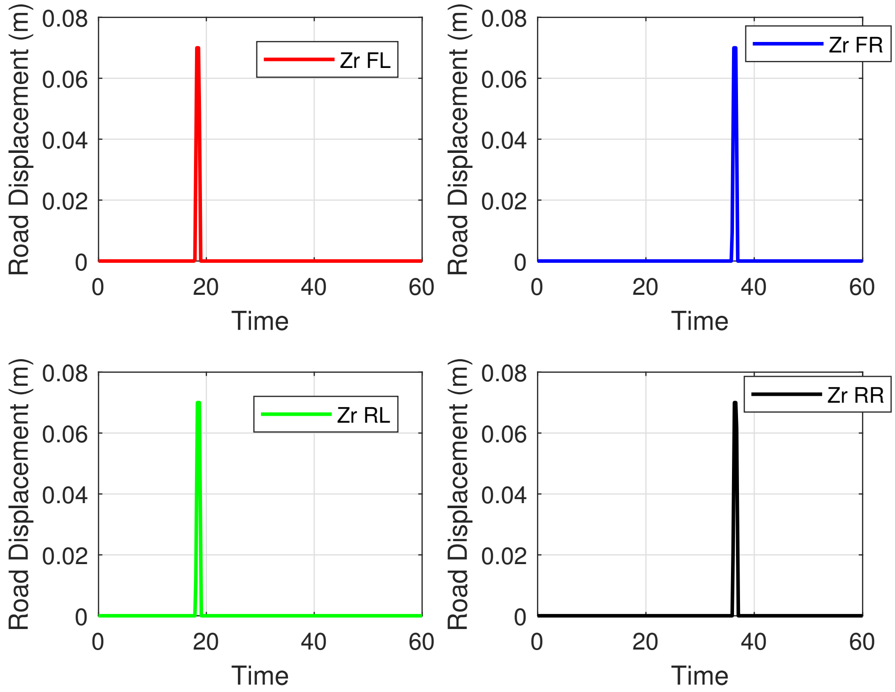

Figure 5.1: Double bump road displacement as disturbance input to the car at 100 km/hr for driver-in-loop case

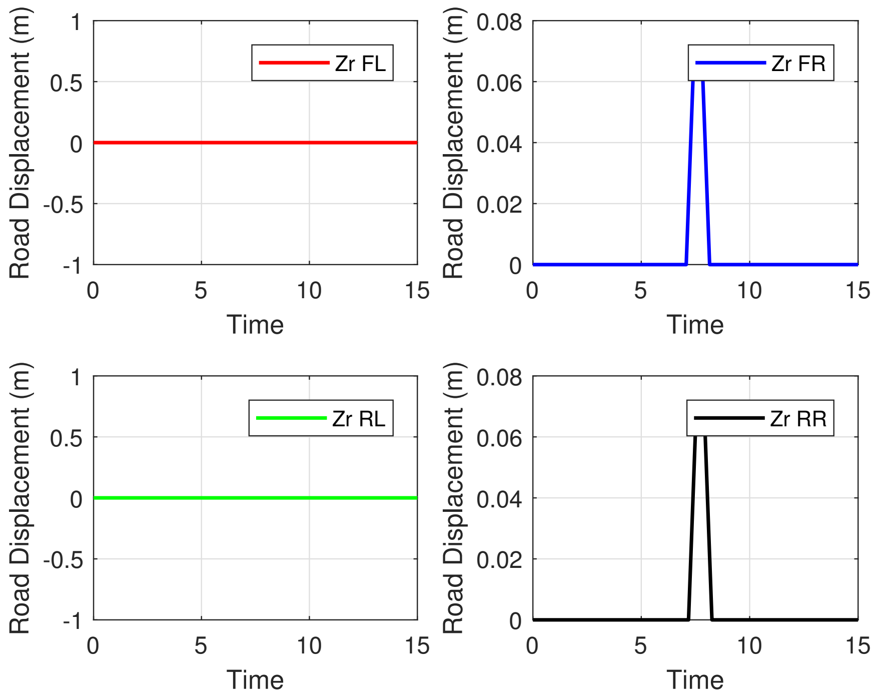

Figure 5.2: Single bump road displacement as disturbance input to the car at 100 km/hr for driver-out-loop case

5.1.1 Driver-In-Loop

The objective of the AARB controller with the driver-in-loop is to reduce the steering effort of the driver which the driver has to apply to keep the car on track. Thus roll and yaw rate disturbances are rejected which are caused by high frequency road bumps by providing extra roll torque by the AARB actuator. This test scenario only involves road disturbances on a straight track. The peak roll angle and yaw rate induced on the car due to bump increases with increase in height of the road bump. The performance of the AARB controller varies with the kinematic setup of the car. Thus, the controller is tested for two different kinematic setups which are introduced in the chapter 4. Also, three different controllers have been investigated i.e. LQR, LQI and robust $\mathcal{H}_\infty$ controller.

In the controller tuning, roll angle and the yaw rate needs to be weighed in-order to achieve the objective. The steering wheel torque reduction and yaw rate reduction are almost the same when roll angle and yaw rate are weighed shown in plots 5.12a and 5.6a. However, weighting body roll angle produces better performance in reducing body roll, lateral deviation, lateral acceleration and steering angle. The controller performance with yaw rate tuning is tested by introducing a delay of 0.5s in driver reaction and results are shown in figures 5.4a, 5.8a, 5.10a and 5.14a.

As a result, for kinematic setup-1 and setup-2, the body roll angle in both the setups shown in figures 5.3a and 5.3c is almost reduced to zero with the AARB controller and there is no much difference in the pitch angle as the road disturbance is a single sided bump.

The yaw rate plots for both the kinematic setups are shown in figures 5.5a and 5.5c. From the plots, it can be seen that the yaw rate with setup-1 is reduced while it increases with setup-2. This contrast result can be seen as the vehicle moves in the direction of the roll torque applied while the behaviour is the opposite with setup-2.

Thus, the lateral deviation of the car with setup-1 is decreased to a great extent while the lateral deviation has increased with setup-2. The lateral deviation plots for setup-1 and setup-2 are shown in figures 5.7a and 5.7c. From these results it can be concluded that there is a fundamental conflict in reduction of body roll angle and yaw rate.

The roll torque produced by the active roll-bar is shown in figure A.1a considerably reduces the lateral acceleration when compared with no controller. The plots are shown in figures 5.9a and 5.9c respectively. The reduction is almost by 50% in case of setup-1 while it is comparatively less with setup-2. From [18], its shown that the steering wheel torque is directly proportional to lateral acceleration up to a certain extent. As a result, steering wheel torque decreases almost by half by the controller with kinematic setup-1 which is shown in figure 5.11a. The steering torque reduction is quite small with setup-2 when compared to that of setup-1 which is shown in the plot 5.11c.

Further, comparing the control methods implemented for the AARB controller it can be seen that all three controllers, LQR, LQI and $\mathcal{H}_\infty$ controller have similar performances for this test scenario in terms of reducing roll angle, lateral acceleration and steering wheel torque. Differences in comparison is more evident in future test scenarios.

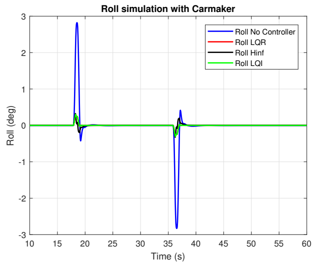

(a) Roll angle with setup-1

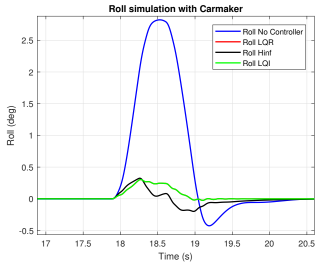

(b) Zoomed-In Roll angle with setup-1

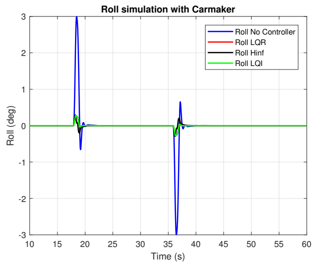

(c) Roll angle with setup-2

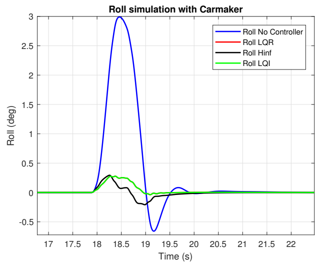

(d) Zoomed-In Roll angle with setup-2

Figure 5.3: Driver-In-Loop: Roll angle comparison for road bumps

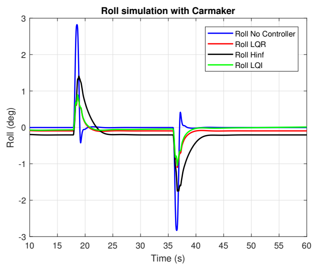

(a) Roll angle with setup-1 with yaw rate weighting

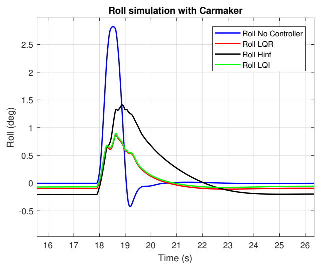

(b) Zoomed-In Roll angle with setup-1 with yaw rate weighting

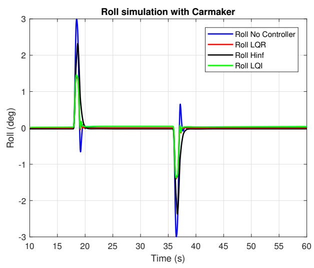

(c) Roll angle with setup-2 with yaw rate weighting

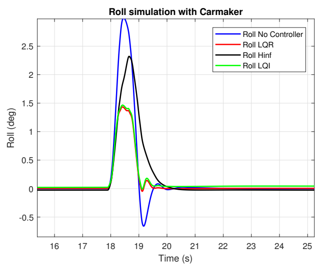

(d) Zoomed-In Roll angle with setup-2 with yaw rate weighting

Figure 5.4: Driver-In-Loop: Roll angle comparison with yaw rate weighting for road bumps

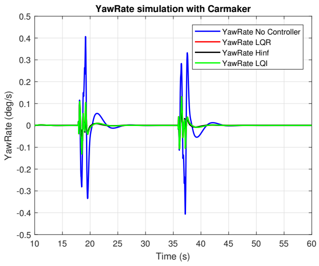

(a) Yaw rate with setup-1

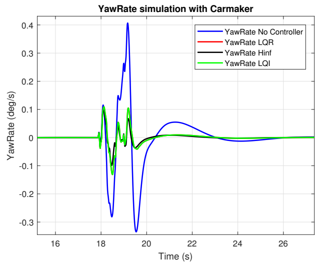

(b) Zoomed-In Yaw rate with setup-1

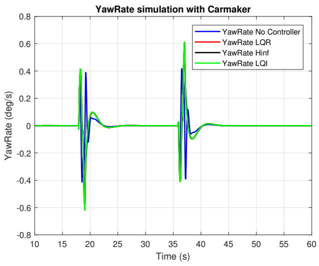

(c) Yaw rate with setup-2

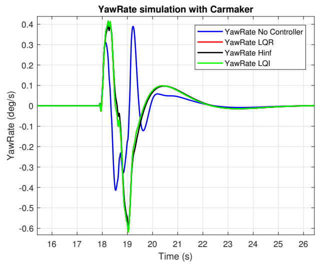

(d) Zoomed-In Yaw rate with setup-2

Figure 5.5: Driver-In-Loop: yaw rate comparison for road bumps

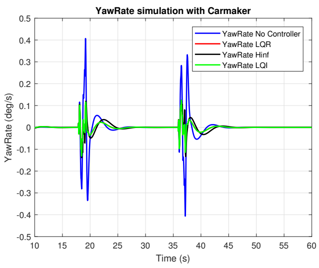

(a) Yaw rate with setup-1 with yaw rate weighting

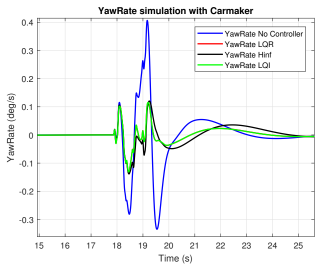

(b) Zoomed-In Yaw rate with setup-1 with yaw rate weighting

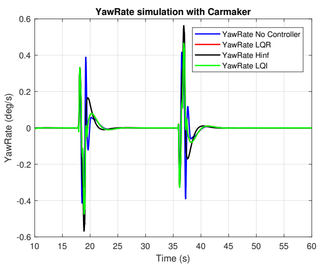

(c) Yaw rate with setup-2 with yaw rate weighting

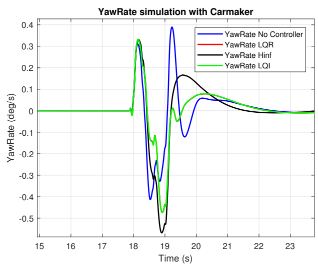

(d) Zoomed-In Yaw rate with setup-2 with yaw rate weighting

Figure 5.6: Driver-In-Loop: yaw rate comparison with yaw rate weighting for road bumps

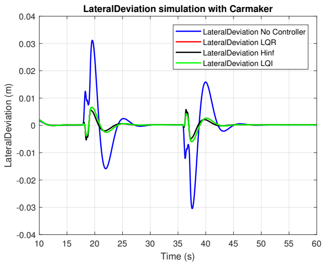

(a) Lateral Deviation with setup-1

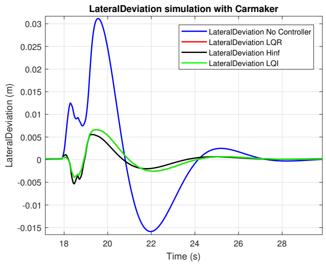

(b) Zoomed-In Lateral Deviation with setup-1

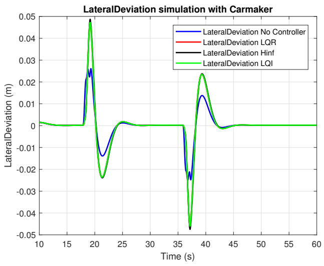

(c) Lateral Deviation with setup-2

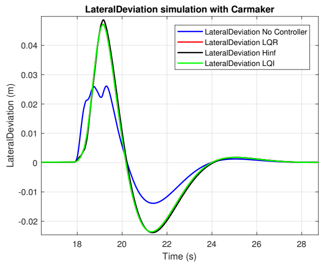

(d) Zoomed-In Lateral Deviation with setup-2

Figure 5.7: Driver-In-Loop: lateral deviation comparison for road bumps

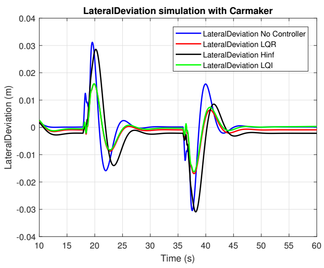

(a) Lateral Deviation with setup-1 with yaw rate weighting

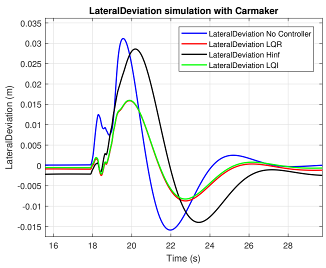

(b) Zoomed-In Lateral Deviation with setup-1 with yaw rate weighting

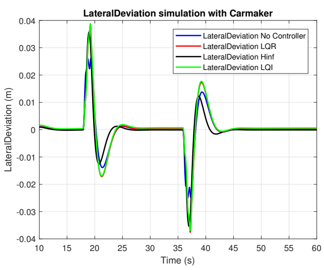

(c) Lateral Deviation with setup-2 with yaw rate weighting

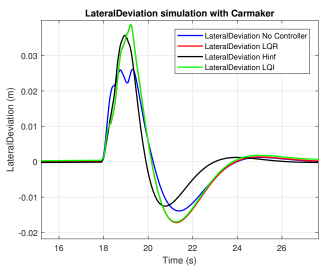

(d) Zoomed-In Lateral Deviation with setup-2 with yaw rate weighting

Figure 5.8: Driver-In-Loop: lateral deviation comparison with yaw rate weighting for road bumps

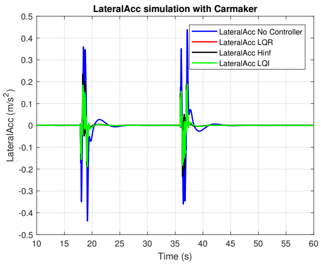

(a) Lateral Acceleration with setup-1

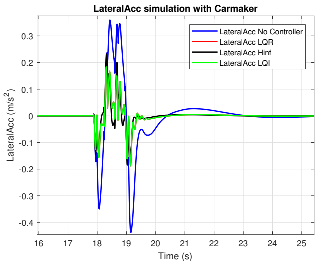

(b) Zoomed-In Lateral Acceleration with setup-1

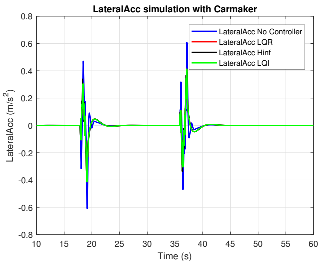

(c) Lateral Acceleration with setup-2

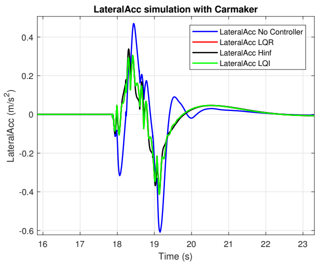

(d) Zoomed-In Lateral Acceleration with setup-2

Figure 5.9: Driver-In-Loop: lateral acceleration comparison for road bumps

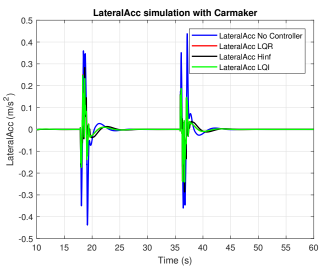

(a) Lateral Acceleration with setup-1 with yaw rate weighting

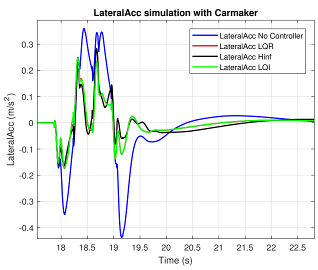

(b) Zoomed-In Lateral Acceleration with setup-1 with yaw rate weighting

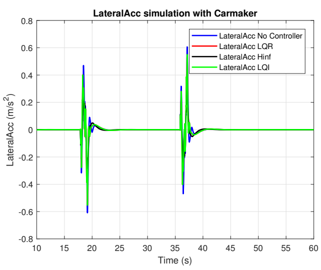

(c) Lateral Acceleration with setup-2 with yaw rate weighting

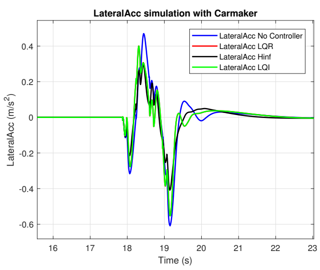

(d) Zoomed-In Lateral Acceleration with setup-2 with yaw rate weighting

Figure 5.10: Driver-In-Loop: lateral acceleration comparison with yaw rate weighting for road bumps

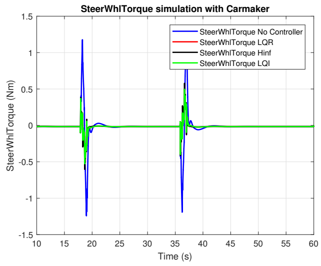

(a) Steering wheel torque with setup-1

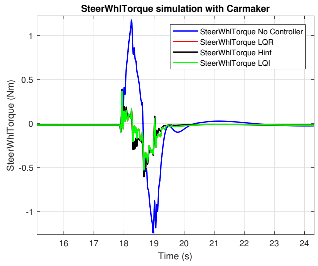

(b) Zoomed-In Steering wheel torque with setup-1

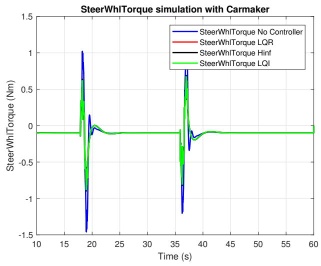

(c) Steering wheel torque with setup-2

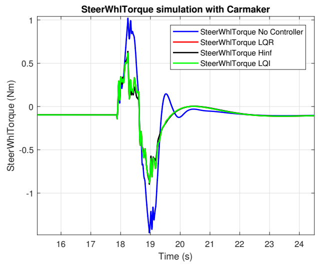

(d) Zoomed-In Steering wheel torque with setup-2

Figure 5.11: Driver-In-Loop: steering wheel torque comparison for road bumps

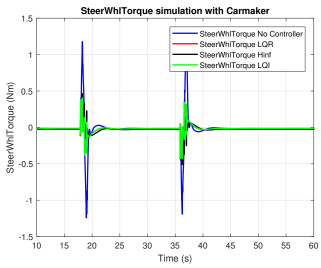

(a) Steering wheel torque with setup-1 with yaw rate weighting

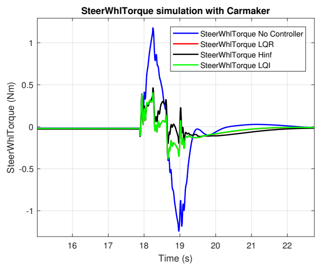

(b) Zoomed-In Steering wheel torque with setup-1 with yaw rate weighting

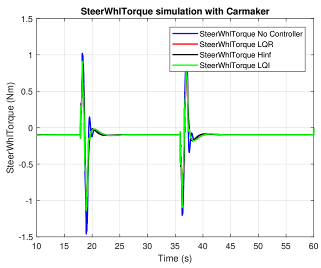

(c) Steering wheel torque with setup-2 with yaw rate weighting

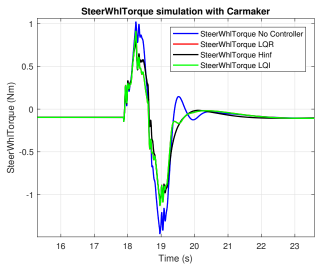

(d) Zoomed-In Steering wheel torque with setup-2 with yaw rate weighting

Figure 5.12: Driver-In-Loop: steering wheel torque comparison with yaw rate weighting for road bumps

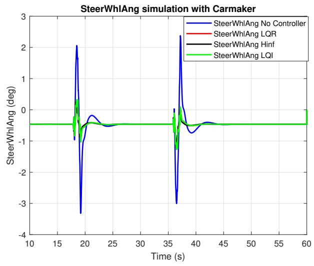

(a) Steering wheel angle with setup-1

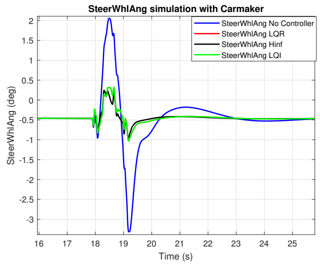

(b) Zoomed-In Steering wheel angle with setup-1

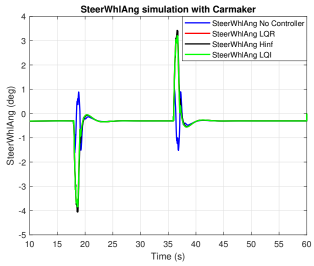

(c) Steering wheel angle with setup-2

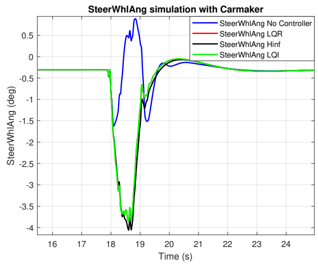

(d) Zoomed-In Steering wheel angle with setup-2

Figure 5.13: Driver-In-Loop: steering wheel angle comparison for road bumps

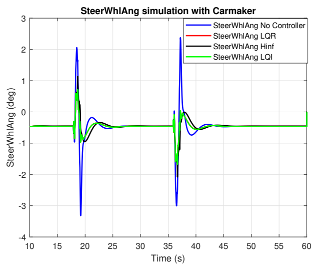

(a) Steering wheel angle with setup-1 with yaw rate weighting

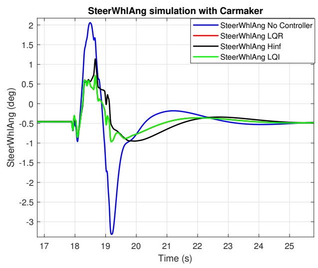

(b) Zoomed-In Steering wheel angle with setup-1 with yaw rate weighting

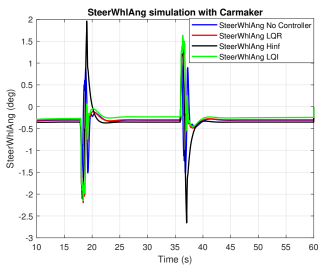

(c) Steering wheel angle with setup-2 with yaw rate weighting

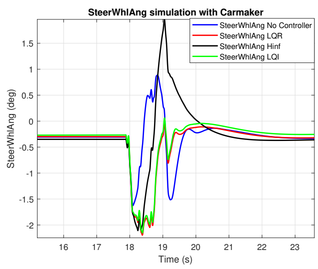

(d) Zoomed-In Steering wheel angle with setup-2 with yaw rate weighting

Figure 5.14: Driver-In-Loop: steering wheel angle comparison with yaw rate weighting for road bumps

5.1.2 Driver-Out-Loop

Another application of the AARB controller is increasing the overall steering ability in the driver-out-loop mode. This can be achieved with AARB controller working in co-ordination with the steering actuator, thus reducing overhead on the steering actuator as well. To achieve this, mainly the yaw rate disturbances induced by the road bumps needs to be attenuated to maintain straight line stability.

The steering ability is improved as the overall steering torque required to decrease the yaw rate is reduced with an active roll torque acting on the car. Yaw rate and its integral state variables are weighed in the controller and the controller is tuned to reduce the overall yaw rate which in turn decreases the over lateral deviation. Thus achieving larger steering angle within the steering torque limits.

In this case, steering actuator is not included and only AARB controller is used for yaw disturbance rejection for controller evaluation purposes. This case is tested as "handsoff" test case in IPG Carmaker. The performance is evaluated for two different kinematic setups.

The body roll angle for kinematic setup-1 and setup-2 are shown in figures 5.15a and 5.15b. It can be seen that roll angle has decreased in the case of setup-1 whereas it increases with setup-2. The yaw rate shown in plots 5.16a and 5.16b, it can be seen that transient oscillations are reduced and the steady state yaw rate is reduced to zero in setup-1 whereas in case of setup-2, it settles to a constant yaw rate value.

Thus, the lateral deviation with and without the controller for setup-2 is almost the same which is shown in figure 5.17b whereas setup-1 with AARB controller produces large reduction in lateral deviations as shown in the plot 5.17a.

Further, lateral acceleration decreases with setup-1 when compared with no AARB controller while it increases with setup-2 thus producing greater steering wheel angle. The steering torque required to correct yaw disturbances in these situation is reduced. The lateral acceleration plots are given in figures 5.18a and 5.18b.

The roll torque produced by weighting the yaw rate and its integral state are shown in A.3a and A.4a results in greater counter steering wheel angle to decrease the lateral deviation. The steering wheel angle for both the setups are shown in the plots 5.19a and 5.19b. A fundamental contrasting behaviour in reducing roll angle and yaw rate is seen in the performance of the AARB controller with setup-2. In the case of setup-1, active roll torque produced reduces both roll angle and yaw rate of the car. There is no much difference in the pitch angle when compared to that of without controller and is shown in A.3b and A.4b.

Further, comparing the control methods implemented for the AARB controller with setup-1, it can be seen that lateral deviation is reduced by tracking of the yaw angle in $\mathcal{H}_\infty$ controller with integral weightings on yaw rate performance and LQI. However, $\mathcal{H}_\infty$ controller shows promising performance as it manages to reduces lateral deviation when compared to others. Performance of controllers in terms of reducing yaw rate and roll angle are quite similar.

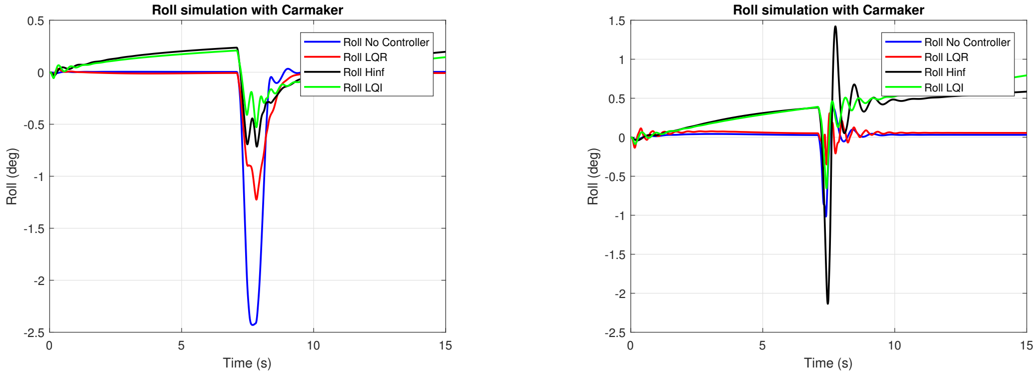

(a) Roll angle with setup-1 **(b)** Roll angle with setup-2

Figure 5.15: Driver-Out-Loop: roll angle comparison for road bumps

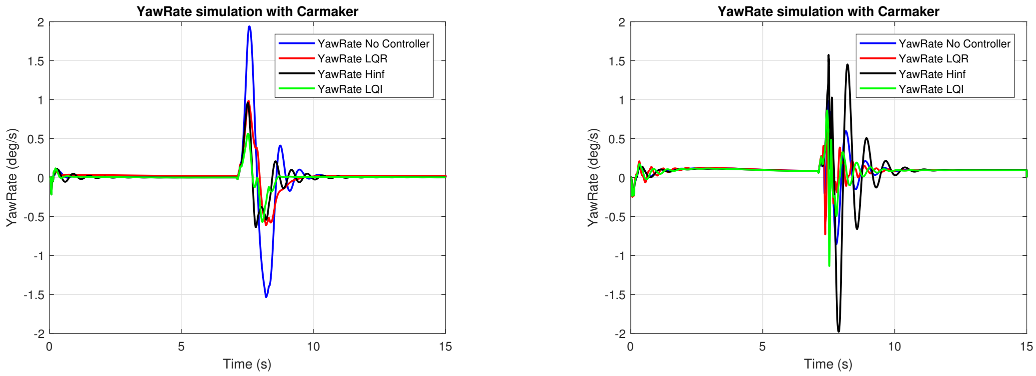

(a) Yaw rate with setup-1 **(b)** Yaw rate with setup-2

Figure 5.16: Driver-Out-Loop: yaw rate comparison for road bumps

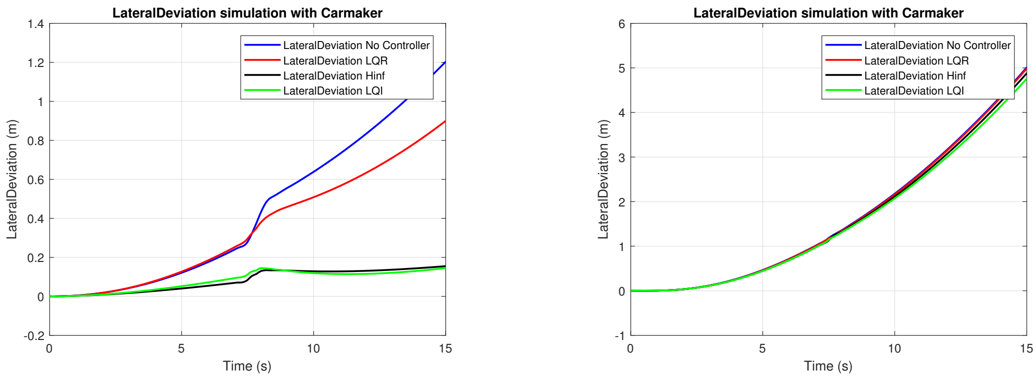

(a) Lateral Deviation with setup-1 **(b)** Lateral Deviation with setup-2

Figure 5.17: Driver-Out-Loop: lateral deviation comparison for road bumps

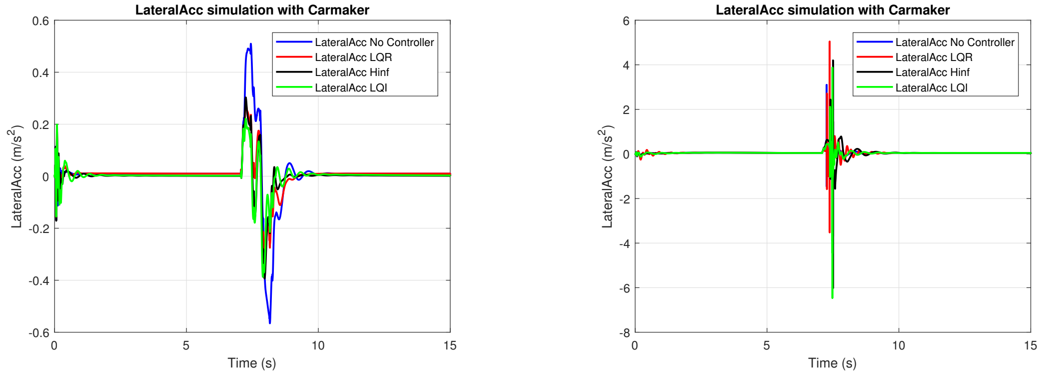

(a) Lateral Acceleration with setup-1 **(b)** Lateral Acceleration with setup-2

Figure 5.18: Driver-Out-Loop: lateral acceleration comparison for road bumps

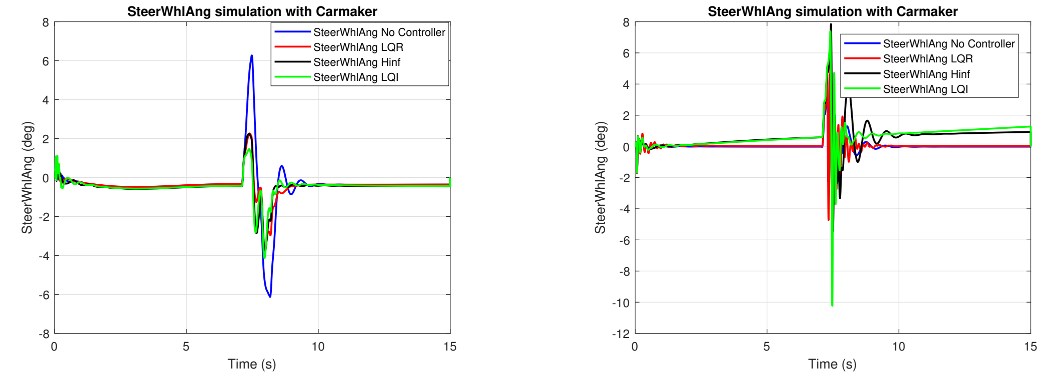

(a) Steering wheel angle with setup-1 **(b)** Steering wheel angle with setup-2

Figure 5.19: Driver-Out-Loop: steering wheel angle comparison for road bumps

5.2 Test Scenario 2 - Banked Roads

In this scenario, the AARB controller performance is tested for a car driven on banked road, one side of the car is in bump where as the other side is in rebound. Low frequency road disturbances such as banked roads and road crowns induces a certain yaw rate on the car which needs to be constantly corrected by the driver or the steering actuator.

The objective of the AARB controller with driver-in-loop is to reduce the overall driving effort, i.e. steering wheel torque by producing a roll torque to reduce the yaw rate error of the car. In driver-out-loop mode, the overhead on the steering actuator is reduced by reducing the yaw rate and lateral deviation of the car using the AARB.

The road profile for this test is that initially, the car is on a straight track for 50m and then road with a continuous slope of 4% is simulated. The road displacement for this test is shown in the 5.20. The test is performed for a constant speed of 100km/h. Same road profile is used for driver-out-loop test case as well.

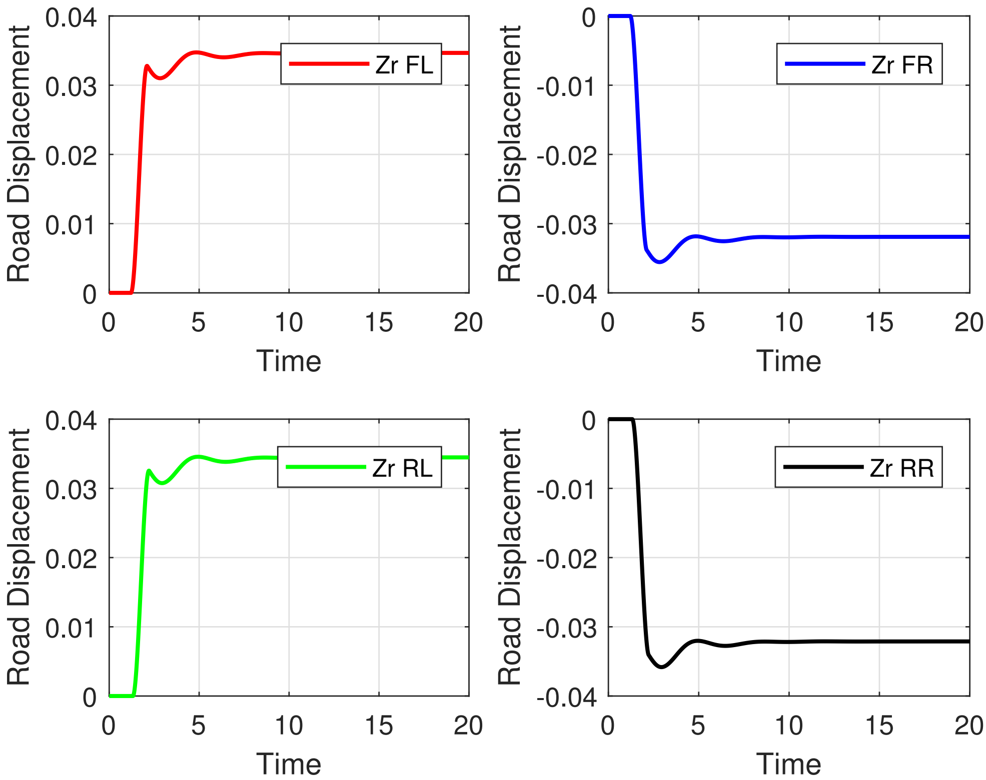

Figure 5.20: Road displacement input on the car due to 4% banked road at 100 km/hr

5.2.1 Driver-In-Loop

The objective of the AARB controller with the driver-in-loop on a banked road is same as the test scenario-1 which is to reduce the steering effort of the driver. This test scenario mainly deals with rejecting roll and yaw rate disturbances induced by low frequency road disturbances such as banked roads, road crowns and wind gusts by using the AARB system.

This test scenario only concerns maintaining the straight line stability of the car. Low frequencies disturbances includes, disturbances in roll angle and yaw rate similar to test scenario-1. The kinematic setup of the car plays a major role on the performance of this AARB controller. Thus, the controller is tested for two different kinematic setups on a 4% banked road.

Ideally the AARB controller is tuned to mitigate the roll and yaw disturbances by weighing roll angle and the yaw rate states in the control design. In the controller tuning, similar situation to test scenario-1 arises i.e weighting the roll angle instead of yaw rate. The controller performance with yaw rate tuning is tested by introducing a delay of 0.5s in driver reaction. The performance of the controller in reducing the steering wheel torque is better in both peak and steady-state error when the roll angle is weighed. this is shown in the plots 5.12a and 5.11a. There is no much change in yaw rate and lateral acceleration reduction as both roll and yaw rate weighting produces almost similar results which is shown in the figure 5.6a, 5.5a, 5.10a and 5.9a. However, better results are obtained by weighting body roll angle in reducing body roll, lateral deviation, and steering angle and results are shown in figures 5.4a, 5.8a, 5.10a and 5.14a.

The body roll angle in for kinematic setup-1 and setup-2 is shown in the figures 5.21a and 5.21b is almost completely reduced to zero by the AARB controller. This shows that the direction of the body roll is against the direction of the slope. However due to the contrasting behaviour of the kinematic setup, the yaw rate has considerably increased while using setup-2 which is shown in 5.22b. There is no change in yaw rate for setup-1 as it is compensated by the driver which can be seen in the plot 5.22a.
Also, the lateral deviation seen with setup-1 is almost zero while the lateral deviation is more with setup-2. The lateral deviation plots for setup-1 and setup-2 are shown in figures 5.23a and 5.23b. The roll torque produced is shown in A.5a and A.6a produces small reduction in lateral acceleration but is not high enough to considerably reduces the lateral acceleration when compared with no controller and the plots are shown in 5.24a and 5.24b respectively. As a result, About 0.4Nm reduction in driving effort can be seen in steady-state while using the AARB controller with setup-1 while steering torque increases with setup-2. Further, there is small increase in the pitch angle which is shown in A.5b and A.6b.

Control methods implemented for the AARB controller are compared and it can be observed that all three controllers, LQR, LQI and $\mathcal{H}_\infty$ controller have similar performances in terms of reducing roll angle, lateral acceleration, steering wheel torque but overall $\mathcal{H}_\infty$ control produces slightly better performance which is evident from the results. The AARB controller performance for kinematic setup-1 and setup-2 are shown in the plots 5.21, 5.22, 5.23, 5.24, 5.25 and 5.26.

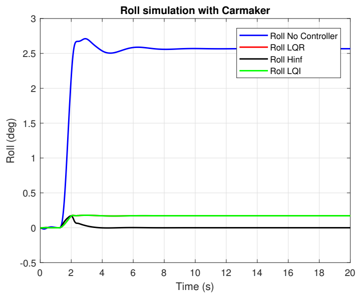

(a) Roll angle with setup-1

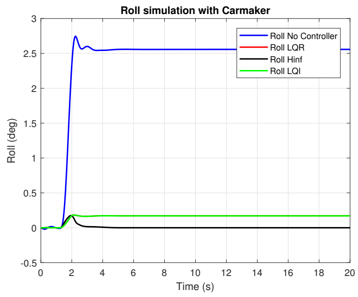

(b) Roll angle with setup-2

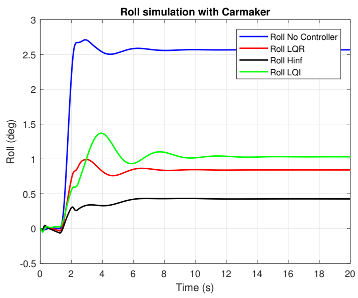

(c) Roll angle with setup-1 with yaw rate weighting

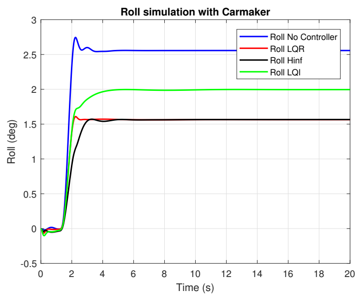

(d) Roll angle with setup-2 with yaw rate weighting

Figure 5.21: Driver-In-Loop: Roll angle comparison for road banking

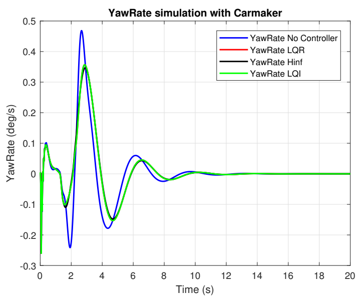

(a) Yaw rate with setup-1

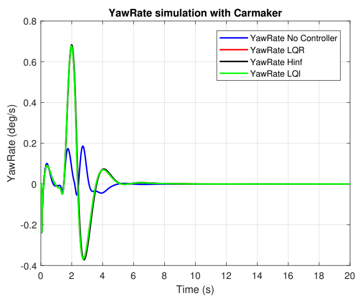

(b) Zoomed-In Yaw rate with setup-1

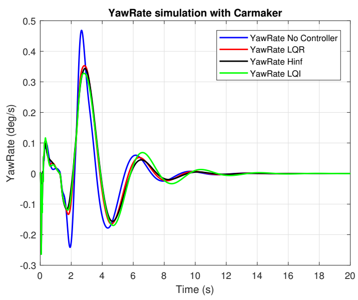

(c) Yaw rate with setup-2 with yaw rate weighting

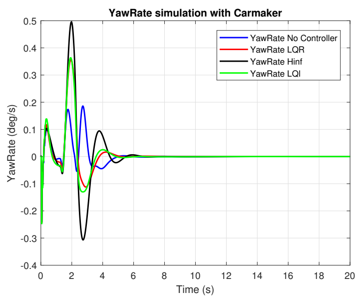

(d) Zoomed-In Yaw rate with setup-2 with yaw rate weighting

Figure 5.22: Driver-In-Loop: yaw rate comparison for road banking

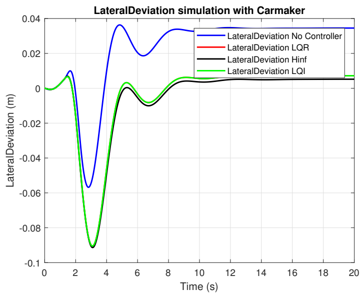

(a) Lateral Deviation with setup-1

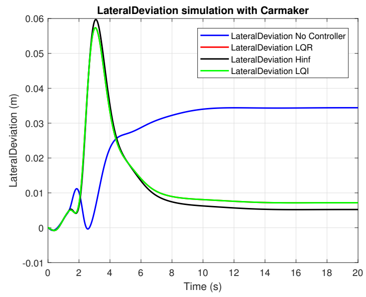

(b) Lateral Deviation with setup-2

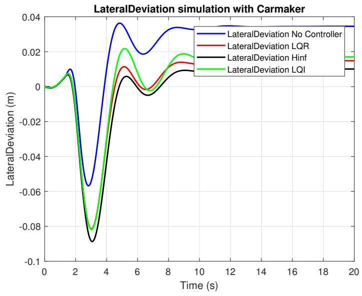

(c) Lateral Deviation with setup-1 with yaw rate weighting

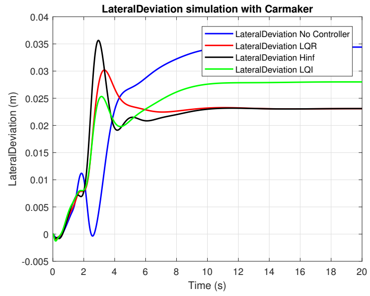

(d) Lateral Deviation with setup-2 with yaw rate weighting

Figure 5.23: Driver-In-Loop: lateral deviation comparison for road banking

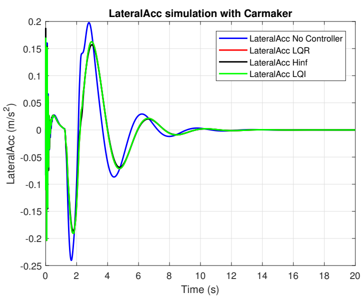

(a) Lateral Acceleration with setup-1

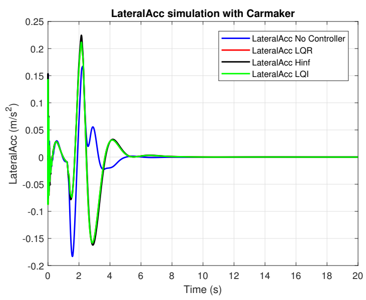

(b) Zoomed-In Lateral Acceleration with setup-1

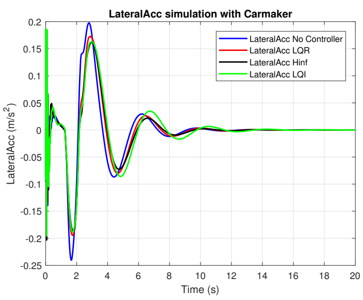

(c) Lateral Acceleration with setup-2 with yaw rate weighting

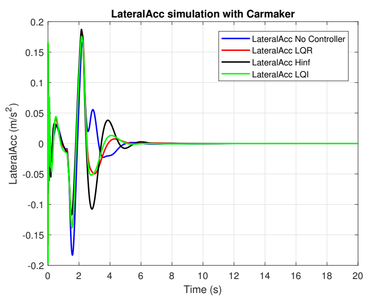

(d) Zoomed-In Lateral Acceleration with setup-2 with yaw rate weighting

Figure 5.24: Driver-In-Loop: lateral acceleration comparison for road banking

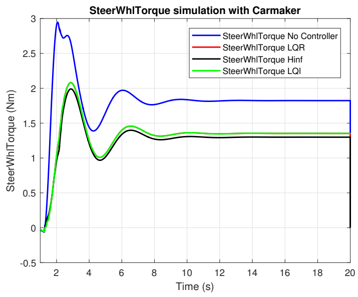

(a) Steering wheel torque with setup-1

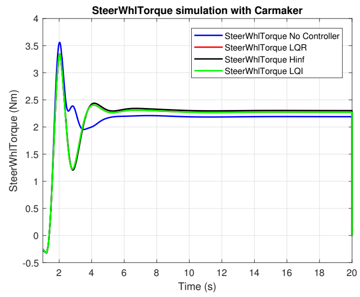

(b) Steering wheel torque with setup-2

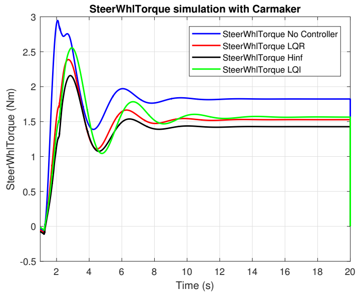

(c) Steering wheel torque with setup-1 with yaw rate weighting

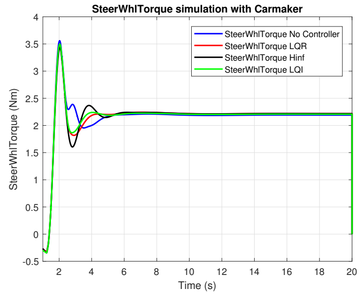

(d) Steering wheel torque with setup-2 with yaw rate weighting

Figure 5.25: Driver-In-Loop: steering wheel torque comparison for road banking

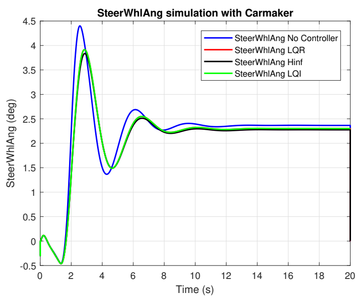

(a) Steering wheel angle with setup-1

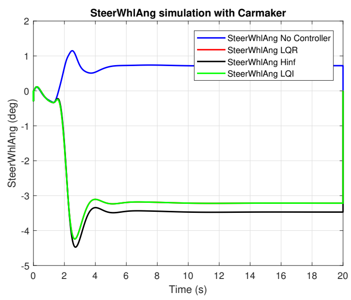

(b) Steering wheel angle with setup-2

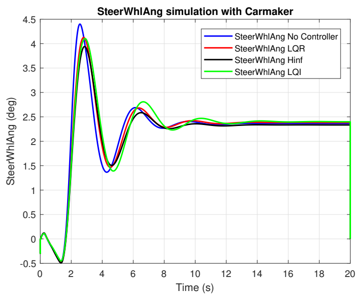

(c) Steering wheel angle with setup-1 with yaw rate weighting

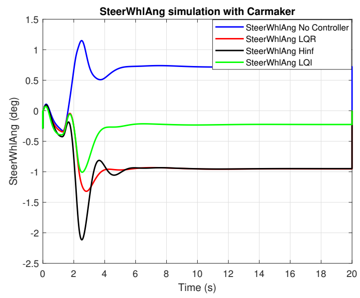

(d) Steering wheel angle with setup-2 with yaw rate weighting

Figure 5.26: Driver-In-Loop: steering wheel angle comparison for road banking

5.2.2 Driver-Out-Loop

Increasing overall steering ability is one of the objective for the AARB controller in the driver-out-loop mode. Thus overhead on the steering actuator is reduced as well. The two main disturbances are the yaw rate and lateral deviation disturbances caused by the banked roads and road crowns which needs to be attenuated to improve straight line stability of the car.

The steering wheel torque required to produce the required yaw rate correction is reduced with the AARB system thus works similarly to the other two scenarios. Also, larger steering angle and larger yaw rate can be achieved within the steering torque limits put on the steering actuator while using the AARB system. The AARB controller performance in attenuating yaw disturbances is evaluated in this test scenario. This case is tested as "handsoff" testcase in IPG Carmaker. The performance is compared for kinematic setup-1 and setup-2.

For setup-1, roll angle is given in the figure 5.27a. It is observed that the body rolls and reaches a steady state value in the direction opposite to the slope in both the setups with the AARB controller. The pitch angle settles to a constant value in case of setup-1. The yaw rate shown in figure 5.28a and major improvement is seen in yaw rate where it is reduced to zero. Thus, AARB controller with setup-1 produces close to zero lateral deviations shown in figure 5.29a. The roll torque produced by yaw rate and its integral state weighting is shown in figure A.7a resulting in greater counter steering wheel angle to decrease the lateral deviation. The steering wheel angle for setup-1 is shown in figure 5.31a. Also, The lateral acceleration for the controller with setup-1 is reduced to zero. Thus when steering actuator is used in co-ordination, small steering torque is required to correct yaw disturbances in these situation. The lateral acceleration plots is given in the plot 5.30a.

For setup-2, roll angle is shown in the plot 5.27b. It is observed that the body rolls and gets unstable in the direction opposite to the slope. Also, the yaw rate increases largely to an extent where it gets unstable which is shown in figure 5.28b. Thus, lateral deviations with setup-2 increases when compared to no controller case. The lateral deviation plot is shown in figure 5.29b. The roll torque produced by yaw rate and its integral state weighting is shown in figure A.8a results in continuously increasing the counter steering wheel angle. The steering wheel angle for setup-2 is shown in figure 5.31b. Also, an increase in lateral acceleration is seen for setup-2. The lateral acceleration plots is given in the plot 5.30b. Thus the AARB controller with setup-2 drives the system towards instability. This happens due to the contrasting behaviour in roll angle and yaw rate reduction as the body rolls opposite to the direction of the slope which increases the yaw rate and lateral deviation of the car.

Comparison of the control methods implemented for the AARB controller are presented with setup-1, it can be seen that lateral deviation reaches zero due to tracking of the yaw angle in $\mathcal{H}_\infty$ controller with integral weightings and LQI while there is some offset using LQR. Performance of controllers in terms of reducing yaw rate and roll angle are quite similar.

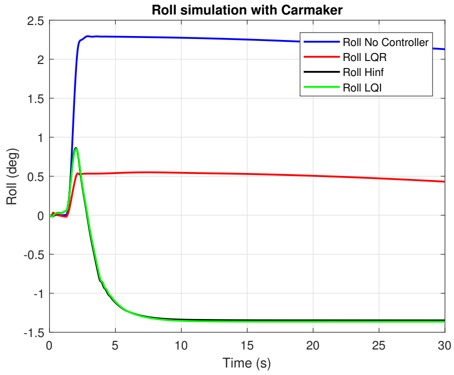

(a) Roll angle with setup-1

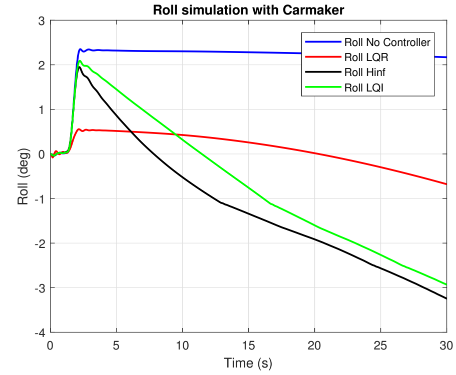

(b) Roll angle with setup-2

Figure 5.27: Driver-Out-Loop: roll angle comparison for road banking

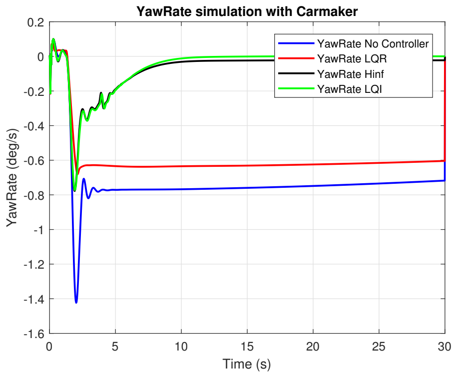

(a) Yaw rate with setup-1

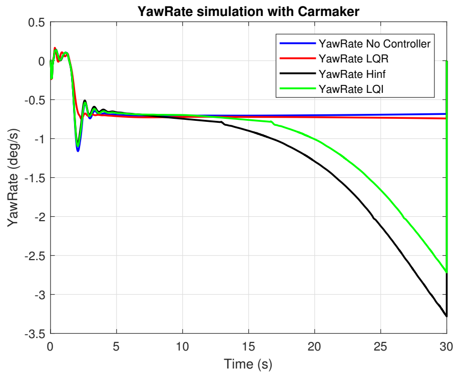

(b) Yaw rate with setup-2

Figure 5.28: Driver-Out-Loop: yaw rate comparison for road banking

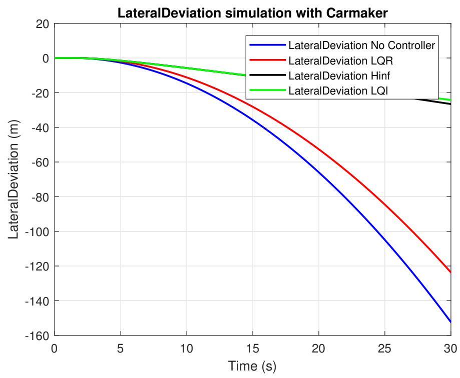

(a) Lateral Deviation with setup-1

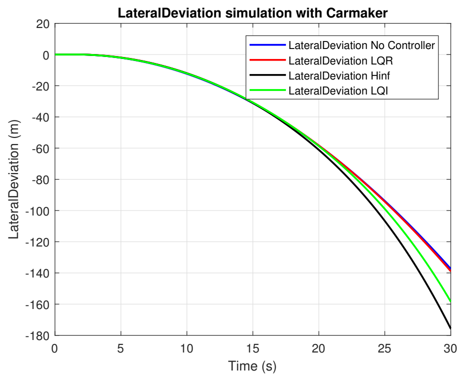

(b) Lateral Deviation with setup-2

Figure 5.29: Driver-Out-Loop: lateral deviation comparison for road banking

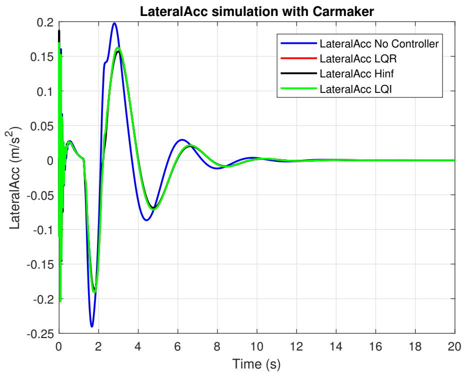

(a) Lateral Acceleration with setup-1

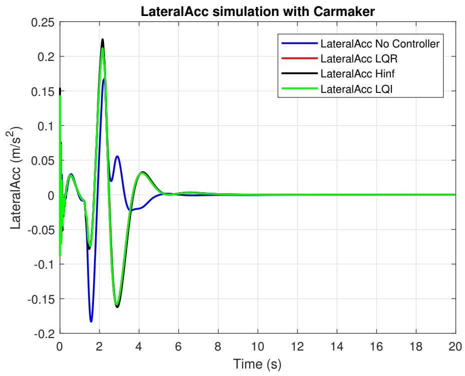

(b) Lateral Acceleration with setup-2

Figure 5.30: Driver-Out-Loop: lateral acceleration comparison for road banking

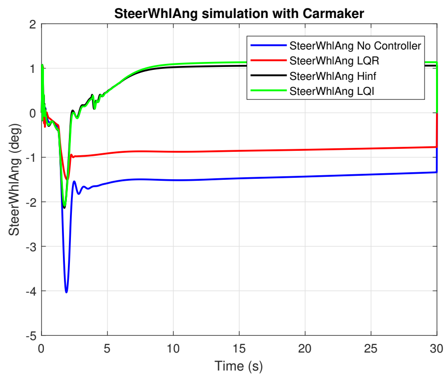

(a) Steering wheel angle with setup-1

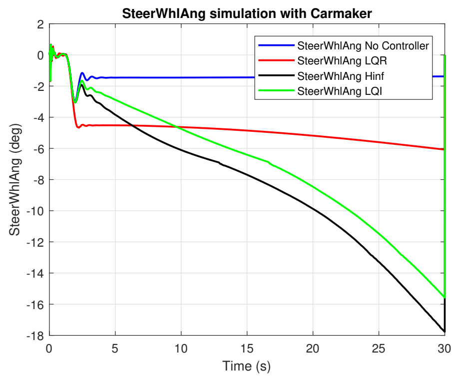

(b) Steering wheel angle with setup-2

Figure 5.31: Driver-Out-Loop: steering wheel angle comparison for road banking

5.3 Test Scenario 3 - Controller Performance for Cornering Scenario

This test scenario is used to test the performance of the AARB controller in low amplitude steady state cornering. The objective of the controller in this scenario is to decrease the steady state steering wheel torque in driver-in-loop case where as increase the steering range in the driver-out-loop mode. While cornering, the car produces a body roll away from the corner due to centrifugal force. The AARB controller produces a roll torque to counteract this body roll and the by utilizing the roll steer effect of the car, the overall driver effort is reduced in a high radius corner. In driver-out-loop mode, the steering actuator torque is limited for safety. The AARB controller is quite useful in reducing the overhead on the steering actuator by achieving the same yaw rate as produced without the controller for a lesser steering torque, thus increasing the steering range in the driver-out-loop. The AARB controller for kinematic setup-1 and setup-2 are compared for driver-in-loop and driver-out-loop cases. The results for driver-in-loop are shown in plots 5.34, 5.35, 5.36, 5.37, 5.38 and 5.39. The results for driver-out-loop are shown in plots 5.40, 5.41, 5.42, 5.43, 5.44 and 5.44. The steering input used in the driver-in-loop test case and the steering torque input in the driver-out-loop case are shown in 5.32a and 5.32b.

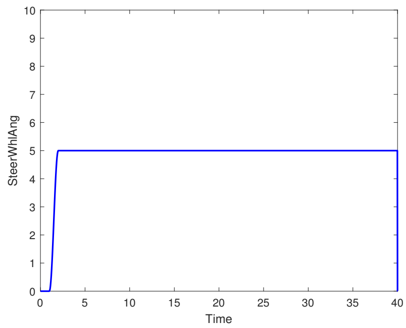

(a) Input Steering wheel angle (deg) for driver-in-loop test case

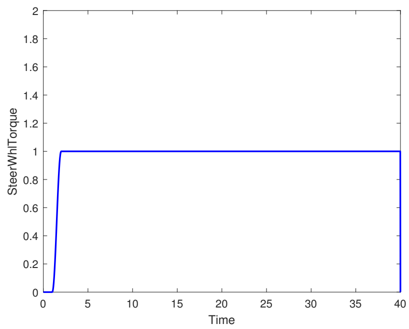

(b) Input Steering wheel torque (Nm) for driver-out-loop test case

Figure 5.32: Inputs signals for the steady-state cornering test case

5.3.1 Driver-In-Loop

The AARB controller was tested for high and low frequency road disturbances in test scenario-1 and test scenario-2. In test scenario-3 with the driver-in-loop, the performance of the controller is evaluated for steady state cornering situations without road disturbances. The main objective of the controller here is to reduce the steering wheel torque while achieving the same yaw rate as without controller. The cornering performance is tested for two different kinematic setups with the AARB controller.

In cornering case, the yaw rate reference is computed by the lateral model based on the steering angle input from the driver. In order to reduce steering wheel torque, the AARB controller needs to produce active roll torque which negates the body roll caused due to cornering. To produce sufficient active roll torque to reduce steering effort, yaw rate needs to be set as the tracking variable as the torque produced due to roll angle is comparatively less. Yaw rate variable is not effective as not much yaw rate error is produced in the driver-in-loop case. However, yaw rate could still be a good variable to control as it hugely reduces the model complexity. Controlling other parameters like Steering Wheel torque would be complex as it would involve driver model, steering model,lateral model and the vertical model.

To overcome this problem we can scale the yaw rate reference and induce a small yaw rate error as shown in 5.33. The roll torque thus produced reduces the steering wheel torque while producing the yaw rate required to follow the path ahead. The magnitude by which the yaw rate reference is scaled is limited by the body roll constraint. This scaling needs to be done in a quasi-static way which is not implemented in this thesis.

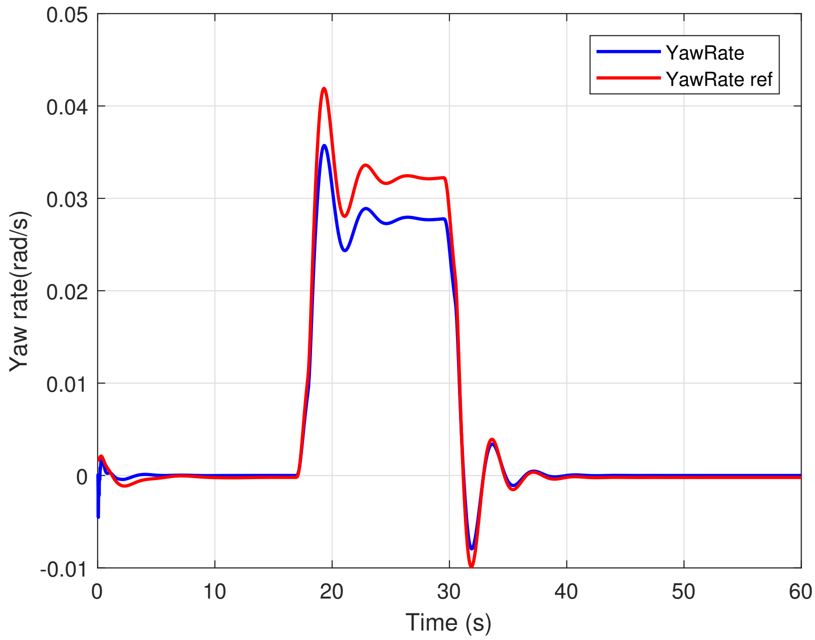

Figure 5.33: the yaw rate reference is scaled by a constant

The yaw rate is shown in 5.35a and 5.35b, it can be seen with AARB controller the desired yaw rate is achieved with both the kinematic setups. Thus, same lateral deviation is achieved with both the setups as shown in 5.36a and 5.36b.

The steady state lateral acceleration for the controller with setup-1 decreases while the lateral acceleration with setup-2 remains unchanged when compared to without controller for the same yaw rate. From [18], its shown that the steering wheel torque is directly proportional to lateral acceleration until certain maximum lateral acceleration is reached. As a result, there is considerable reduction in steady state steering wheel torque which is shown for both the setups in 5.38a and 5.38b. The lateral acceleration plots are given in 5.37a and 5.37b.

The body roll angle for setup-1 and setup-2 are shown in 5.34a and 5.34b. It is observed that the body rolls into the corner and reaches a steady state in setup-1 while roll angle is slightly reduced with setup-2. The pitch angle plots are shown in A.9b and A.10b. The roll torque produced are shown in A.9a and A.10a. From this test scenario it can seen that cornering with large radius, with body roll, the steering effort can be reduced considerably while having setup-1 but cannot be achieved by using setup-2.

The control methods implemented for the AARB controller with setup-1 are compared, it can be seen that yaw rate and lateral deviation reaches a desired value by tracking of the yaw angle in $\mathcal{H}_\infty$ controller and LQI. It can be noted that both $\mathcal{H}_\infty$ controller and LQI performed equally well while comparing all other parameters.

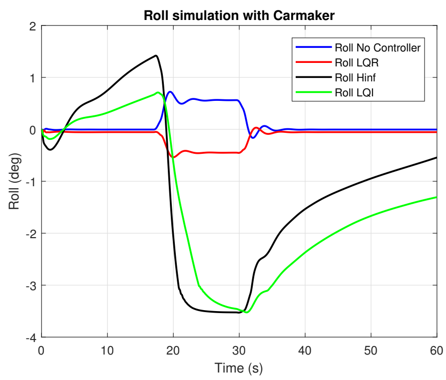

(a) Roll angle with setup-1

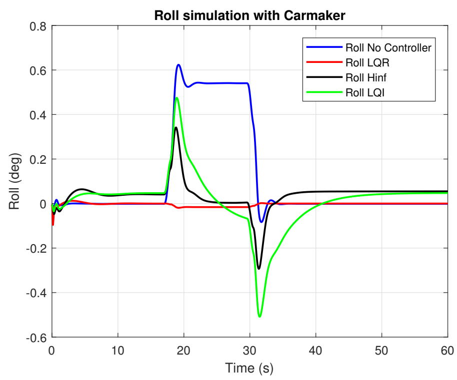

(b) Roll angle with setup-2

Figure 5.34: Driver-In-Loop: roll angle comparison for cornering scenario

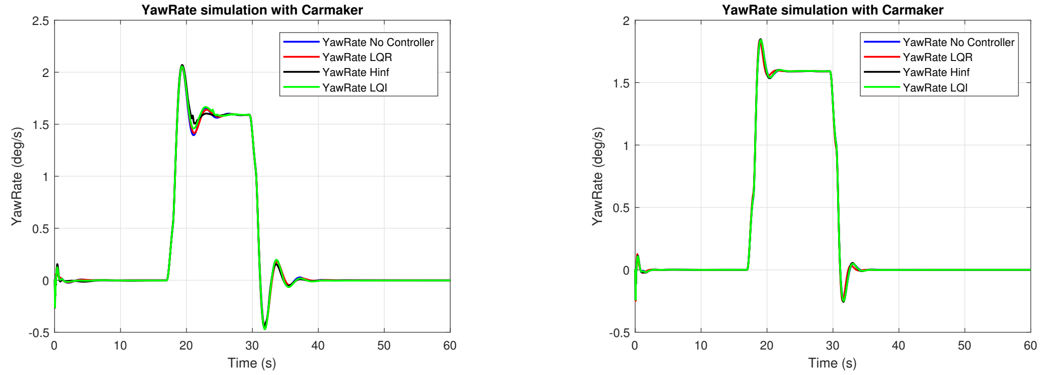

(a) Yaw rate with setup-1 **(b)** Yaw rate with setup-2

Figure 5.35: Driver-In-Loop: yaw rate comparison for cornering scenario

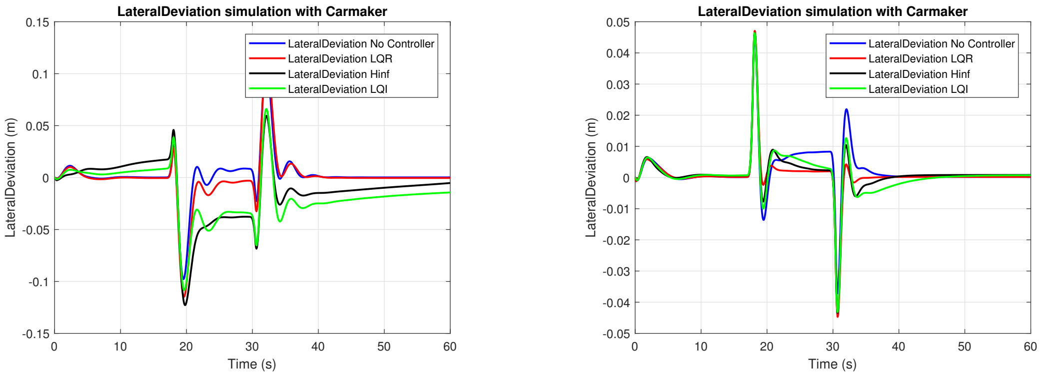

(a) Lateral Deviation with setup-1 **(b)** Lateral Deviation with setup-2

Figure 5.36: Driver-In-Loop: lateral deviation comparison for cornering scenario

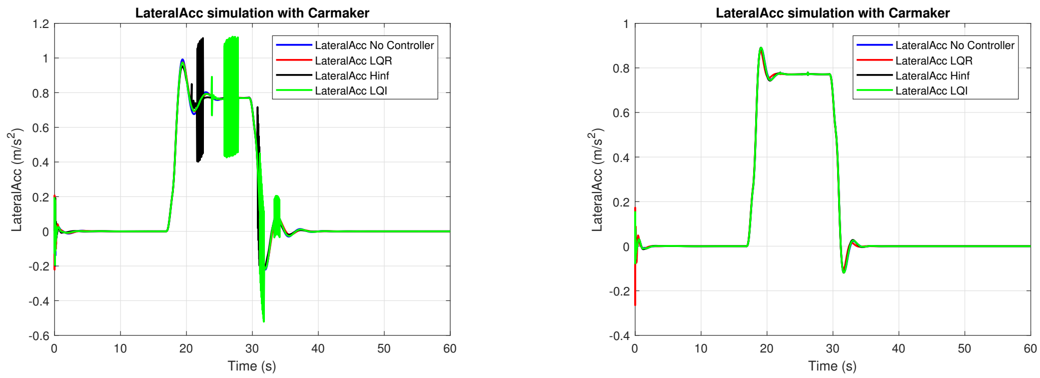

(a) Lateral Acceleration with setup-1 **(b)** Lateral Acceleration with setup-2

Figure 5.37: Driver-In-Loop: lateral acceleration comparison for cornering scenario

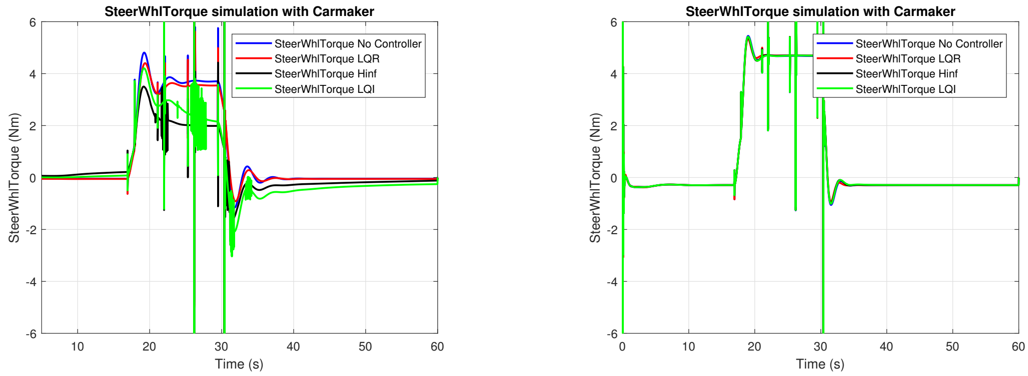

(a) Steering wheel torque with setup-1 **(b)** Steering wheel torque with setup-2

Figure 5.38: Driver-In-Loop: steering wheel torque comparison for cornering scenario

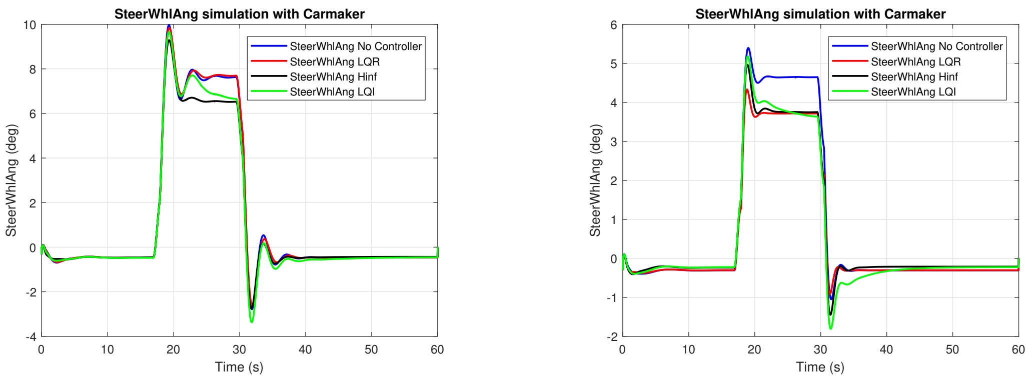

(a) Steering wheel angle with setup-1 **(b)** Steering wheel angle with setup-2

Figure 5.39: Driver-In-Loop: steering wheel angle comparison for cornering scenario

5.3.2 Driver-Out-Loop

The objective of overall steering ability remains the same as test scenario-1 and scenario-2 but the major difference is that here the controller performance is evaluated in cornering/-turning situations in the driver-out-loop mode. AARB controller increases the steering angle considerably while maintaining steering torque with the prescribed actuator limits. Thus higher yaw rate can be reached using a lesser steering wheel torque as some part of it is produced with the AARB system. This can be attained with AARB controller working in co-ordination with the steering, thus providing more room for the steering actuator to achieve higher steering angles.

This test case mainly deals with evaluating how steering range is improved, thus road disturbances are not considered. The steering actuator is not included and only AARB controller is used for yaw rate reference tracking for controller evaluation purposes. This case is tested with 1Nm of steering torque in IPG Carmaker and its performance with kinematic setup-1 and setup-2 are compared. For AARB testing purpose, the reference yaw rate is scaled considering the AARB actuator limits to produce yaw rate error required to produce roll torque which increases the yaw rate and lateral deviation of the vehicle.

From the yaw rate shown in 5.41a and 5.41b, it can be seen how the AARB kicks in to increase the steady state yaw rate with setup-1 but no improvements can be seen with setup-2. Thus, the lateral deviation with setup-1 increases considerably shown in 5.42a while it remains same with setup-2 and without the controller which is shown in 5.42b.

The roll torque produced by both setups are shown in A.11a and A.12a resulting in increase in steering wheel angle with setup-1 to increase the lateral deviation while steering wheel angles decreases with setup-2. The steering wheel angle for both the setups are shown in 5.44a and 5.44b.

Similar to yaw rate, lateral acceleration for the controller with setup-1 is increases to new steady state value while the lateral acceleration with setup-2 remains unchanged when compared to without controller. The lateral acceleration plots are given in 5.43a and 5.43b.

The body roll angle for setup-1 and setup-2 are shown in 5.40a and 5.40b. It is observed that the body rolls and reaches a steady state into the corner in setup-1 while roll angle is close to zero with setup-2. The pitch angle plots are shown in A.11b and A.12b.

The control methods implemented for the AARB controller with setup-1 are compared, it can be seen that yaw rate and lateral deviation is increased greatly by tracking of the yaw angle in $\mathcal{H}_\infty$ controller and LQI while LQR performance is not satisfactory. It can be noted that $\mathcal{H}_\infty$ controller performed slightly better than LQI as it provides greater design flexibility.

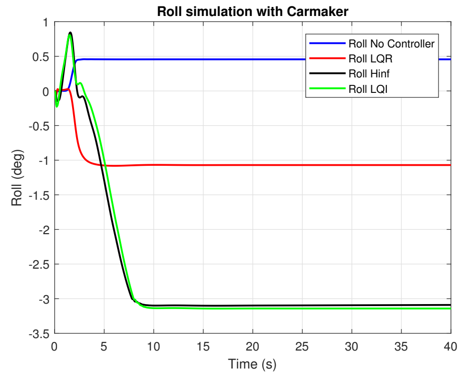

(a) Roll angle with setup-1

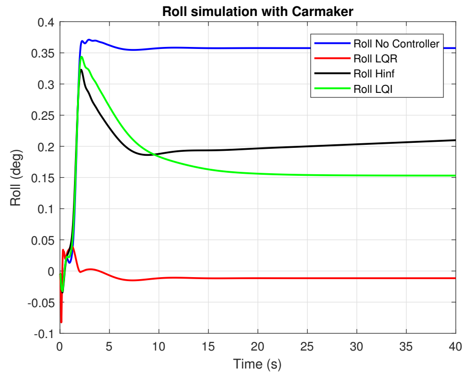

(b) Roll angle with setup-2

Figure 5.40: Driver-Out-Loop: roll angle comparison for cornering scenario

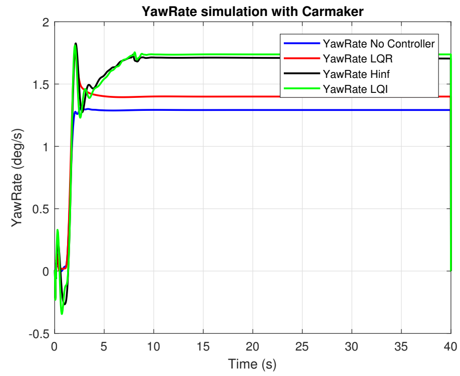

(a) Yaw rate with setup-1

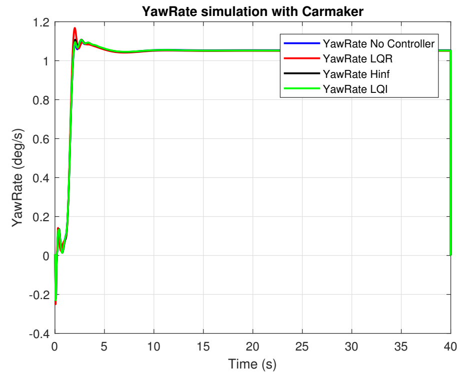

(b) Yaw rate with setup-2

Figure 5.41: Driver-Out-Loop: yaw rate comparison for cornering scenario

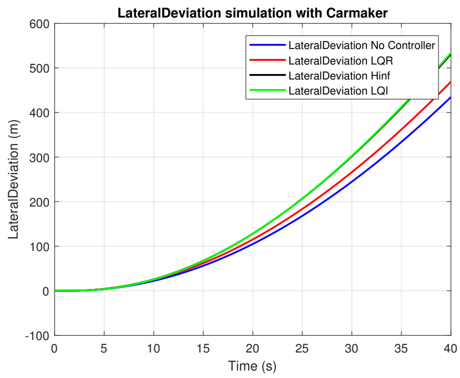

(a) Lateral Deviation with setup-1

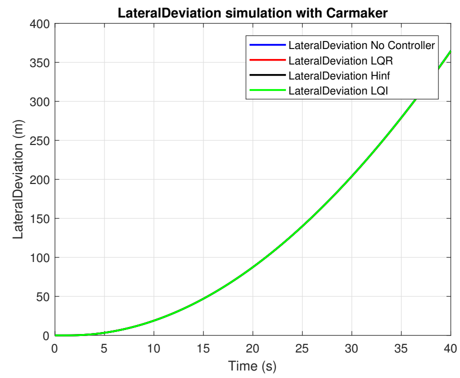

(b) Lateral Deviation with setup-2

Figure 5.42: Driver-Out-Loop: lateral deviation comparison for cornering scenario

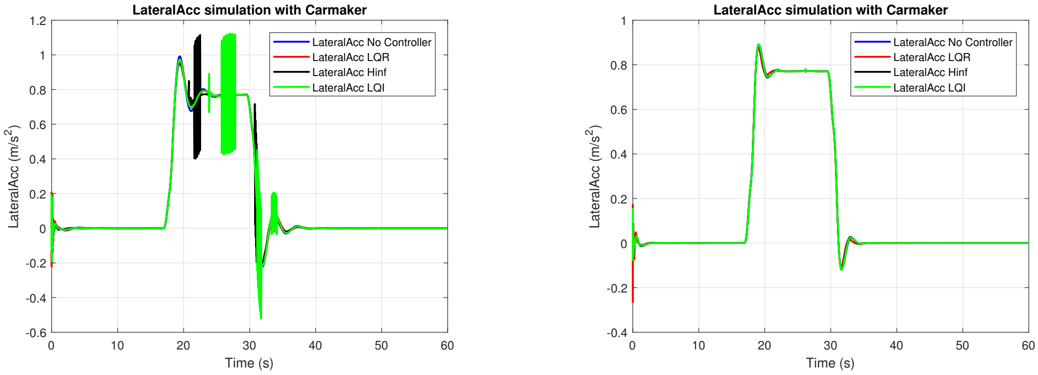

(a) Lateral Acceleration with setup-1 **(b)** Lateral Acceleration with setup-2

Figure 5.43: Driver-Out-Loop: lateral acceleration comparison for cornering scenario

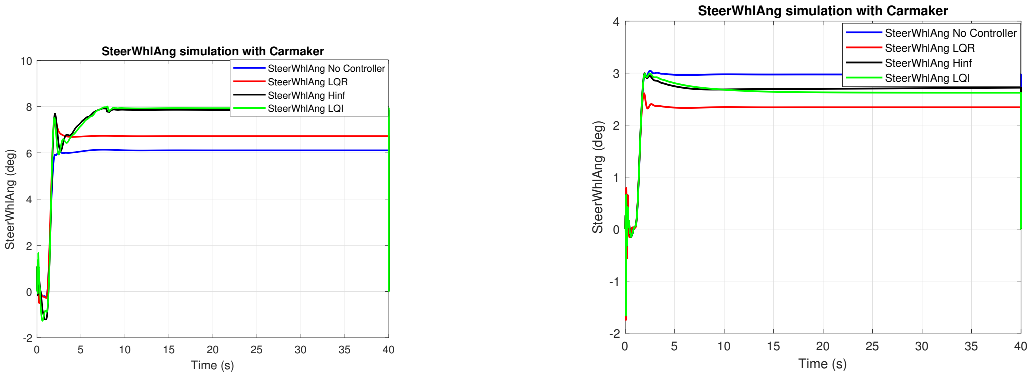

(a) Steering wheel angle with setup-1 **(b)** Steering wheel angle with setup-2

Figure 5.44: Driver-Out-Loop: steering wheel angle comparison for cornering scenario

6 Conclusion and Future Work

In this chapter, the objective of the thesis is recalled and discussed in concurrence with the obtained results. Furthermore, actions for future work are suggested. Then conclusions are drawn regarding how well the purpose of the thesis was achieved.

6.1 Conclusion

The purpose of the thesis is to study the effects of the active suspension system on steering and yaw motion of the vehicle and to decrease driver steering effort for various road disturbances with driver-in-loop and to improve the auto-pilot steering ability using the active anti-roll bar system . For this purpose, various model based control methods such as LQR, LQI and robust $\mathcal{H}_\infty$ control method was implemented. The common way to formulate the control problem is to use a roll-yaw model which include full car suspension dynamics with roll, pitch and heave and one track lateral dynamics model with the link between suspension deflection and steering is established by a linear suspension kinematics and compliance model. The research questions on formulation of transfer function between steering angle and ΔF_z caused due to suspension deflection is obtained through kinematics model and relation between suspension deflection and yaw rate is established in roll-yaw model. The reduced order roll-yaw model is derived by removing the unsprung mass states as these states needs to be estimated and unsprung mass acceleration measurements are not available. The full and reduced order model is validated using the CarMaker model and compared with each other. It can be seen that the full roll-yaw model and the reduced roll-yaw model behaves very similar to each other.

Three different types of model based controllers were implemented and tested in simulation environment for three different road scenarios. The different road scenarios include high frequency disturbances such as road bumps, low frequency disturbances like banked roads and road crowns in straight line driving while the third scenario includes cornering situations. Thus yaw rate reference generator model is derived to produce yaw rate reference to the AARB controller.

From the results obtained, the first and foremost conclusion is that the performance of the AARB controller largely depends on kinematic setup of the car. The results from all the test scenarios prove that the AARB controller performance with kinematic setup-1 makes it feasible to meet all the objectives which is to reduce steering wheel torque in the driver-in-loop case and increase steering ability in driver-out-loop case. It was also observed that there is no much effect on steering wheel torque and steer-ability with kinematic setup-2.

To implement of the AARB system, the suspension kinematics needs to be setup similar to setup-1. Kinematic analysis was carried out in chapter 4 using a linear kinematic model in CarMaker to quantitatively analyze the effects of kinematic parameters and its effects on lateral acceleration and steering wheel torque during AARB intervention.
From the tables 4.1 and 4.2, it can be concluded that the bump steer has the highest effect on the steering wheel torque and yaw rate under the influence of active roll torque.

The AARB controller needs to be tuned separately for different kinematic setups. Also, it needs different tuning for driver-in-loop and driver-out-loop cases. This is because the controller performs better when roll angle is weighed compared to yaw rate in the driver-in-loop case. To prove this, driver delay of 0.5s was introduced earlier and the comparative results are presented in the chapter 5. Whereas, yaw rate and yaw angle needs to be weighed in driver-out-loop case to attenuated yaw disturbances caused due to road disturbances. However, the controller tuning remains same for different frequencies of road disturbances and cornering scenarios for a particular vehicle speed.

Linear Quadratic Integral control has promising results as it minimizes yaw rate error and its integral state error with less oscillations but is not as effective as the $\mathcal{H}_\infty$ controller in cornering scenario. The Linear Quadratic Regulator is promising for high frequency disturbance rejection, however its performances is limited in low frequency scenarios as large yaw angle error is induced in the low frequency scenario which the LQR will not be able to handle.

The real-time implementation of this controller, the AARB system utilizes lot of energy as large roll torque is needed to correct small yaw rate error which is explained in 2.11. However, the performance of the AARB controller showed great potential in the simulation results in decreasing the overhead on the steering actuator and increasing driving comfort by decreasing driver effort.

6.2 Future Work

Below are the future work recommendations for real-time implementations of the AARB controller.

6.2.1 Dynamic Model

- The lateral dynamics model can be implemented to include different wheel angles due to steering geometry and non-linear bump steer effects can be included.
- The model needs to be extended in order to handle road disturbances in cornering scenarios. The present model does not include the kinematic effects caused due to both steering and road disturbances.

6.2.2 Control Design

- Quasi-static method needs to be implemented to select the gain by which the yaw rate reference needs to be scaled. This scaling factor needs to selected depending on the steering angle and the vehicle speed while considering the constraint of the body roll angle.
- The full state feedback is developed using reduced roll-yaw model as unsprung states needs to be estimated. An observer can be implemented to estimate the unsprung mass states to successfully utilize full roll-yaw model.
- The controller implemented in this thesis assumes constant vehicle speed. So, Linear Parameter Varying (LPV) controller can be designed with vehicle speed being the varying parameter.
- Control allocation techniques can be implemented as a vehicle is an over-actuated system and the yaw moment can be distributed between multiple actuators satisfying actuator constraints and minimal control effort objectives.

6.2.3 Suspension Kinematics

- Kinematic parameters are quantified in the tables 4.1 and 4.2 using linear 3-DOF Model in IPG Carmaker to lay down a marker for suspension design. Suspension kinematics needs to be designed accordingly if it is desired to affect steering with the AARB system.

Bibliography

[1] Jacob Gustafsson, Harshit. *Investigation of active anti-roll bars and development of control algorithm* Diploma work - Department of Applied Mechanics, Chalmers University of Technology, Gothenburg, Sweden, ISSN 1652-8557; 2017: 30, 2017

[2] Van-Tan Vu, Olivier Sename, Luc Dugard, Peter Gáspár. *$\mathcal{H}_\infty$ active anti-roll bar control to prevent rollover of heavy vehicles: a robustness analysis.* 6th IFAC International Symposium on System Structure and Control (SSSC 2016), Jun 2016, Istanbul, Turkey. 2016.

[3] Skogestad Sigurd, Postlethwaite Ian, *Multivariable Feedback Control: Analysis and Design*,2015, New York,Wiley-Interscience, Edition Number 2, ISBN: 9780470011683

[4] Rajamani, R *Vehicle Dynamics and Control*,Springer, Mechanical Engineering Series, 2005.

[5] Vu, V.T., Sename, O., Dugard, L., and Gaspar, P. (2016). *Active anti-roll bar control using electronic servo-valve hydraulic damper on single unit heavy vehicle* in IFAC Symposium on Advances in Automotive Control - 8th AAC 2016. Sweden.

[6] Gaspar, P., Szabo, Z., and Bokor, J. (2005b). *Prediction based combined control to prevent the rollover of heavy vehicles* in Proceedings of the 13th Mediterranean Conference on Control and Automation. Limassol, Cyprus.

[7] Jacobson, Bengt, et al. 2018. *Vehicle Dynamics Compendium for Course MMF062* Göteborg : Chalmers University of Technology, 2018

[8] Samuel Joseph. *Design and development of steering and suspension system of a concept car* Master of Science Thesis Stockholm, Sweden 2013

[9] ISO 8855.*Road vehicle – Vehicle dynamics and road holding ability* Vocabulary. s.l. : International Organization for Standardization, Genève, Switzerland.

[10] Martin Mondek and Martin Hromcık.*Linear analysis of lateral vehicle dynamics* Czech Technical University in Prague

[11] Reza N. Jazar. 2008. *Reza N Jazar Vehicle Dynamics. Theory and Application*, Springer, Mechanical Engineering Series, 2005.

[12] CarMaker. 2018. *Reference Manual Version 7.0*,1999 - 2018 by IPG Automotive GmbH – www.ipg-automotive.com

[13] Skogestad Sigurd, Postlethwaite Ian, *Multivariable Feedback Control: Analysis and Design*,2015, New York,Wiley-Interscience, Edition Number 2, ISBN: 9780470011683

[14] Bal´azs Kulcs´ar, *Linear Control System Design (SSY285) - System Modeling for Control* Göteborg : Chalmers University of Technology, 2017

[15] Bal´azs Kulcs´ar, *Linear Control System Design (SSY285) - Controller synthesis for LTI systems* Göteborg : Chalmers University of Technology, 2017

[16] Bal´azs Kulcs´ar, *Robust and Nonlinear Control Design (ESS076)- Robust control* Göteborg : Chalmers University of Technology, 2018

[17] Hartley, Gerald A,*F-18 robust control design using H2 and H-infinity methods*, M.S. Thesis, Naval Postgraduate School, Monterey, California, December, 1990.

[18] Philipp Kautzmann,Jürgen Römer, Michael Frey,*A Novel Chassis Concept for Power Steering Systems Driven by Wheel Individual Torque at the Front Axle*,25th Aachen Colloquium Automobile and Engine Technology 2016.

[19] x-engineer.org, *Tire axis system and terminology defined by SAE standards*, 2019 x-engineer.org

[20] Rachid Attia, Rodolfo Orjuela, Michel Basset,*Combined longitudinal and lateral control for automated vehicle guidance*,Vehicle System Dynamics, Taylor,Francis, 2014, 52 (2), pp.261-279. ff10.1080/00423114.2013.874563ff. ffhal-01027591

[21] Kwan-Woong Gwak and Glenn Y. Masada,*Nonlinear Optimal Control of an Input-Constrained and Enclosed Thermal Processing System*International Journal of Control, Automation, and Systems, vol. 6, no. 2, pp. 160-170, April 2008

A

Appendix 1

A.1 Results

The roll torque and pitch angle plots for all the test scenarios and shown below.

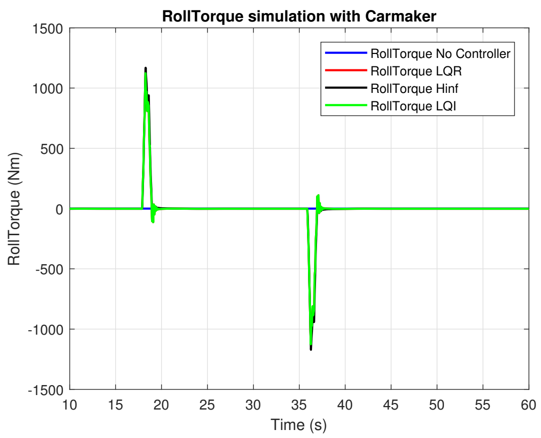

(a) Roll torque with setup-1

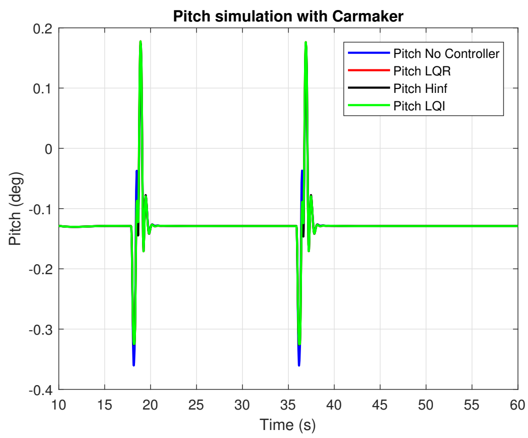

(b) Pitch with setup-1

Figure A.1: Roll torque and Pitch plots for kinematic setup-1 and high frequency road disturbances with driver-in-loop

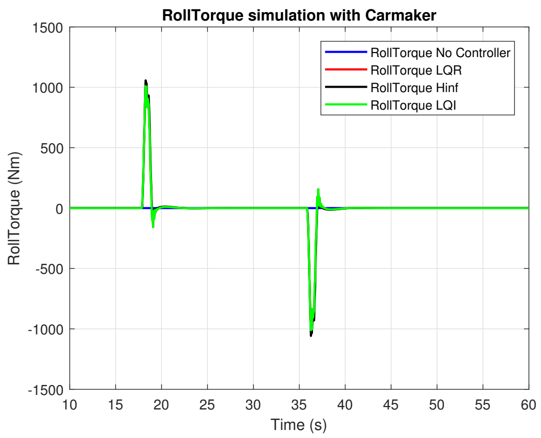

(a) Roll torque with setup-2

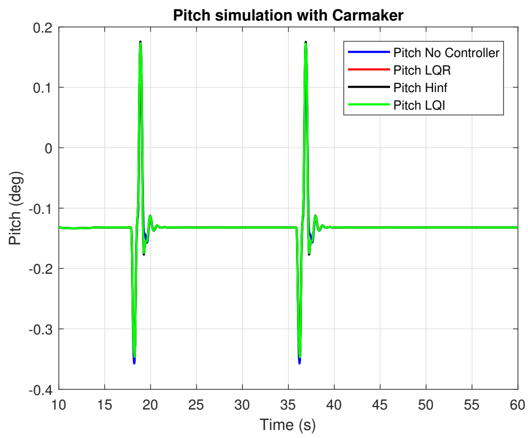

(b) Pitch with setup-2

Figure A.2: Roll torque and Pitch plots for kinematic setup-2 and high frequency road disturbances with driver-in-loop

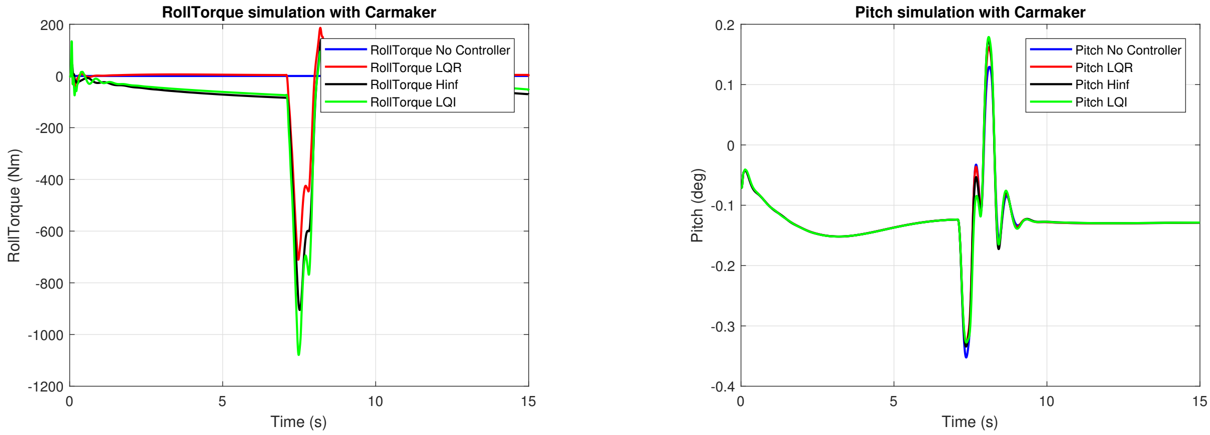

(a) Roll torque with setup-1 **(b)** Pitch with setup-1

Figure A.3: Roll torque and Pitch plots for kinematic setup-1 and high frequency road disturbances with driver-out-loop

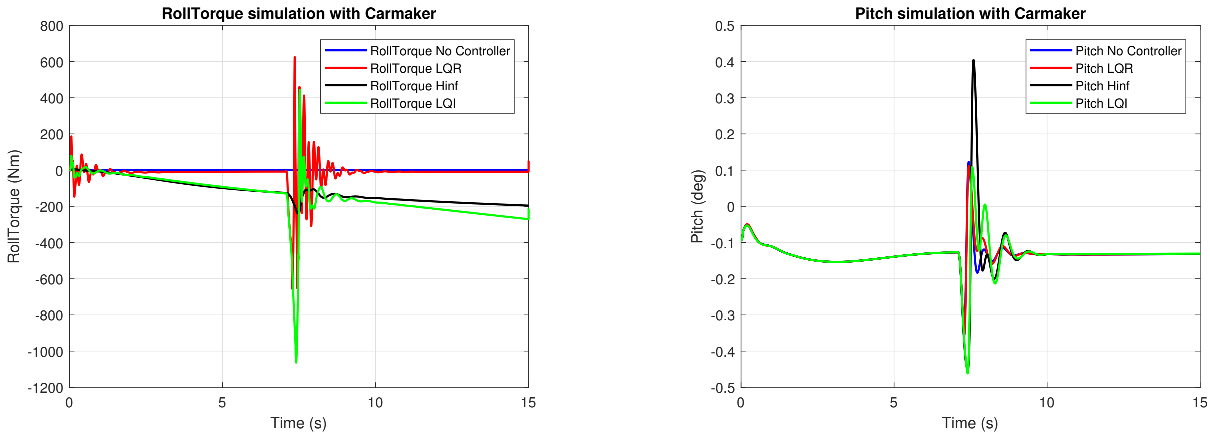

(a) Roll torque with setup-2 **(b)** Pitch with setup-2

Figure A.4: Roll torque and Pitch plots for kinematic setup-2 and high frequency road disturbances with driver-out-loop

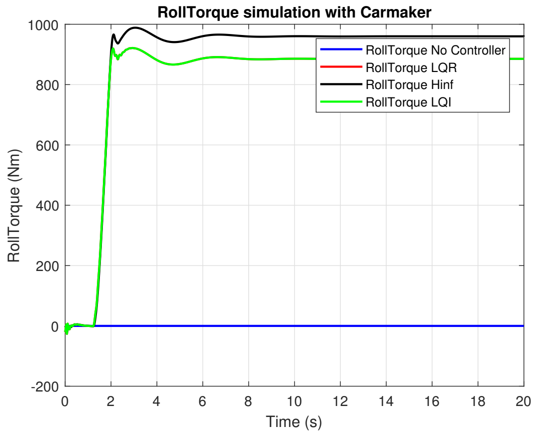

(a) Roll torque with setup-1

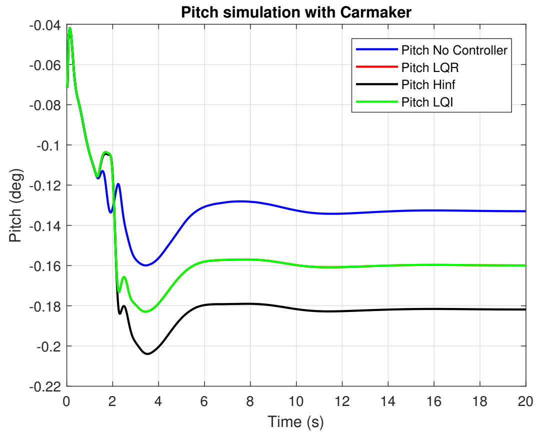

(b) Pitch with setup-1

Figure A.5: Roll torque and Pitch plots for kinematic setup-1 and banked road with driver-in-loop

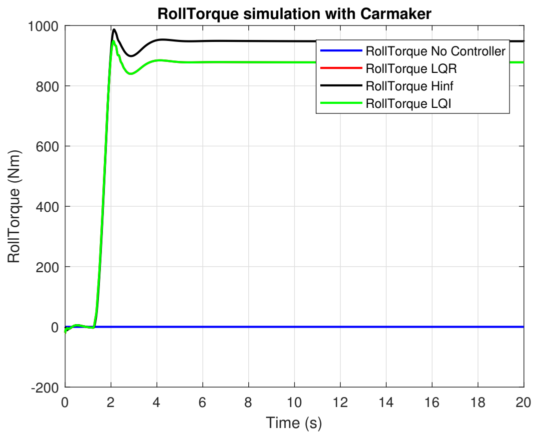

(a) Roll torque with setup-2

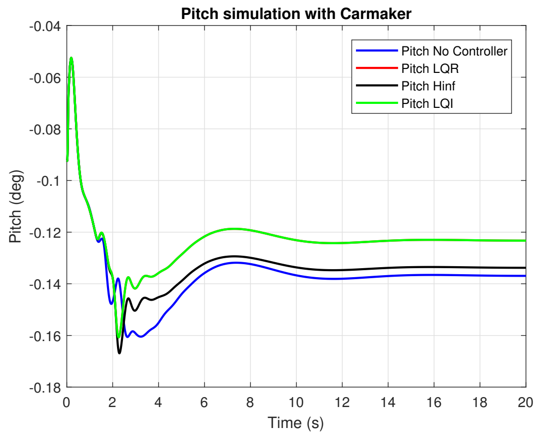

(b) Pitch with setup-2

Figure A.6: Roll torque and Pitch plots for kinematic setup-2 and banked road with driver-in-loop

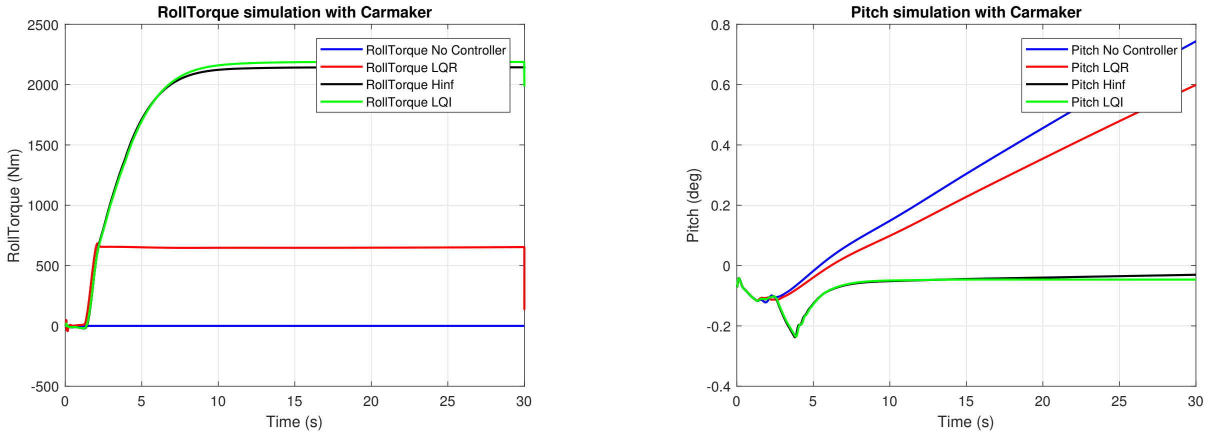

(a) Roll torque with setup-1 **(b)** Pitch with setup-1

Figure A.7: Roll torque and Pitch plots for kinematic setup-1 and banked road with driver-out-loop

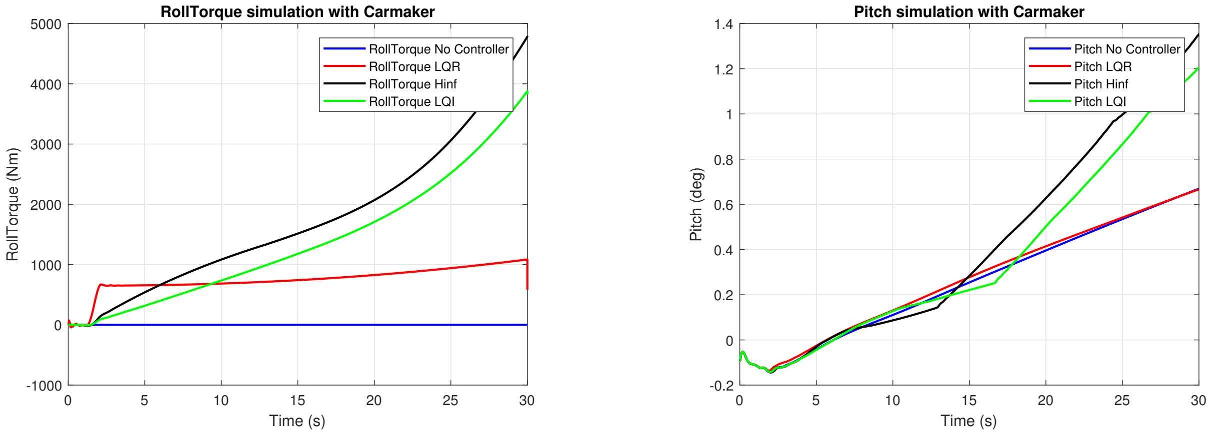

(a) Roll torque with setup-2 **(b)** Pitch with setup-2

Figure A.8: Roll torque and Pitch plots for kinematic setup-2 and banked road with driver-out-loop

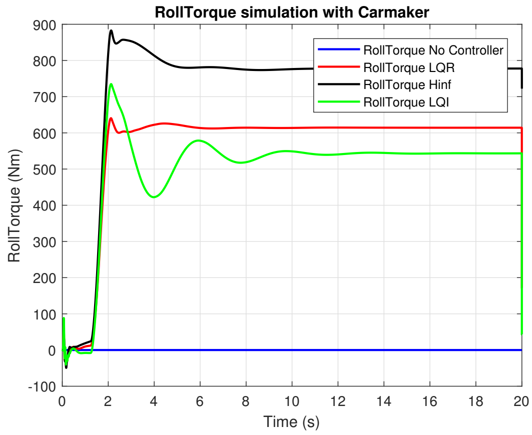

(a) Roll torque with setup-1

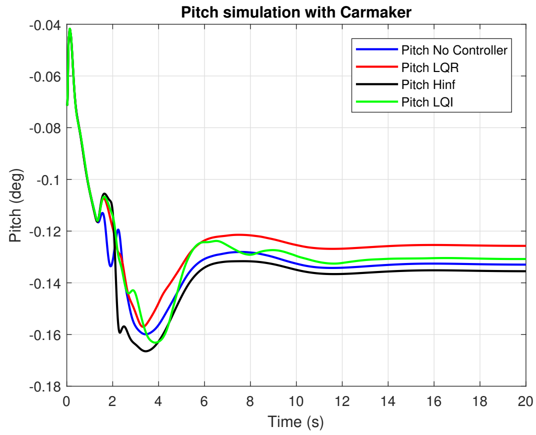

(b) Pitch with setup-1

Figure A.9: Roll torque and Pitch plots for kinematic setup-1 and cornering with driver-in-loop

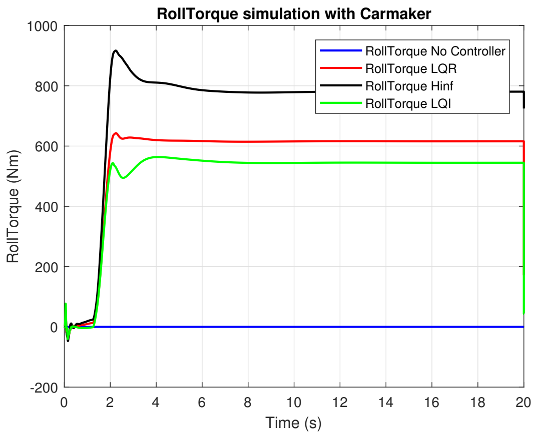

(a) Roll torque with setup-2

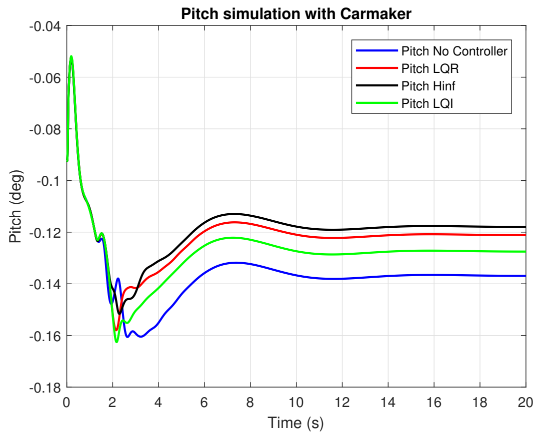

(b) Pitch with setup-2

Figure A.10: Roll torque and Pitch plots for kinematic setup-2 and cornering with driver-in-loop

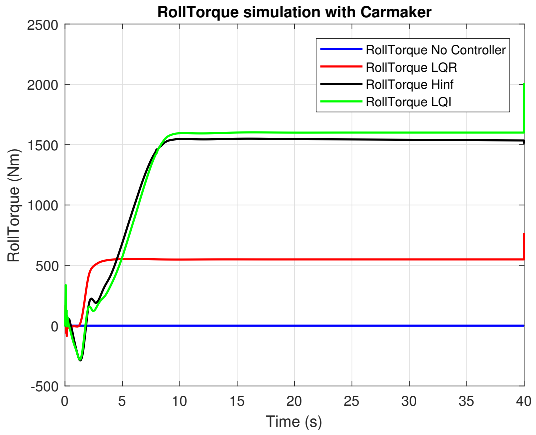

(a) Roll torque with setup-1

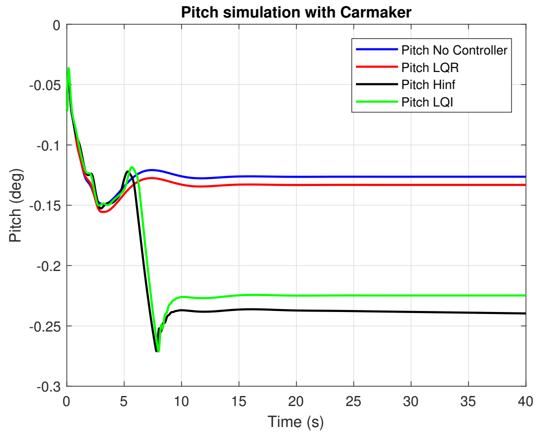

(b) Pitch with setup-1

Figure A.11: Roll torque and Pitch plots for kinematic setup-1 and cornering with driver-out-loop

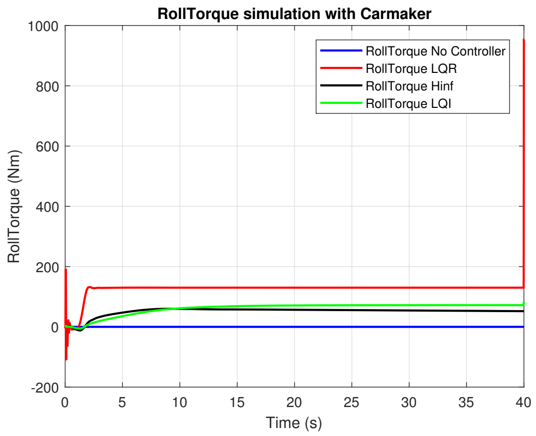

(a) Roll torque with setup-2

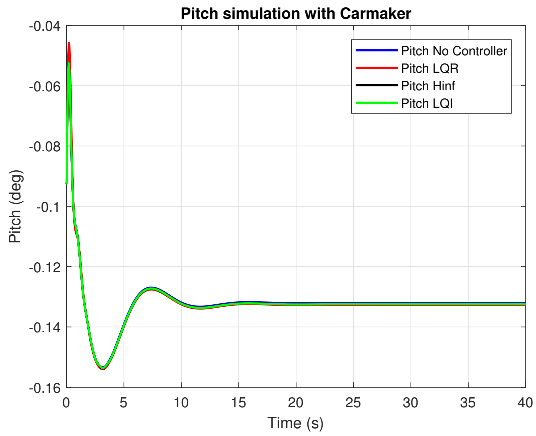

(b) Pitch with setup-2

Figure A.12: Roll torque and Pitch plots for kinematic setup-2 and cornering with driver-out-loop

A.2 Modeling

The reduced roll-yaw model matrices are given by -

$$A_{AARB} = \begin{pmatrix} 0 & 1 & 0 & 0 & 0 & 0 & 0 & 0 \\ -82.51 & -4.716 & -21.62 & -1.417 & 0 & 0 & 0 & 0 \\ 0 & 0 & 0 & 1 & 0 & 0 & 0 & 0 \\ -11.89 & -0.7794 & -102.7 & -5.883 & 0 & 0 & 0 & 0 \\ 0 & 0 & 0 & 0 & 0 & 1 & 0 & 0 \\ 0 & 0 & 0 & 0 & -186.1 & -10.64 & 0 & 0 \\ 0.06419 & 0 & 0.1008 & 0 & 0.8595 & 0 & -5.543 & -24.07 \\ -0.0531 & 0 & 0.7754 & 0 & -3.991 & 0 & 1.956 & -6.791 \end{pmatrix} \tag{A.1}$$

$$B_{AARB} = \begin{pmatrix} 0 \\ 0 \\ 0 \\ 0 \\ 0 \\ -0.00846 \\ 0 \\ 0 \end{pmatrix} \tag{A.2}$$

$$C_{AARB} = \begin{pmatrix} 1 & 0 & 0 & 0 & 0 & 0 & 0 & 0 \\ 0 & 1 & 0 & 0 & 0 & 0 & 0 & 0 \\ 0 & 0 & 1 & 0 & 0 & 0 & 0 & 0 \\ 0 & 0 & 0 & 1 & 0 & 0 & 0 & 0 \\ 0 & 0 & 0 & 0 & 1 & 0 & 0 & 0 \\ 0 & 0 & 0 & 0 & 0 & 1 & 0 & 0 \\ 0 & 0 & 0 & 0 & 0 & 0 & 1 & 0 \\ 0 & 0 & 0 & 0 & 0 & 0 & 0 & 1 \end{pmatrix} \tag{A.3}$$

$$D_{AARB} = \begin{pmatrix} 0 \\ 0 \\ 0 \\ 0 \\ 0 \\ 0 \\ 0 \\ 0 \end{pmatrix} \tag{A.4}$$

$$
E = \begin{pmatrix}
0 & 0 & 0 & 0 & 0 & 0 & 0 & 0 & 0 & 0 \\
0 & 0 & & & & & & & & \\
18.0777 & 18.0777 & 23.1796 & 23.1796 & 1.0028 & 1.0028 & 1.3551 & 1.3551 & 0 & 0 \\
0 & 0 & & & & & & & & \\
0 & 0 & 0 & 0 & 0 & 0 & 0 & 0 & 0 & 0 \\
0 & 0 & & & & & & & & \\
-14.0682 & -14.0682 & 20.0145 & 20.0145 & -0.7804 & -0.7804 & 1.1701 & 1.1701 & 0 & 0 \\
0 & 0 & & & & & & & & \\
0 & 0 & 0 & 0 & 0 & 0 & 0 & 0 & 0 & 0 \\
0 & 0 & & & & & & & & \\
-47.9632 & 47.9632 & -61.4994 & 61.4994 & -2.6606 & 2.6606 & -3.5954 & 3.5954 & 0 & 0 \\
0 & 0 & & & & & & & & \\
-1.4006 & 1.4006 & 1.8741 & -1.9383 & 0 & 0 & 0 & 0 & 23.2208 & 23.2208 \\
53.7633 & 53.7633 & & & & & & & & \\
-1.0443 & 1.0443 & -1.5503 & 1.6034 & 0 & 0 & 0 & 0 & 17.3123 & 17.3123 \\
-44.4742 & -44.4742 & & & & & & & &
\end{pmatrix}
\quad \text{(A.5)}
$$